SYNTHESIS, CHARACTERIZATION, AND HYPERTHERMIA STUDIES OF THERMOSENSITIVE HYDROGELS ASSOCIATED WITH MAGNETIC NANOEMULSIONS

A Dissertation by

Aybala Usta

Master of Science, Wichita State University, 2014

Bachelor of Science, Sakarya University, 2011

Submitted to the Department of Mechanical Engineering
and the faculty of the Graduate School of
Wichita State University
in partial fulfillment of
the requirements for the degree of
Doctor of Philosopy

July 2018

SYNTHESIS, CHARACTERIZATION, AND HYPERTHERMIA STUDIES OF THERMOSENSITIVE HYDROGELS ASSOCIATED WITH MAGNETIC NANOEMULSIONS

The following faculty members have examined the final copy of this dissertation for form and content, and recommend that it be accepted in partial fulfillment of the requirement for the degree of Doctor of Philosophy, with a major in Mechanical Engineering.

_____
Ramazan Asmatulu, Committee Chair

_____
Gamal Weheba, Committee Member

_____
Shang-You Yang, Committee Member

_____
Bin Li, Committee Member

_____
Shuang Gu, Committee Member

Accepted for the College of Engineering

_____
Steven Skinner, Interim Dean

Accepted for the Graduate School

_____
Dennis Livesay, Dean

DEDICATION

To my family and my dear friends

ACKNOWLEDGEMENTS

I would like to express my heartfelt gratitude to my advisor, Dr. Ramazan Asmatulu, Professor in the Department of Mechanical Engineering, for his guidance in accomplishing this research work. He has always been a great support throughout my Ph.D. program. With his humble heart and great personality, the time I spent throughout my research work has become more enjoyable and has added great value to my knowledge.

I am also very grateful to Dr. Gamal Weheba, Professor in the Department of Industrial and Manufacturing Engineering, and Dr. Bin Li, Assistant Professor in the Department of Mechanical Engineering, for their interest in my thesis and attendance at my defense, and also for teaching me many valuable concepts. The subjects I learned from them have added great value to my knowledge and have been very important while working on this research project. I wish to thank Dr. Shang-You Yang, Associate Professor in the Department of Biological Sciences, for sharing his valuable knowledge of the biological field. His suggestions and advice have given me ideas for further studies and designing biological tests. I am also very thankful to Dr. Shuang Gu, Assistant Professor in the Department of Mechanical Engineering, for his interest in my thesis and attendance at my defense. His suggestions and questions helped me conduct a better research study.

I am also very thankful to my best friend, Vinay Patil. He has always been a great support and listener, and most importantly, he has been very encouraging and patient. He has provided the best advice and helped me during difficult times. Vinay has become one of the unforgettable people in my life.

Hajar El Makhloufi, Haneen Abu Al Rob, and Jayangika Niroshani Dahanayake, my chosen sisters, have been my biggest supporters and have provided unforgettable moments along

with endless joy. Without them in my life, my journey would have been more tedious and difficult. I express my heartfelt appreciation for them touching my life.

Next, my relatives who have always prayed for and supported me, especially my grandparents Mariye and Ahmet Akbudak, and my aunt Gul Akbudak Aykac, deserve a big thank. Their support and prayers from far away were felt in my heart.

Finally, knowing that I can never be thankful enough, my sincerest appreciation and gratitude goes to my father Hacı Numan Usta, my mother Betul Sukran Usta, and my brother Atalay Usta, for their endless inspiration, guidance, support, and prayers in order for me to complete this research work. No words can explain their place in and impact on my life. Their influence on my life always will always be the most meaningful gift.

ABSTRACT

Targeted drug delivery is of great importance in cancer treatment and has become the interest of many scientists worldwide. Targeted drug delivery renders local treatment of cancerous cells possible without affecting healthy cells. Hydrogels are promising materials to be used in targeted drug delivery systems due to their biocompatible nature and injectable behavior whereby they can be used to load drugs. However, considering that not all the drugs are water soluble, entrapment of some drugs in hydrogels is not practical in terms of poor drug solubility and burst drug release. An oil phase can be considered as a drug-carrying agent, and entrapment of this oil phase into the hydrogel would make it possible for the *in-situ* injection of a dissolved drug into the oil phase. Moreover, incorporation of hydrogels with magnetic nanoparticles can create a double effect, making hyperthermia treatment possible and also controlling the flow of magnetic nanoparticles out of the concerned region using a hydrogel matrix.

In this study, oil-in-water (O/W)-type nanoemulsions were prepared using a combination of black seed oil (which is known to cause apoptosis via a p-53 dependent mechanism), water, and Triton X-100 and Span-80 surfactants. Three different oil percentages and three different surfactant percentages were tested, and the stability behavior of these nanoemulsions were investigated and compared. Dynamic light scattering analysis and zeta potential measurements were conducted for determining particles sizes and surface charges of the nanoemulsions. The most stable nanoemulsion with the smallest diameter and lowest polydispersity index (PDI) was used in the synthesis of nanoparticle-added magnetic nanoemulsion hydrogels (MNHs) for the hyperthermia study. Results have indicated that time, concentration, and magnetic field strength (MFS) can significantly affect the heating ability of the samples, which can be promising candidates for further hyperthermia studies.

TABLE OF CONTENTS

TABLE OF CONTENTS (continued)

LIST OF TABLES

LIST OF TABLES (continued)

Table Page

LIST OF FIGURES

LIST OF FIGURES (continued)

LIST OF FIGURES (continued)

LIST OF FIGURES (continued)

LIST OF FIGURES (continued)

LIST OF ABBREVIATIONS

5-FU	5-Flouracil
AC	Alternating Current
AMF	Alternating Magnetic Field
ANOVA	Analysis of Variance
AR	Androgen Receptor
ATR	Attenuated Total Reflection
CDR	Cumulative Drug Release
CMC	Critical Micelle Concentration
DFFITS	Difference in Fits
DLS	Dynamic Light Scattering
DLVO	Derjaguin, Landau, Verwey, and Overbeek (Theory)
DOX	Doxorubicin
FTIR	Fourier Transform Infrared Spectroscopy
GSH	Glutathione
HCl	Hydrochloric Acid
HLB	Hydrophilic-Lipophilic Balance
HPLC	High-Performance Liquid Chromatography
IR	Infrared
LCST	Lower Critical Solution Temperature
LSW	Lifshitz-Slesov-Wagner (Theory)
MFS	Magnetic Field Strength
MHz	Megahertz

MNH	Magnetic Nanoemulsion Hydrogel
MNP	Magnetic Nanoparticle
NIPAAm	N-isopropylacrylamide
NIR	Near-Infrared
O/W	Oil-in-Water
PBS	Phosphate-Buffered Saline
PDI	Polydispersity Index
PEC	Polyelectrolyte Complex
PDI	Polydispersity Index
PVA	Polyvinyl Alcohol
ROS	Reactive Oxygen Species
SAR	Specific Absorption Rate
SD	Standard Deviation
SLP	Specific Loss Power
SQRT	Square Root
SR	Swelling Ratio
TQ	Thymoquinone
UCST	Upper Critical Solution Temperature
UV-Vis	Ultraviolet Visible
WC	Water Content
WHO	World Health Organization
W/O	Water-in-Oil

LIST OF SYMBOLS

A	Hamaker Constant
D	Diffusivity
g	Gravitational Constant
h	Distance between Two Droplets
N_{av}	Avogadro Number
r	Radius
R	Inert Gas Constant
T	Temperature
t	Time
U	Velocity of Rising Droplet
Z_i	Valency of Ions
χ	Flory-Huggins Interaction Parameter
υ	Molar volume of dispersed phase
δ	Polymer Chain Thickness
C_∞	Solubility of Dispersed Phase
φ_2	Volume Fraction
γ	Interface Energy
μ_c	Viscosity of Continuous Medium
μ_d	Viscosity of Dispersed Medium
$\Delta\rho$	Density Difference
ε_r	Relative Permittivity
ε_o	Permittivity of Free Space

κ	Debye-Huckel Parameter
$1/\kappa$	Thickness of Double Layer
Ψ_o	Surface Potential

CHAPTER 1

INTRODUCTION

Nanoemulsions are systems that are thermodynamically stable, and their size is in the range of 20 to 200 nm. They are used in numerous pharmaceutical products such as vaccines [1] and in potential drug delivery applications such as intranasal drug delivery [2], pulmonary drug delivery [3, 4], parenteral drug delivery [5], and transdermal drug delivery [6-8].

Targeted drug delivery is a trending approach in drug delivery, and hydrogels hold great potential in this field because of their biocompatible and biodegradable properties. Hydrogels have been used in drug delivery applications, and drugs have been entrapped in a hydrogel network [9-12]. The challenging part of this application is that the watery structure of the hydrogel does not always provide a good environment for drugs that are weakly soluble in water. At this point, the use of nanoemulsions, which consist of oil and water together, offers a great path for reaching the target. Drugs dissolved in the oil phase can be dispersed homogeneously in the water phase, so that the dissolved drug amount sent to the target area will increase. Moreover, release properties and treatment efficiency would also be enhanced. This renders the delivery of both hydrophilic and lipophilic drugs together possible.

Nanoemulsion can be generated using various methods including high-energy emulsification methods such as high-pressure homogenization and ultrasonication, and low-energy methods such as phase inversion composition, phase inversion temperature, and solvent displacement. Among these methods, ultrasonic emulsification is an easy, cost-effective, clean, and fast technique for nanoemulsion preparation [13]. Ultrasonic emulsification utilizes a probe that generates ultrasonic waves to break apart the macroemulsion by cavitation forces.

1.1 Significance of Study

The importance of this study is that it shows how lipophilic drugs can be delivered to a targeted area of the body. Hydrogels as a water-based drug delivery material are not always appropriate for delivering drugs with low water solubility, because they cause a burst release of the drug, which can be toxic to healthy cells. However, by using nanoemulsions, entrapment of these drugs in a water phase can be made possible by means of an oil phase dispersed into a water phase. Here, water used in the system can be used in preparation of hydrogels with stimulus sensitivity. Once the stimulus-sensitive hydrogel is injected into the body, gelation occurs, and drugs dissolved in the oil phase can be delivered to the targeted area.

1.2 Objectives of Study

One of the objectives of this study was to prepare nanoemulsions with different oil and surfactant percentages, and then investigate the long-term stability behavior of these oil-in-water (O/W) nanoemulsions. The hydrophilic-lipophilic balance (HLB) is crucial for nanoemulsion applications. In the current study, the effect of the HLB change on nanoemulsion characteristics was investigated. Results from numerous tests over the course of 30 days were used for further studies in drug delivery applications. Moreover, chitosan hydrogels, which are known for their excellent biocompatibility and biodegradability, were combined with nanoemulsions so that they could be fabricated and injected into targeted areas of the body.

Another aim of this study was to increase the mechanical properties of injectable chitosan-based hydrogels impregnated with the above-mentioned nanoemulsions that have the best stability, zeta potential, and particle size properties. Chitosan hydrogels are known for their low mechanical properties and fast biodegradation, which causes inefficiency in drug delivery. In

this study, the mechanical properties of the chitosan hydrogel were increased by adding polyvinyl alcohol (PVA).

This study also contributes to the understanding and treatment of localized cancer using O/W nanoemulsion hydrogels incorporated with magnetic nanoparticles (MNPs) along with the treatment effect of hyperthermia. Studies involving materials science and biology have opened up new investigations in the field of biotechnology.

The overall focus of this study was on incorporation of the physical properties of magnetic nanoparticles, nanoemulsions and hydrogels, thus increasing the treatment efficiency of cancer cells with the help hyperthermia. Nanoemulsions were investigated for the best stability conditions. Moreover, the principles of heat generation mechanism by induction heating from source to the cells are considered, and temperature rise in targeted area is aimed to be controlled for a safe treatment.

CHAPTER 2

LITERATURE REVIEW

2.1 Overview of Cancer

Cancer is one of the leading causes of death in the world. About 2.5 million cancer patients are found in the world, and one million new cases are added each year, with a chance of the disease rising fivefold by 2025 [14]. According to a World Health Organization (WHO) report, premature death involving no communicable diseases is the highest in the world. In spite of new discoveries of drugs and treatment combinations, as evidenced by reports of close to 200,000 experimental studies on mice, two million scientific publications, and an annual spending of around 15 billion U.S. dollars worldwide, the death rate due to cancer has not changed in the past five to six decades [15]. Therefore, there is still a strong need for a shift in the approach to cancer diagnosis and therapy.

Until today, cancer treatments have been based on conventional techniques involving radiological and histopathological examinations. The most common cancer treatments are restricted to surgery, radiation, and chemotherapy [16]. Cancer can basically be defined as the abnormal growth of cells caused by multiple changes in gene expression leading to a deregulated balance of cell proliferation and cell death [17]. These changes in genetic expressions can be caused by genetic or environmental factors. Once gene mutation occurs, cells keep proliferating, as opposed to healthy cells that go through apoptosis in the case of faulty genes. Thus, cancer forms as a tumor. On the other hand, not all tumors are cancerous. While some tumors do not metastasize (spread), which are referred to as benign (non-cancerous), others are malignant, which are cancerous tumors. Moreover, some cancers, like leukemia, do not form tumors. Instead, these cancer cells involve the blood and blood-forming organs and circulate through

other tissues where they grow. Figure 1 represents the difference between normal and cancer cells.

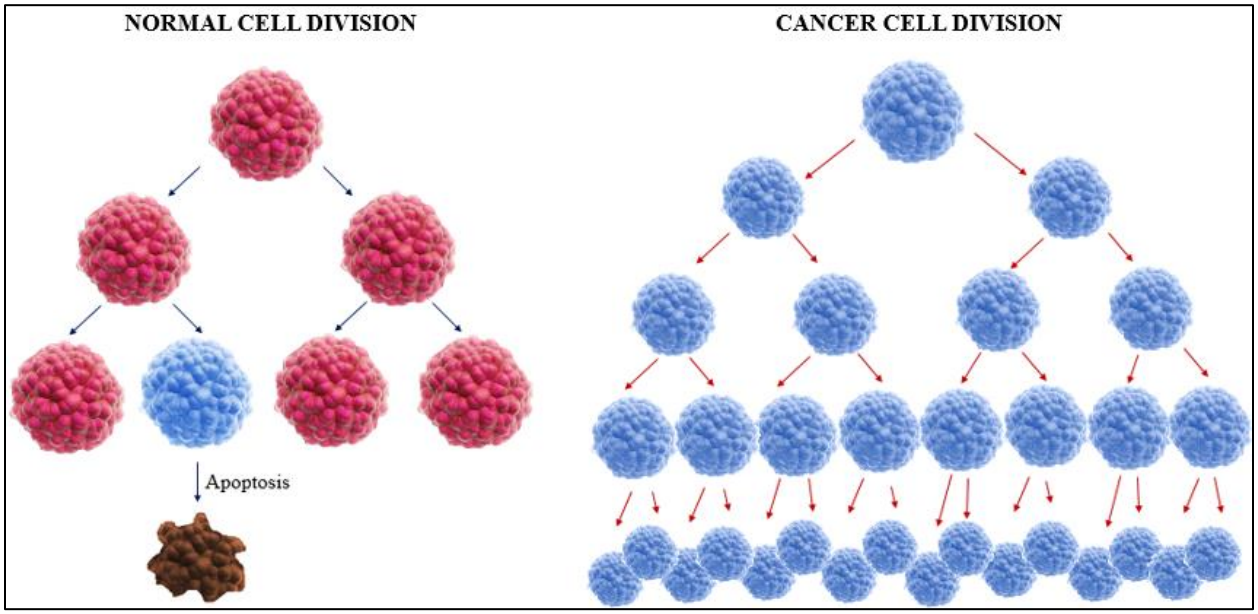

Figure 1. Comparison of normal cell division and cancerous cell division.

2.1.1 Surgery Treatment

Surgery is the oldest form of treatment for many cancer types [18]. Considering the types of cancer that have not yet metastasized offers one of the greatest opportunities to cure many types of cancer, but not for late-stage cancer. The goal of treating cancer with surgery is complete removal of the cancer without damage to the rest of the body; however, surgery is not only used in the treatment of cancer but also to prevent, determine the stage of, and diagnose the cancer. Surgery is often required to remove a wide surgical margin or a free margin. Width of the free margin depends on the type of cancer and the method of removal.

2.1.2 Radiotherapy Treatment

Radiation therapy is a clinical treatment method for cancer that uses ionizing radiation to treat patients with malignant excessive growth of tissue, or neoplasias (and occasionally benign diseases). The purpose of radiation therapy is to deliver a precisely measured dose of irradiation

to a defined tumor volume with as minimal damage to the surrounding healthy tissue as possible, using an appropriate radiation technique, thus resulting in destruction of the tumor [19]. Radiation therapy involves exposing cancer cells to beams of high-energy particles, or waves (radiation), such as x-rays, gamma rays, neutrons, pi-mesons, or radioactive seeds. Radiotherapists often implant radioactive materials or radioisotopes into tumors. The particles transfer their energy into electrons, which ionize the matter, thus damaging the molecules and causing the free radicals to react with oxygen that is present in the environment. This can change the biological properties of the biomolecules and cause cell death or stop cell proliferation. Radiation is much more harmful to cancer cells than to normal cells. This is because cancer cells divide more rapidly than healthy cells [20]. Cells are more vulnerable to damage when they are dividing, making cancer cells more susceptible to radiation than normal cells. In addition, normal cells can recover from the effects of radiation more easily than cancer cells. Nevertheless, it is impossible to kill a tumor without harming the surrounding healthy cells. Radiation can also cause damage to normal tissue [21].

2.1.3 Chemotherapy Treatment

Chemotherapy is one of the major the treatment technique of localized or metastasized cancers, which involves the use of one or more anti-cancer drug to destroy cancer cells. Considering that anticancer drugs are not specific to cancer cells holds a great importance to deliver anticancer agents to the concerned area only and enhance the selective increase in tumor tissue uptake. For optimization of drug therapy, administration routes, bio distribution and elimination of available chemotherapeutic agents can be modified by drug delivery systems.

Most often, chemotherapy means taking medicines, or drugs, to treat the cancer, especially cancer that is spread out and cannot be treated using local methods such as surgery

and radiation. The effectiveness of chemotherapy is often limited by its toxicity to other tissues in the body. Anticancer drugs destroy cancer cells by stopping them from growing or multiplying. They also target and damage any healthy cells that are quickly dividing, whether or not those cells are cancerous. Up until today, the treatments mentioned above have been used to treat cancer efficiently. However, these techniques have major side effects, the most common of which are bleeding, hair loss, high pain, and infection. Figure 2 presents a diagram of the progression of cancer and how it is halted using chemotherapy.

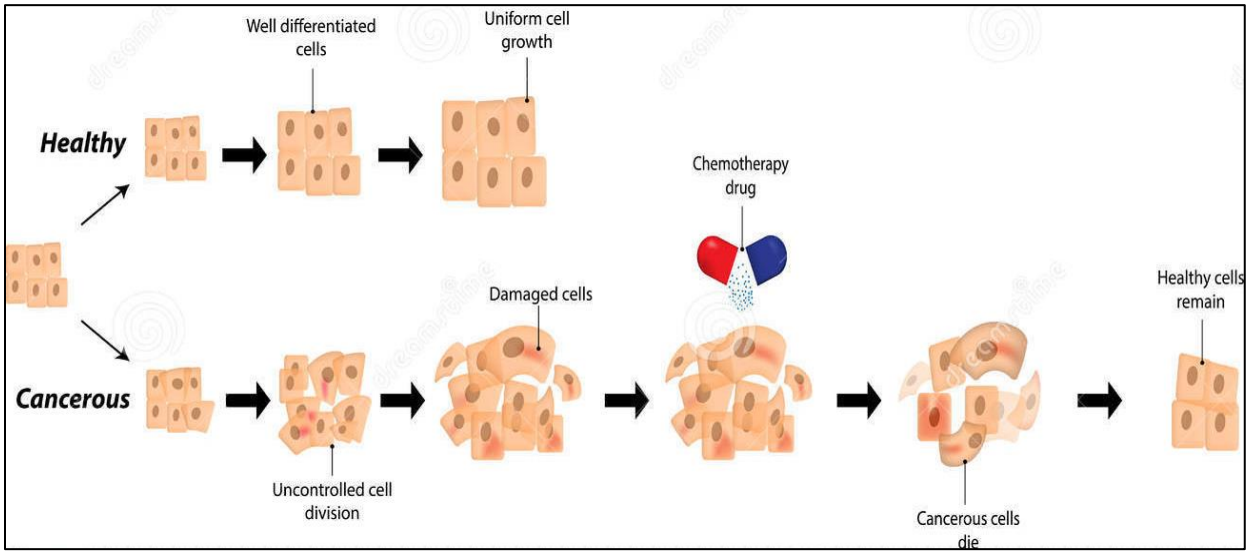

Figure 2. Progression of cancer and how it is halted using chemotherapy [22].

2.1.4 Hyperthermia Treatment and Selective Cell-Killing Mechanism

Hyperthermia is a cancer treatment that destroys a tumor by elevating the temperature of the cancerous tissue to approximately 42°C –45°C for 20 to 60 minutes [23]. Even though there have been studies on using hyperthermia alone as a cancer treatment technique, it is almost always used in combination with conventional cancer treatment techniques to increase the treatment efficacy [24, 25] and make the cancer cells more sensitive to treatment. Research has shown that elevated temperatures can damage or kill cancer cells, while normal tissues are

injured minimally during hyperthermia [25]. A number of mechanisms are used in the selective killing of cancerous cells by hyperthermia. One of these mechanisms involves the protein denaturation energy of cancerous cells and is similar to the energy applied during hyperthermia, which eventually damages the proteins and kill the cancer cells [26]. Another mechanism is due to the physiological differences between cancerous and normal cells. While cancer cells have a strong orientation in the vascular network, abnormal cells have a poor orientation [27], and at elevated temperatures, increasing the blood flow can transfer the generated heat easily, due to the well-oriented vascular network. On the other hand, because of the poor orientation of the vascular network in tumor cells, the blood flow is disturbed, and the heat generated by hyperthermia is not transferred. Because of the low heat-dissipation rate, the temperature rises more easily in tumor tissues than in normal tissues [28]. For a small percentage of patients, the hyperthermia therapeutic technique is used against tumors in conjunction with other techniques such as surgical operation, chemotherapy, and radiotherapy. However, in the future, this technique is expected to be one of the most important treatments for many kinds of cancer. Another mechanism involved here comes from the higher sensitivity of cells to heat during the mitosis phase of proliferation. In normal cells, mitosis is negligible due to controlled division; however, mitosis is prominent in cancerous cells that have a high cell proliferation rate, which increases the mitosis phase number and renders the cancer cells more vulnerable to elevated temperatures.

2.2 Breast Cancer

Among women living in Western countries, breast cancer is an important disease in terms of incidence and mortality. This disease occurs when cells in the breast grow out of control, usually forming a tumor that can often be seen on an x-ray or felt as a lump. The tumor is

considered to be malignant (cancerous) if the cells grow into (invade) surrounding tissues or spread to distant areas of the body, which is called metastasis. A model of the breast with breast cancer is shown in Figure 3.

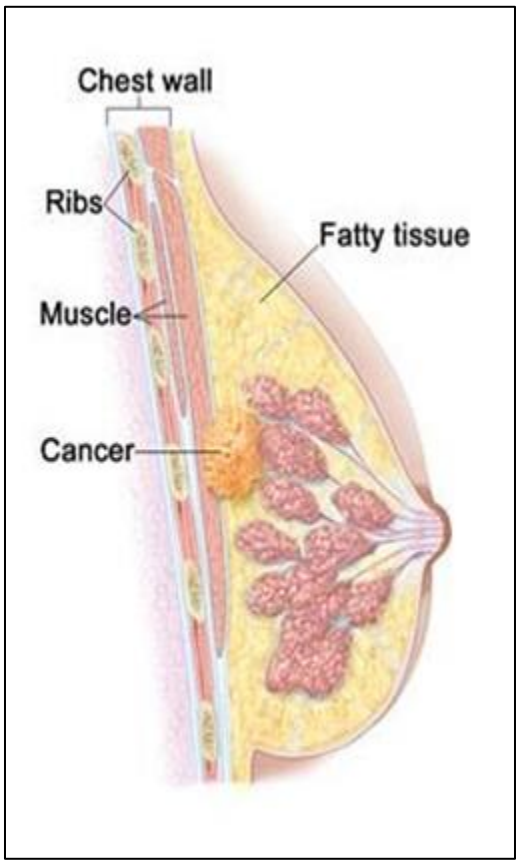

Figure 3. Model of the breast showing breast cancer [31].

Breast cancer occurs almost entirely in women, but men can also get breast cancer [29]. According to a statistical study by the American Cancer Society in 2016, invasive breast cancer was diagnosed in approximately 246,660 women and 2,600 men. About 61,000 cases of *in situ* breast cancer were diagnosed in 2016, and an estimated 40,890 breast cancer deaths (40,450 women, 440 men) were expected in that year. According to these statistics, breast cancer is the most frequently diagnosed cancer and ranks second as the cause of cancer death in women [30].

From 2003 to 2012, breast cancer death rates decreased by 1.9% per year in white women and by 1.4% per year in black women. Overall, breast cancer death rates declined by 36% from 1989 to 2012, due to improvements in early detection and treatment, translating to the avoidance of approximately 249,000 breast cancer deaths.

Changes or mutations in DNA can cause normal breast cells to become cancerous. Certain DNA changes are passed on from parents (inherited) and can greatly increase the risk for breast cancer. Other lifestyle-related risk factors, such as what you eat and how much you exercise, can increase your chance of developing breast cancer, but it is not yet known exactly how some of these risk factors cause normal cells to become cancer. Hormones seem to play a role in many cases of breast cancer, but just how this happens is not fully understood [29].

Breast cancers can begin in different parts of the breast, primarily in the ducts that carry milk to the nipple (ductal cancers). Some begin in the glands that make breast milk (lobular cancers). There are also other types of breast cancer that are less common. A small number of cancers start in other breast tissue, which are referred to as sarcomas and lymphomas and are not really considered to be breast cancers. Breast cancer can spread when cancer cells enter the blood or lymph system and are carried to other parts of the body [29].

2.3 Nanoemulsions

Emulsion technology is generally applied to the encapsulation of bioactive compounds in aqueous solutions through the production of nanoemulsions. The high kinetic stability of nanoemulsions is a real benefit for encapsulation purposes and plays a critical role in retaining the surface oil content of the product [32]. Nanoemulsions, being non-equilibrium systems, cannot be formed spontaneously, consequently needing energy input, generally from mechanical devices or from the chemical potential of the components. Therefore, nanoemulsion formation is

generally achieved using high-energy emulsification methods such as high-shear stirring, high-speed or high-pressure homogenization, ultra-sonication, and micro-fluidization. These methods supply the available energy in the shortest period of time and possess the most homogeneous flow to produce the smallest droplet sizes [33-35].

Nanosystems such as liposomes, dendrimers, micelles, nanocapsules, and nanoemulsions are some of the targeting agents that have been used in various applications such as pharmaceuticals and cosmetics, and in this area of study. Among the nanosystems, nanoemulsions can be defined as emulsions that contain nanoscaled water or oil droplets dispersed in the external phase of opposite polarity by the effect of surfactants arranging at the interface of oil and water [36], as shown in Figure 4.

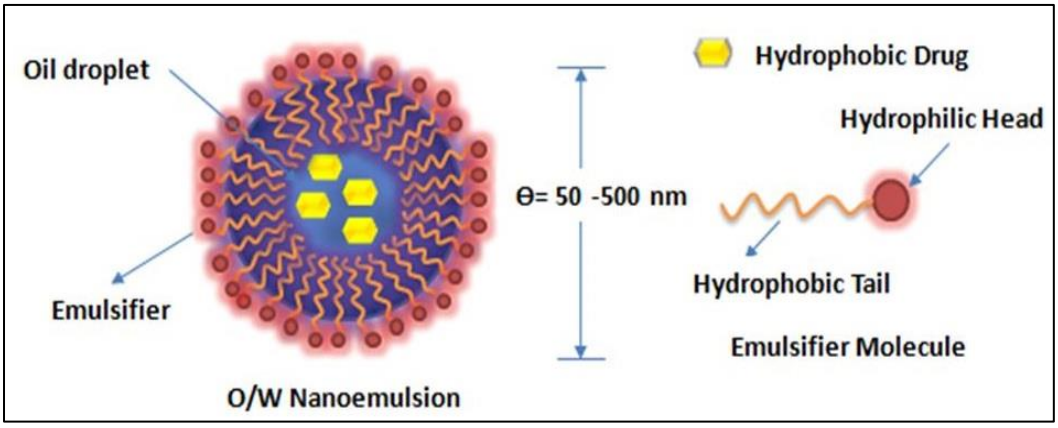

Figure 4. Schematic of oil-in-water nanoemulsion droplet [37].

2.3.1 Thymoquinone

Thymoquinone (TQ) is the most abundant bioactive constituent of the volatile oil of black seed (Nigella sativa [N. sativa]) (54%) and was first extracted by El-Dakhakhny [38]. This ingredient has been found to cause TQ-induced p53-independent apoptosis through caspase-8 activation in myeloblastic leukemia HL-60 cells [39]. Moreover, p53-dependent apoptosis has been shown in HCT-116 human colon cancer cells [40]. Nigella sativa extract in combination

with an oxidative stress agent has exhibited significant anticancer activity in MCF-7 breast cancer cells [41].

In a study by Ghosheh et al. [42], TQ was found to be not the only bioactive constituent of nigella sativa oil, but also other pharmacologically active constituents such as dithymoquinone, thymohydroquinone, and thymol were identified by high-performance liquid chromatography (HPLC). Other fractionated proteins of N. sativa ranging in their molecular mass from 10 to 94 kDa were purified by ion exchange chromatography and have also been found to be bioactive [43].

In 2010, the mechanism of action of TQ on androgen receptor (AR)-independent (C4-2B) and AR-naive (PC-3) prostate cancer cells was studied by Koka et al. [44] . Results suggested that TQ-induced cell death is primarily due to increased reactive oxygen species (ROS) generation and decreased glutathione (GSH) levels, and is independent of AR activity. In 2011, Arafa et al., studied the effect of TQ on cell signaling and survival pathways in resistant cancer cells. Study results indicated that TQ greatly inhibits doxorubicin (DOX)-resistant human breast cancer MCF-7/DOX cell proliferation [45].

2.3.2 Considerations in Formation of Nanoemulsions

2.3.2.1 Importance of Small Diameter

Reducing droplet sizes to the nanoscale leads to some very interesting physical properties, such as optical transparency and unusual elastic behavior [46]. Due to their small droplet size, nanoemulsions appear to be transparent or translucent. The main difference between a nanoemulsion and an emulsion is in the size of the water particles. When the size of the oil particles becomes small, the stability of the emulsion significantly improves. Due to Brownian

motion of the small micelles, the system is prevented from incurring any instability mechanisms such as flocculation, coalescence, creaming, and sedimentation.

Another importance of small diameter is that this would lead to an increase in surface area. In this sense, nanoemulsions also have a high interfacial area, a characteristic that influences the transport properties of drugs [47] and provides better absorption.

2.3.2.2 Importance of Oil Nature and Amount

The amount of oil has been seen to be important in terms of stability. A study by Peng et al. in 2010 [48] found that in the case of a 25 percentage of oil, the system exhibited coalescence and particle-size increase because the oil droplets became very close to each other even though more surfactant was used. For this reason, it is recommended that the oil percentage should not exceed 25%.

2.3.2.3 Importance of Surfactant Nature and Amount

Surfactants are the most important compound in nanoemulsion preparation due to the impact of their nature and concentration in systems. To enhance the kinetic stability of a system, surfactants are usually added to an oil-water mixture. A surfactant is an amphiphilic molecule that has a hydrophilic head group (polar region), which has a high affinity for water, and a lipophilic tail group (non-polar region), which has a high affinity for oil [49]. Surfactants are basically found in four forms: anionic, cationic, nonionic, and zwitterionic (or amphoteric). Their polar and non-polar characteristics affect system stability and droplet size. Figure 5 illustrates four different surfactant structures based on charge characteristics.

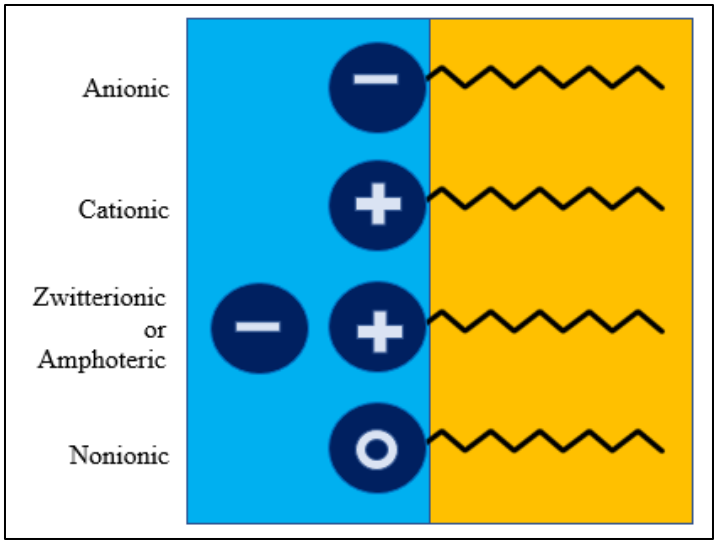

Figure 5. Four different surfactant structures based on charge characteristics.

Moreover, surfactant length is important, impacting nanoemulsion properties such as droplet size, surface tension [50], and stability. It was reported that for a non-ionic surfactant system, by adding a second surfactant with the same alkyl chain length, the Oswald ripening rate can be decreased [35]. Also, using a surfactant along with a co-surfactant can also improve the size and stability characteristics of nanoemulsions. Transient negative tension and a fluid interfacial film are rarely achieved with the use of a single surfactant, usually necessitating the addition of a co-surfactant. The presence of co-surfactants decreases the bending stress of the interface and allows an interfacial film with sufficient flexibility to assume different curvatures required to form a nanoemulsion over a wide range of compositions. Hence, the use of co-surfactant stabilizes the formed nanoemulsion [51].

Surfactants are crucial in preparing emulsions. While 10%–20% of surfactant is required to prepare microemulsions, this number is 5–10% for nanoemulsion preparation [52]. A certain amount of surfactant is needed for nanoemulsions depending on the desired final emulsion diameter and stability. There is also a limit for surfactant concentration because an excess amount of it might result in poor stability as the result of gel breakdown. This phenomenon is

referred to as depletion stabilization. Basically, at a high level of surfactant concentration, there would be layering around the micelles, and this results in a lower osmotic imbalance [53]. Figure 6 shows two types of polymeric stabilization of colloids—steric and depletion.

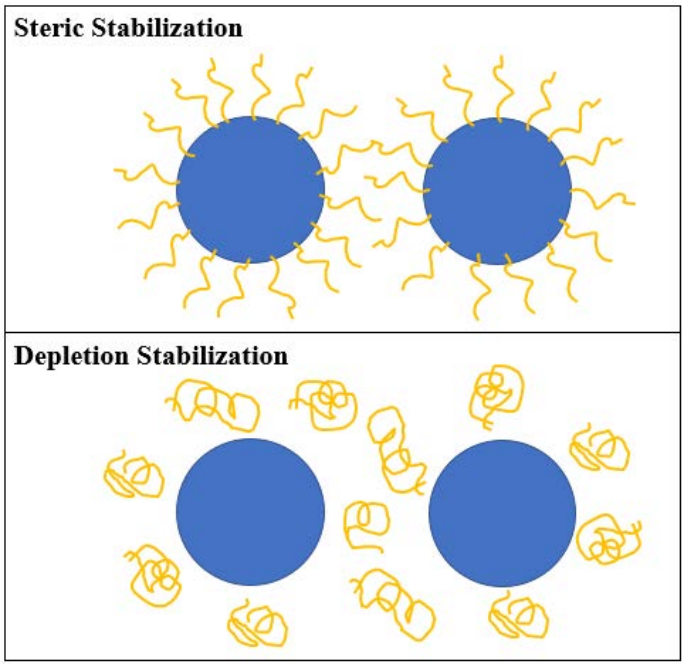

Figure 6. Two types of polymeric stabilization of colloids.

2.3.2.4 Importance of Viscosity and Relative Viscosity

The relative viscosity of the oil and water phases (ηd/ηc) is another term used to determine the stability level of nanoemulsion-based systems. When the relative viscosity is between 0.1 and 5, the system shows excellent droplet break-up properties, which makes it easier to obtain droplets that are smaller in diameter.

2.3.2.5 Hydrophilic-Lipophilic Balance

The hydrophilic-lipophilic balance is another crucial point in nanoemulsion preparation. It can be said that a surfactant with a high HLB value forms oil-in-water emulsions, while a low HLB value forms water-in-oil (W/O) emulsions. Basically, a surfactant and a co-surfactant having an HLB value > 0 are considered for making an O/W nanoemulsion [54]. The right blend

of low and high HLB surfactants leads to the formation of a stable nanoemulsion upon dilution with water [55]. Table 1 shows the HLB range and its applications.

TABLE 1

HLB RANGE AND ITS APPLICATIONS

HLB Range	Application
4–6	W/O Emulsions
7–9	Wetting
8–16	O/W Emulsions
3–15	Detergency
13–18	Solubilization

Various HLB values can be obtained by mixing surfactants. Depending on the volume fraction of surfactants, the final mixture will give the desired HLB value. The HLB value of a final mixture can be calculated as

$$\mathrm{HLB_{mix}} = \mathrm{x_A HLB_A} + (1 - \mathrm{X_A})\mathrm{HLB_B} \quad (1)$$

In 2014, Syed and Peh [56] studied the identification of phases in terms of using different oils, surfactants, co-surfactants, and water system. Their results indicated that using a co-surfactant improved the stability of the system. Moreover, the HLB of the surfactant and co-surfactant was seen to be very important in system stability. Results indicated that a non-ionic surfactant and co-surfactant mixture with a large HLB difference tends to form more stable emulsions because both high- and low-HLB surfactants dissolve better in the water and oil phases, respectively, and function well together.

2.3.2.6 Polydispersity Index

The polydispersity index (PDI) describes the variation in droplet size: the higher the PDI, the wider the droplet size distributed. Nanoemulsions with PDI values below 0.2 indicate the high fidelity of the system (low polydispersity), which may reflect the overall stability of this formulation and synthesis method. Polydispersity values near 1.0 are indicative of a polydispersive system [57]. Polydispersive systems can trigger droplet breakup via the Ostwald ripening mechanism, which might eventually cause separation.

2.3.2.7 Surfactant Toxicity

Surfactant selection plays a crucial role in the preparation of nanoemulsions. Their amount, ratio, and HLB values directly affect emulsion properties such as particle size stability and viscosity. As mentioned previously, there are four types of surfactants: anionic, cationic, nonionic, and zwitterionic (or amphoteric). Even though cationic surfactants have recently been of interest for targeted drug delivery because their positive charge can be utilized to target negatively charged cells, non-ionic surfactants are those that are most commonly used due to their least sensitivity against ions and pH. Also, they are usually preferred because they have good cutaneous tolerance and lower irritation potential and toxicity [58].

Components of nanoemulsion-based systems are associated with toxicity concerns. Large amounts of surfactants may cause gastrointestinal and skin irritation when administered orally and topically, respectively. Therefore, the proper selection of surfactants is essential. Rational use of the minimum concentration of surfactant in the formulation is advocated. Nonionic surfactants are relatively less toxic than their ionic counterparts and typically have a lower critical micelle concentration (CMC). Also, O/W nanoemulsion dosage forms for oral or

parenteral use based on nonionic surfactants are likely to offer *in vivo* stability [59]. Therefore, proper selection of surfactants is a crucial factor.

The distribution of small-molecular-weight surfactants in equilibrium is determined by the ratio of adsorption-to-desorption rates at the interface. Accordingly, a relatively large number of free surfactants are required to increase the number of surfactants bound to the surface of droplets, which is critically important in the stabilization of emulsions. However, it is desirable to avoid the use of a large number of free surfactants, particularly for biological applications, because of their deleterious activities, including disintegration of biological membranes, protein denaturation, lipid extraction, and cytotoxicity [60-62].

2.3.3 Theory of Nanoemulsion Formation

Key physical concepts behind the nanoemulsion formation will be explained here in detail. Although nanoemulsion formation seems to be a simple type of colloidal dispersion, an enormous knowledge of physics and chemistry is involved.

As simply known in daily life, liquids with different densities are immiscible, and no matter how much mechanical force is applied to mix them, eventually they separate. An emulsion is basically a combination of the continuous phase, dispersed phase, and surfactant. In addition to these three main constituents, several important concepts must be considered: surface tension, interfacial tension, dispersed phase volume fraction, shear rate, and Laplace pressure.

Since emulsification is the formation of miscible liquids from immiscible liquids, it is important to understand what make liquids immiscible or miscible. Interfacial tension (σ) is the difference between attractive interactions of the molecules of two liquids at their interface [63] and is responsible for their miscibility characteristics. In terms of low interfacial tension, one

liquid phase tends to disperse in the other continuous phase more easily, and this enables the formation of emulsions.

As is well known, everything in the universe tends to decrease its energy over time at thermodynamic equilibrium. This phenomenon is the reason behind the tendency of separation of phases in nanoemulsion systems. While dispersing one phase into another, due to the formation of droplets, the area of the interfacial surface will increase, in turn automatically increasing the energy at the interface. As a result, droplets tend to merge, decreasing the specific surface area so that energy will decrease. This eventually causes the separation of two phases. Surfactants come into play at this point by positioning themselves at the interface of these two phases and reducing the interfacial tension, which makes the dispersion of one phase into the other phase possible.

Laplace pressure in the mechanism of droplet formation in the continuous phase must also be understood. As is known, to form a nanoemulsion, an enormous amount of energy is required, which increases when the desired emulsion is smaller in size. The reason for this is the Laplace pressure of the droplets in the continuous phase. It is known that the pressure inside a nanoemulsion droplet is always greater than the surrounding phase pressure due to the additional contribution from the Laplace pressure resulting from the curvature effect. The Laplace pressure can become very large as the nanoemulsion becomes very small [64]. When shear force that is applied to the system exceeds the Laplace pressure of the droplets, droplet breakup occurs, and smaller-size droplets form.

In nanoemulsions, two types of Laplace pressure must be mentioned. One is the Laplace pressure of the spherical droplets, which is observed when the dispersed phase holds a small volume fraction, and can be calculated as

$$P = 2\gamma/r \tag{2}$$

where γ is the interfacial energy, and r is the radius of the droplet.

The second type of Laplace pressure applies to non-spherical droplets, calculated as

$$P = \gamma \left({}^{1}/_{r_1} + {}^{1}/_{r_2} \right) \quad (3)$$

where γ is the interfacial energy, and r_1 and r_2 are the radii of the curvature of the droplets. As can be understood from equation (3), when the droplet size is larger, the Laplace pressure decreases, and when the droplet size is smaller, the Laplace pressure increases. As a result of the higher Laplace pressure generated inside the droplets, the shear energy required to break the droplets into smaller-size nanoemulsions increases. This explains the reason behind the great energy need to fabricate nanoemulsions with a diameter below 100 nm. In addition to the radii of the droplets, interfacial tension has an impact on Laplace pressure. As can be seen in equations (2) and (3), at a higher level of interfacial tension, the Laplace pressure increases, and this value decreases with a reduction in the interfacial tension value. This shows the importance of surfactants in the making of nanoemulsions. They basically lower the interfacial tension, which causes the Laplace pressure to drop, so that it is possible to obtain a smaller diameter with applied shear stress.

2.3.4 Stability of Nanoemulsions

Two of the main challenges in nanoemulsion preparation are the formation of droplets below 80 nm in size and maintaining this diameter, which indicates the stability of the system. Emulsion stabilization is controlled by multiple molecular interactions, including electrostatic interactions, steric hindrance, the Gibbs-Marangoni effect, and mechanical forces [65-67]. Also, van der Waals forces also affect nanoemulsion stability.

Van der Waals interactions can be classified into three groups: dipole-dipole interaction (also known as Keesom), dipole-induced dipole (Debye), and London interaction. The most

important of these is the London interaction, which plays an significant role in the stability behavior of nanoemulsions. London forces occur from temporary dipoles created from electrons rotating around the nucleus. The relationship of London forces and emulsions was revealed by Hamaker [68], who posited that van der Waals attraction between droplets is related to the radii of the droplets and the distance between them. The equation to calculate van der Waals energy is expressed as

$$G_A = -AR/12h \tag{4}$$

where A is the Hamaker constant, R is the droplet radii, and h is the distance between two droplets.

As can be understood from equation (4), the smaller h causes an increment in van der Waals energy, G_A, which in turn causes the flocculation of droplets. To overcome this phenomenon, a repulsion force between the droplets must be created. Two types of repulsive forces are steric hindrance and electrostatic repulsion.

Electrostatic repulsion applies to systems using an ionic surfactant. Due to the charged head groups of surfactants, they attract counter ions which create a double layer. The double-layer extension depends on electrolyte concentration and valency (the lower the electrolyte concentration and the lower the valency, the more extended the double layer) [69], that is, the smaller the thickness of the double layer. When two charged droplets with a double layer come close to each other, their double layers overlap, and h, which is the separation distance, becomes smaller than twice the double-layer thickness. Thus, repulsion occurs, and separation of the droplets results. The repulsive interaction can be given by the following expression:

$$G_{el} = 2\pi R\varepsilon_r\varepsilon_o\psi_o^2 \ln(1 + \exp(-\kappa h)) \tag{5}$$

where R is the radii of the droplets, ε_r is the relative permittivity, ε_o is the permittivity of free space, ψ_o is the surface potential, κ represents the Debye-Huckel parameter, and $1/\kappa$ is the thickness of the double layer, and is equal to

$$\left(1/\kappa\right) = \left(\varepsilon_r \varepsilon_o kT \Big/ 2n_o z_i^2 e^2\right) \tag{6}$$

where k is the Boltzmann constant, T is the absolute temperature, n_o is the number of ions per unit volume of each type present in the bulk solution, Z_i is the valency of ions, and e is the electronic charge.

As mentioned above, with a higher electrolyte concentration and greater valency, the extension of the double layer drops, which causes a decrement in the repulsion force of the droplets. Under the two conditions mentioned above, van der Waals attractions and electrostatic repulsion, the total energy of the interaction is given as

$$G_T = G_{el} + G_A \tag{7}$$

and this interaction is schematically shown in Figure 7.

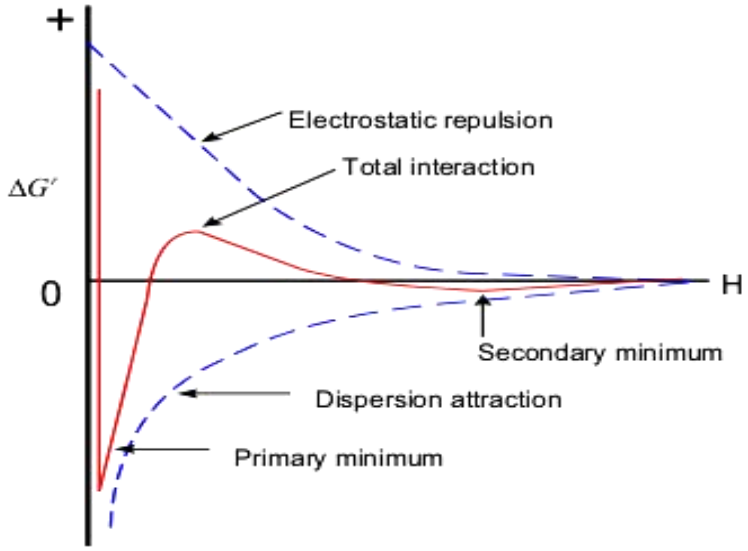

Figure 7. Electrostatic stability of dispersions based on DLVO theory [71].

According to the Derjaguin, Landau, Verwey, and Overbeek (DLVO) theory, when the repulsive maximum of the droplet-droplet interaction potential is low, droplets come close to each other and fall into the primary minimum, i.e., the irreversibly flocculated state. During this process, when the droplets come into "primary" contact, they tend to coalesce [70]. This is experienced in the case of when h is very low and $G_A >> G_{el}$. At a large h, attraction prevails, resulting in a shallow minimum (G_{sec}) of the order of a few kilotesla units [69]. Finally, at intermediate h levels, the $G_{el} > G_A$ maximum energy barrier is reached. Gmax is dependent on zeta potential as well as electrolyte concentration and valency. In this situation, the repulsive force is greater than the attractive force, resulting in a net repulsive force. Thus, droplets are prevented from flocculating [69].

Another phenomenon causing repulsion between droplets is steric hindrance, which is experienced when non-ionic surfactants or polymers are used in a nanoemulsion system [69]. In this case, hydrophilic chains of surfactants or polymers create a repulsion force based on two main effects [72], which are caused from the unfavorable mixing of chains and elastic interactions. Basically, in the case of unfavorable mixing, the Flory Hugging interaction parameter is acting, and according to its value, the G_{mix} (osmotic free energy) can predict whether it is attractive or repulsive. When the Flory-Huggins interaction parameter $\chi < 0.5$, the G_{mix} will be positive, and the interaction becomes repulsive, and in the opposite scenario, the interaction will be attractive ($\chi > 0.5$):

$$\frac{G_{mix}}{kT} = \left(\frac{4\pi}{V_1}\right) \varphi_2^2 N_{av} \left(\frac{1}{2} - \chi\right) (\delta - \frac{h}{2})^2 \left(3R + 2\delta + \frac{h}{2}\right) \quad (8)$$

where V_1 is the molar volume of the solvent, N_{av} is the Avogadro number, φ_2 is the volume fraction of the polymer chain, δ is the chain thickness, and χ is the Flory-Huggins interaction

parameter. Also, elastic interactions result from the loss in the configurational entropy of the chains. Entropy loss causes G_{el} to be positive and repulsion occurs:

$$G_T = G_{mix} + G_{el} + G_A \quad (9)$$

One of the mechanisms in emulsion stabilization is using surfactants to stabilize newly formed droplets against recoalescence, which can be achieved via the Gibbs-Marangoni effect [73]. According to this effect, when two droplets approach each other, they acquire more surfactant at their interfaces. However, this adsorption of surfactant is uneven, because the amount of surfactant available is lower in the region of the closest approach than in the bulk. This uneven adsorption creates a surface tension gradient that pulls more surfactant to the depleted region. The accompanying influx of water drives the two droplets apart, stabilizing them against recoalescence. The power of this effect is a function of both the surfactant concentration and the Gibbs elasticity of the interface [73-75].

Factors that greatly influence formation and stabilization are the nature of the oil phase, relative viscosity, surfactant length, and surfactant concentration. In addition, controlling the order of adding the components and applying the way shear stress can be added are also influential.

Nanoemulsions are known to be kinetically stable and thermodynamically non-stable, which means they will eventually separate into the phases from which they are formed. This destabilization (breakdown) process can be in different forms, such as Oswald ripening, coalescence, flocculation, creaming, and sedimentation. Among these, Oswald ripening is the primary mechanism in destabilization, followed by coalescence.

To begin, in flocculation, due to the attractive interactions, droplets move closer to each other and as a single entity; however, the size of droplets that attach to each other does not

change. As explained in detail above, the time flocculation occurs can be predicted via the DLVO theory. Flocculation is the result of van der Waals attraction, which is universal for all dispersal systems. Flocculation occurs when there is not sufficient repulsion to keep the droplets apart to distances where the van der Waals attraction is weak. Flocculation may be "strong" or "weak," depending on the magnitude of the attractive energy involved [69].

In contrast to flocculation, during coalescence, the droplets merge into each other and form a larger droplet. The complete separation of the emulsion into two distinct liquid phases is the limiting case for coalescence. Here, the driving force is the surface or film fluctuations, which cause a close approach of the droplets, whereby the van der Waals forces are strong so that their separation is prevented [69]. Explaining coalescence in detail begins by explaining the role of surfactants, one of the roles of which is to provide a repulsion force between droplets. In case this repulsion force is not high enough, droplets rupture and fuse together, which is called coalescence, and this is one of the primary mechanisms causing destabilization in systems. Coalescence becomes a potential instability mechanism when the critical disjoining pressure is low [76]. For many surfactants, this critical disjoining pressure can be quite large relative to thermal fluctuations and external mechanical perturbations, thereby providing a mechanism for long-term persistence of interfaces without coalescence [76]. By choosing a surfactant that provides a strong repulsion between droplet interfaces, coarsening through coalescence can also be effectively eliminated even at large φ, provided that ηd is not exceeded [76].

When creaming or sedimentation is the case, three forces should be mentioned: buoyancy forces, gravitational forces, and Brownian motion, which is driven by thermal fluctuations. Basically, very small droplets in a colloidal solution stay separated because of Brownian motion, which is created as the result of thermal fluctuations. To explain in more detail, Brownian

motion is observed in very small molecules or droplets in a colloidal suspension, such as a nanoemulsion system. Due to the very small size of the colloids, the effect of molecules hitting their surfaces does not cancel out, and colloids are continually hit by the surrounding molecules, thereby always undergoing a certain force, making a zigzag motion that prevents them from undergoing creaming or sedimentation. However, if the buoyancy forces overcome the Brownian motion and gravitational forces in a system, then oil droplets rise, and separation occurs. This phenomenon is seen when the buoyant force dominates over the thermal fluctuations, and this phenomenon occurs when the particle or droplet size is larger. The reason for this is explained above: for larger particles or droplets, forces applied on them by surrounding molecules cancel each other. Under this situation, gravitational forces, buoyant forces, and viscous drag forces come into action. This can be explained using the Peclet number, which is the ratio of viscous stress to thermal stress:

$$Pe \sim \mu_C U d^2 / k_B T \tag{10}$$

where μ_c is the viscosity of the continuous medium, U is the velocity of the rising droplet (terminal velocity), and k_B represents the Boltzmann constant [77]. The velocity of a rising droplet, U, can be expressed by

$$U = 2a^2 \Delta\rho g / 9\mu_c \tag{11}$$

where a is the radius of droplet, $\Delta\rho$ is the density difference of the dispersed and continuous phases, g is the gravitational constant, and μ_c is the viscosity of the continuous medium.

As mentioned previously, the nature of the components is very crucial in the stability of a nanoemulsion. The nature of the components refers to solubility behavior and viscosity of the oil. When aiming at good stability, it should be noted that the dispersed phase should have good insolubility in the continuous phase. Viscosity of the oil phase and insolubility have a direct

relationship. The physical properties of oil, such as fatty acid length, is crucial in stable nanoemulsion preparation because it is directly related to viscosity of the oil. Long-chain triglycerides are known to have higher viscosity compared to medium-chain and short-chain triglycerides. Due to the long chain length and higher viscosity, the oil phase tends not to mix with water phase, and therefore good stability can be obtained. In the case of high solubility, micelles with high Laplace pressure will merge into larger micelles, which are known to have a lower Laplace pressure. This will cause system instability, which is known as Oswald ripening. This process is driven by the Kelvin effect where the small emulsion droplets have higher local oil solubility than the larger droplets because of the difference in Laplace pressures driven by the curvature effect. The rate of Ostwald ripening is largely dictated by the solubility of the oil in the continuous phase C(∞) as described by the Lifshitz-Slesov-Wagner (LSW) theory [78, 79]:

$$d^3 = {d_o}^3 + (64\sigma C_\infty \upsilon^3 D/9RT)t \quad (12)$$

where d_o is the initial average diameter, σ is the interfacial tension, C_∞ is the solubility of the dispersed phase in the continuous phase, υ is the molar volume of the dispersed phase, D is the diffusivity of the dispersed phase, R is the ideal gas constant, and T is the temperature.

2.3.5 Advantages of Nanoemulsions

Nanoemulsions in drug delivery have numerous advantages compared to traditional drug-carrying agents, the major of which are increased drug loading, enhanced drug solubility and bioavailability, reduced patient variability, controlled drug release, and protection from enzymatic degradation [80]. Because of the oil phase trapped in the continuous water phase, the solubility of poor water-soluble drugs increases. Due to better dissolution, the drug release is controlled better and not released as fast, which improves the bioviability of drugs and possible toxic effects resulting from burst release. Other advantages of nanoemulsions are as follows:

- Ease of fabrication in various ways, including both high-energy and low-energy methods.
- Long period of circulation in the bloodstream, and tumor targeting achieved by surface modification with hydrophilic polymer chains and active targeting ligands [81]. As known, a smaller-diameter emulsion would lead to an increase in surface area, meaning that nanoemulsions have a high interfacial area, a characteristic that would influence the transport properties and better absorption of drugs [82, 83].
- High loading capacity.
- Less affected by gravitational and buoyancy forces, and a dominance of Brownian motion, which provides good shelf stability by keeping the micelles always suspended. The small droplets also prevent their coalescence due to droplet elasticity, and weak flocculation is prevented, thus enabling the system to remain dispersed with no separation [46].
- Suitable for efficient delivery and rapid penetration of active ingredients through the skin, due to the large surface area of the emulsion system, and their non-toxic and non-irritant nature, which means that they can be easily applied to skin and mucous membranes.
- Site-specific delivery of drugs, the capacity to dissolve large quantities of hydrophobics, and the ability to protect drugs from degradation with long-term stability, thus making them an ideal drug delivery system. The frequency and dosage of injections can be reduced throughout the therapy because the release pattern of drugs takes place in a sustained and controlled mode over long periods of time [46].
- Product delivery through various routes—topical, oral, and intravenous.
- Increase in the rate of absorption, increase bioavailability, and eliminate variability in absorption.

- Possibility of controlled drug release and drug targeting, and the incorporation of a great variety of therapeutic active ingredients.
- Better uptake of oil-soluble supplements in cell cultures, improvement in growth and vitality of cultured cells, and toxicity studies of oil-soluble drugs in cell cultures.
- Due to small droplet size, resistance to physical destabilization caused by gravitational separation, flocculation, and/or coalescence. Also, avoidance of the creaming process because the droplet's Brownian motion is enough to overcome the gravitational separation force.

2.3.6 Disadvantages of Nanoemulsions

Nanoemulsions have attracted interest in recent years for the following reasons [84]:

- Difficult stability of nanosystems because of their large surface area, which naturally has higher energy due to more surface atom concentration compared to the whole volume.
- Preparation requiring, in many cases, special application techniques, such as the use of high-pressure homogenizers as well as ultrasonic equipment (such as the microfluidizer), which became available only in recent years.
- Perception in the personal care and cosmetic industry that nanoemulsions are expensive to produce because of the expensive equipment that is required as well as the use of high concentrations of emulsifiers.
- Lack of understanding of the mechanism of production of submicron droplets and the role of surfactants and co-surfactants.
- Lack of understanding of interfacial physics.
- Lack of demonstration of the benefits that can be obtained from using nanoemulsions when compared with classical macroemulsion systems.

- Lack of understanding of the interfacial chemistry involved in their production.
- Limited solubility capacity for high-melting substances.
- Sensitivity and environmental factors such as pH and temperature, which greatly impact their stability.

2.4 Hydrogels

Over the past two decades, controlled drug delivery has attracted considerable attention as an alternative to conventional drug delivery routes such as oral administration and injections. The fact that drugs are not directed to the concerned area using conventional techniques creates some problems. First, with techniques of oral administration and injection, targeting therapeutic agents to a particular area in the body is too low due to pharmacokinetics and the clearance rate. Also, drugs are released over a short period of time, which increases the toxic side effects [85]. However, by using polymers, targeted and controlled drug release can be achieved. By targeting the drug directly to the concerned area, toxic effects can be reduced, and the total amount of the drug reaching the cancer area can be increased. Also, loading drugs into polymer carriers for delivery induces a controllable release mechanism.

Hydrogels have been used extensively in the development of smart drug delivery systems. A hydrogel is a network of hydrophilic polymers that can swell and hold a large amount of water while maintaining their structure. A three-dimensional network is generated by crosslinking polymer chains, which can be provided by covalent bonds, hydrogen bonding, van der Waals interactions, or physical entanglements [86, 87]. Smart hydrogels can be used in various applications, such as artificial muscles, chemical valves, immobilization of enzymes and cells, and dilute solutions in bioseparation [88]. Figure 8 shows the classification of hydrogels.

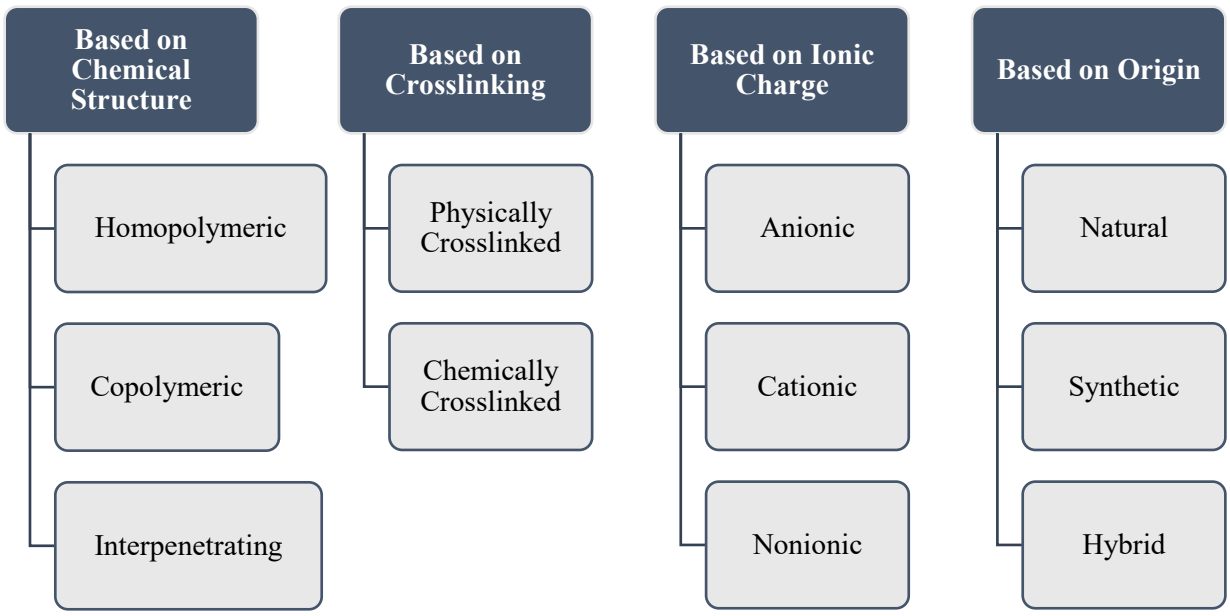

Figure 8. Classification of hydrogels [89].

2.4.1 Drug Delivery

Targeted drug delivery is a way of delivering a drug to a certain area rather than releasing the drug into the entire body. With targeted drug delivery, only a certain part of the body is affected by the drug so that side effects are reduced, and the bioviability of the cells is increased.

Hydrogels are advantageous materials in drug delivery due to some of their characteristics. First, their nature is similar to biological tissue. The hydrophilic nature and three-dimensional polymer network allows them to embed a large amount of biological fluid easily into their structure [90]. Also, their biocompatibility and least mechanical irritation to tissues are other advantages in their use as biomaterial. Moreover, due to the lowest interfacial stress between the hydrogel surface and surrounding fluid, protein adsorption and cell adhesion onto gel can be minimized [91]. Another important characteristic of hydrogels is that they can be produced in a variety of shapes, such as thin films, rods, disks, and nanoparticles. The type of hydrogel fabrication is dependent on the intended application and the application site. Also, they can be washed easily in order to remove unreacted initiators, monomers, etc. [92]. In drug

delivery techniques, using hydrogel is in a researcher's best interest because their environmentally sensitive behavior makes them attractive in cancer treatment. They can be directed to the desired area, and the drug to which they are attached can be released by means of the response of the hydrogel to that environment. Environmentally sensitive hydrogels can be classified as thermosensitive, photosensitive, pH sensitive, enzyme sensitive, and electric sensitive. Moreover, the water absorption property of hydrogels makes them a good candidate for drug loading and releasing.

2.4.2 Stimulus Sensitivity

Environmentally sensitive hydrogels are the best candidates for generating self-regulated drug delivery systems because they can defend the drug from adverse environments, e.g., the presence of enzymes and acidity (low pH) in the stomach. Hydrogels can also control drug-release behavior by altering the gel structure in response to environmental stimuli [88]. Some environmental variables, such as low pH and elevated temperatures, are found in the body. These characteristic pH-sensitive and temperature-sensitive hydrogels can be used for targeted controlled drug delivery systems. Also, it is possible to use hydrogels that are responsive to specific molecules, such as glucose or antigens, as biosensors and drug delivery systems. Additionally, light-sensitive, pressure-responsive, and electrosensitive hydrogels have the potential to be used in drug delivery and bioseparation [88]. Basically, a hydrogel's response might be physical, chemical, or biochemical, depending on the type of stimuli. Physically sensitive hydrogels can be classified as temperature sensitive, light sensitive, magnetic field sensitive, pressure responsive, and electric field responsive. Chemically sensitive hydrogels can be subdivided into two types: pH-responsive and glucose-sensitive. Biochemically responsive

hydrogels can be divided into three subgroups: antigen-, enzyme-, and ligand-responsive hydrogels. Table 2 provides a schematic classification of smart hydrogels.

Among the stimuli sensitivity mechanisms of a hydrogel, the most important is phase separation, which has both hydrophobic and hydrophilic chemical structures, such as poly(N-isopropylacrylamide) (poly-NIPAAm). Another important mechanism is the volume change of a hydrogel's polyelectrolytes due to the conformation change by ionic interaction between the polymeric ion and the counter ion in the solvent [93, 94].

TABLE 2

CLASSIFICATION OF STIMULI-SENSITIVE HYDROGELS [89]

<table>
<tr><th>Physically Responsive Hydrogels</th><th>Chemically Responsive Hydrogels</th></tr>
<tr><td>Temperature Sensitive</td><td>pH Sensitive</td></tr>
<tr><td>Light Sensitive</td><td rowspan="3">Molecular Species Sensitive
Glucose Sensitive
Protein Sensitive
Enzyme Sensitive</td></tr>
<tr><td>Magnetic Field Sensitive</td></tr>
<tr><td>Pressure Sensitive</td></tr>
<tr><td>Electric Field Sensitive</td><td>Ionic Strength</td></tr>
<tr><td>Ultrasound Sensitive</td><td>Solvent Composition</td></tr>
</table>

Response time is one of the most important properties to be considered in the production of hydrogels because slow response time is the most significant weakness of all external stimuli-sensitive hydrogels. Thus, fast-acting hydrogels are desired, and the easiest way to accomplish this goal is to generate thinner and smaller hydrogels. This usually makes hydrogel systems fragile and fail to meet the mechanical strength values desired in many applications [88]. Therefore, it should be noted that in addition to having good release and response characteristics, the mechanical properties of a hydrogel should be considered for developing a suitable structure in drug delivery applications.

2.4.2.1 Thermosensitivity

Thermosensitive hydrogels are those that provide a response to changes in temperature. While they are in a sol phase before an *in vivo* injection, they turn into gel with the increased temperature after injection. This characteristic induces an easy injection of drug-loaded hydrogel into the body.

Most thermosensitive polymers contain some hydrophobic groups such as propyl, ethyl, and methyl groups. Basically, they have two important parameters: a lower critical solution temperature (LCST) and an upper critical solution temperature (UCST). According to the phase response of a temperature change, polymers are subdivided into negatively thermosensitive, positively thermosensitive, and thermoreversible types [95]. Negatively sensitive systems are also known as inverse temperature-dependent systems. Generally, the water solubility of hydrogels is directly proportional to increasing temperature. For a negatively sensitive system, this relation is inversely proportional, meaning that with increasing temperature, the water solubility drops. When the temperature reaches the LCST, the hydrogel starts shrinking. Because hydrophobic interaction becomes more dominant above the LCST, hydrogen bonding will lose its strength, which is dominant below the LCST. While hydrogel becomes insoluble above the LCST, it becomes soluble under the LCST. In contrast, as positive temperature-sensitive systems swell at high temperatures, they shrink at low temperatures. In contrast to UCST systems, an LCST system is mostly preferred for drug delivery technologies because UCST systems require higher temperatures, which is unfavorable for heat-labile drugs and biomolecules [96].

Thermosensitive hydrogels have several advantages and disadvantages. The first major advantage is their avoidance of toxic organic solvents. They also have the ability to carry both hydrophilic and lipophilic drugs. In addition, site-specific delivery, reduced side effects, and

sustained release properties are important advantages. Some drawbacks are high burst release, low biocompatibility, low mechanical strength, and gradual lowering of the system's pH due to acidic degradation [97, 98]. Figure 9 shows the sol-gel transition of thermosensitive hydrogels in response to temperature change [89].

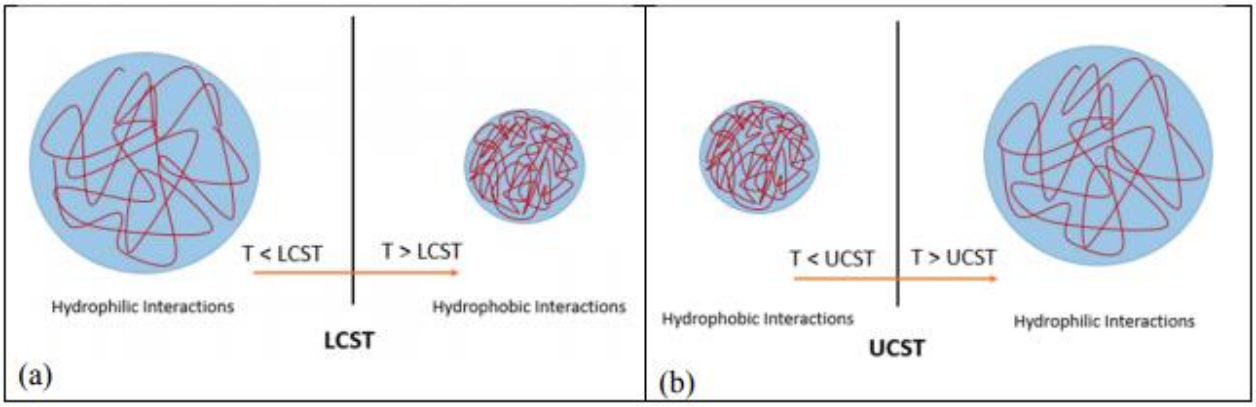

Figure 9. Sol-gel transition of thermosensitive hydrogels in response to temperature change: (a) lower critical solution temperature, (b) upper critical solution temperature [89].

2.4.2.2 pH Sensitivity

The pH is another stimulus to which some hydrogels show sensitivity, and this property can be used in drug delivery applications since the pH value varies in different parts of the body. Hydrogels that are pH-sensitive consist of weak acidic or basic groups and are also in the polyelectrolyte complex (PEC) group. While cationic hydrogels shrink at high pH values, anionic hydrogels swell in a high pH environment. As the environmental pH changes, the pendant acidic group undergoes ionization at a specific pH known as the pKa [96]. The major advantage in utilizing this stimulus is that it is suitable for thermolabile drugs. On the other hand, several disadvantages are lack of toxicity data and low mechanical strength [96]. Figure 10 displays the pH responsive swelling of anionic and cationic hydrogels.

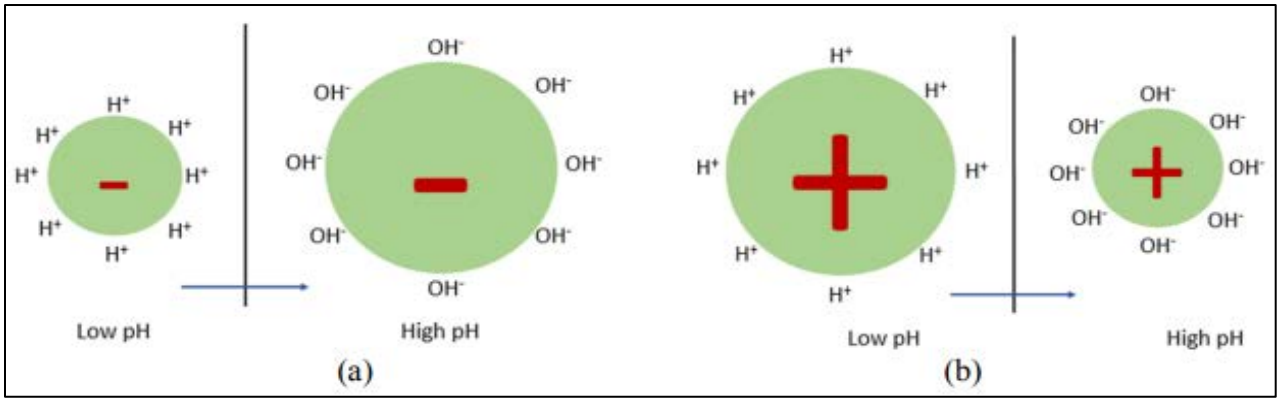

Figure 10. pH responsive swelling: (a) anionic hydrogels, (b) cationic hydrogels.

2.5 Swelling Kinetics

The swelling phenomenon shows itself in applications in various fields such as biomedical, pharmaceutical, environmental, and agricultural engineering. This leads to the need for a better understanding of the mechanisms of water diffusion in swelling polymeric systems. Studies on the swelling kinetics of polymeric structures have received a great deal of attention. Controlled drug delivery is another field where analysis of the swelling properties holds great importance because it is correlated with the diffusion rates of both the penetrant into the matrix and the drug throughout the gel layer of the matrix [90, 99, 100]. Moreover, structural changes resulting from the degree of crosslinking and the drug-release behavior of different materials can be investigated by the observing the swelling behavior of hydrogels [101].

Water diffusion into hydrogels can be studied by the Fickian diffusion law given in equation (13). This equation can only be applied for the onset of swelling (first 60% of swelling). For example, a 60% increase in the mass of hydrogel ($M_t/M_\infty \leq 0.6$; $\log(M_t/M_\infty) \leq -0.22$) [102].

$$F = M_t/M_\infty = kt^n \tag{13}$$

where M_t is the amount of solvent that diffuses into the sample at any time t, M_∞ is the amount of solvent that diffuses into the hydrogel at infinite time (at equilibrium state), k is the diffusion constant correlated to the network structure, and n is the exponent characteristic representing the

type of diffusion taking place in the hydrogel. According to n, the swelling kinetics can be classified under three main groups, as provided in Table 3. Once the n is calculated, it suggests the water-uptake characteristics of the hydrogel, depending on the values indicated in Table 3. In the case of n = 0.5, the swelling mechanism is called Fickian diffusion (Case I), and transport is diffusion controlled, that is, the rate of diffusion is much smaller than the rate of relaxation. If n is between 0.5 and 1, then this mechanism is called non-Fickian (anomalous) diffusion, and it is both diffusion and swelling controlled, meaning that the rate of diffusion and the rate of relaxation are comparable. Finally, if n is equal to 1, then the mechanism is called Case II transport, whereby the water-transport mechanism is totally swelling controlled, and the release rate is independent of time. The rate of diffusion is much faster than the rate of relaxation [103, 104].

TABLE 3

WATER TRANSPORT MECHANISMS AND DIFFUSIONAL EXPONENTS (n) FOR DIFFERENT HYDROGEL SHAPES

Diffusional Exponent (n)			**Mechanism**	**Time Dependence**
Film	**Cylinder**	**Sphere**		
0.5	0.45	0.43	Fickian Diffusion (Case I)	$t^{1/2}$
$0.5 < n < 1$	$0.45 < n < 0.89$	$0.43 < n < 0.85$	Non-Fickian (Anomalous) Diffusion	t^{n-1}
1	0.89	0.85	Case II Transport	Time Independent

2.6 Drug-Release Kinetics

When a new solid drug delivery system is developed, it is highly important to investigate the drug release or dissolution of the new material, which will make the quantitative analysis of the release phenomena easier. The mathematical modeling enables optimization of the design of a therapeutic device to yield information on the efficacy of various release models [105]. Some

of the mathematical models and their corresponding equations that are used to determine the kinetics of drug release from drug delivery systems are listed in Table 4.

TABLE 4

MATHEMATICAL MODELS AND EQUATIONS FOR DRUG-RELEASE KINETICS

Model	**Equation**
Zero-Order Model	$M_t/M_\infty = kt + C$
First-Order Model	$\ln(1 - M_t/M_\infty) = kt + C$
Higuchi Model	$M_t/M_\infty = kt^{1/2} + C$
Korsmeyer-Peppas Model	$\ln(M_t/M_\infty) = k\ln t + C$
Hixson-Crowell Model	$(1 - M_t/M\infty)^{1/3} = kt + C$
Baker-Lonsdale Model	$3/2(1-(1 - M_t/M_\infty)^{2/3})- M_t/M_\infty = kt$

2.7 Hyperthermia Study

Under very abnormal circumstances such as fever, heatstroke, or malaria does the body temperature increase dramatically to as high as 39℃ or above. These types of conditions can affect the normal physiological, biochemical, and chemical processes of body cells, which are caused by low heat dissipation rate due to limited blood perfusion. Hyperthermia is the intended exposure of cancer cells and tissue to higher temperatures in a range of 40℃ to 46℃ [24, 106-108], which is sufficient to activate responsive biochemical and physiological changes as well as possible complete eradication. In this temperature range, tumor cells are generally found to be more vulnerable to heat compared to normal cells because they are hypoxic (poorly oxygenated) while normal cells are euoxic (well oxygenated) [109, 110]. Hyperthermia temperature ranges are supported by the established observation [111] that the lowest temperature of the first protein denaturation is detectable in the range of 40℃ to 45℃ for mammalian cells, and cell membrane

lipids transitionally melt before any protein structural alteration can occur. Yang et al. [112] indicated that the elevation of temperature to 40℃ to 44℃ could improve tumor control.

One hyperthermia study showed that the power of heating depends on the intrinsic and extrinsic properties such as size, composition, properties of nanoparticles, frequency and amplitude of the electromagnetic waves based on output current, etc. Furthermore, the actual increase in temperature at a targeted site depends on magnetic losses, local blood circulation, thermal conductivity, and heat capacity of the surrounding medium, which can diffuse the heat. Figure 11 demonstrates the principles of this magnetic hyperthermia study.

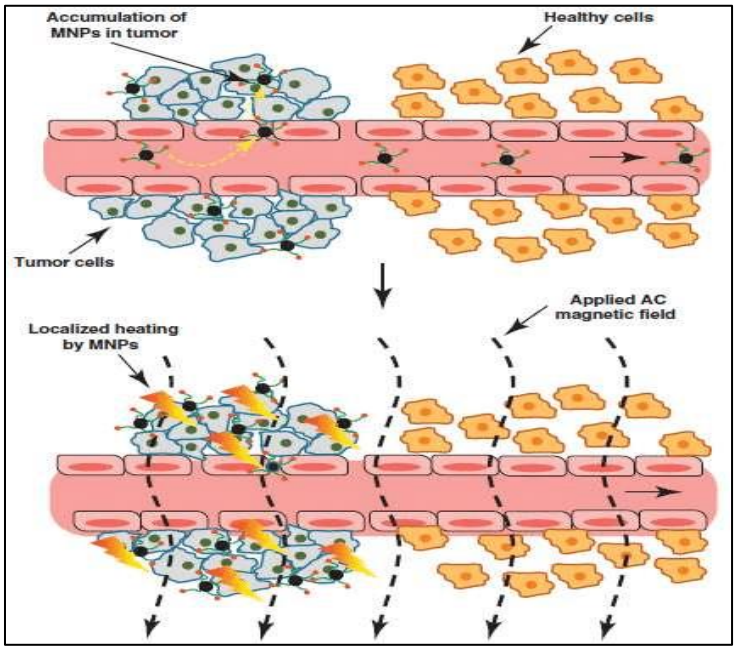

Figure 11. Illustration demonstrating principles of magnetic hyperthermia study [113].

It has been observed that when cells are introduced to magnetic nanoparticles, they uptake them by a process called endocytosis. Furthermore, cancerous tissue is known to absorb a much larger amount of magnetic nanoparticles than normal tissue due to its leaky vasculature [23]. One of the advantageous of using MNPs is the use of localized magnetic field gradients to direct the particles to a selected site, thus holding them there until the therapy is completed. Later, these particles can be removed. In addition, magnetic nanoparticles may easily be tagged

to biomolecules such as folate or antibodies and can be targeted to specific tissues. In addition, magnetic nanoparticles, such as iron oxides, can be developed easily into multifunctional agents, thus making it possible to take advantage of their diagnostic imaging capabilities and magnetic properties in targeting drugs [114, 115]. Drugs can be immobilized on the surface of magnetic nanoparticles and can be targeted to a specific exposed tumor region with the help of a magnetic field.

Compared to traditional cancer therapies such as chemotherapy and radiotherapy, hyperthermia in general and hyperthermia using magnetic nanoparticles can reduce the severe side effects caused to normal tissue [116-119]. Achieving controlled and uniform heating is the limitation of existing heating methods, such as the capacitive or inductive coupling of radiofrequency fields, microwave, ultrasound, and heat administered by external contacts. It is suggested that regulated and uniform heating can be achieved by hyperthermia treatment [120], whereby heat can be applied locally with no systemic effects, and hence, the side effects become further reduced. In view of this discussion, it is apparent that there are distinct advantages of hyperthermia treatment over other hyperthermia processes.

There are various requirements for magnetic nanoparticles in order to use them in hyperthermia treatment applications:

- Nature and size of magnetic nanoparticles
- Uniform and controlled heating
- Biocompatibility
- Site specificity
- Colloidal stability
- High specific loss power (SLP)

- Applied frequency and magnetic field strength

2.7.1 Limitations of Hyperthermia

One of the greatest challenges in the use of hyperthermia in the treatment of breast cancer and other types of diseases has been how to achieve an above-normal temperature and keep it within a relatively cancer-cell catastrophic range without severely damaging neighboring healthy tissue. Therefore, this key limitation has resulted in a limited use of the treatment method. Based on a review [24], the vanishing of the hyperthermia application in the treatment of cancer was due to lack of a hyperthermia technique used at that time. The method remained at the experimental level and evolved with advancements in science and technological innovations of more-accurate application techniques, and continued to improve with nanoscience and nanotechnologies that have supported the evolution of superior biomaterials and fabrication techniques.

The side effects experienced during hyperthermia is another limitation of hyperthermia. Some of these side effects are pain at the target site, bleeding, blood clots, infection, swelling, burns, blistering, and damage to skin, nerves, and muscles around the treated area [121].

Based on these limitations, the importance of improved heat-delivery techniques and temperature control at the targeted area in hyperthermia treatment should not be underestimated. At this point, understanding heat generation and transfer at cancer cells is indispensable to the development of efficient devices and controls. Modeling the effects of heating temperature and time contribute to better control of hyperthermia parameters, thus ensuring a safe treatment condition.

2.7.2 Magnetic Nanoparticles for Hyperthermia Study

Magnetic nanoparticles have been extensively used as a promising tool for therapeutics, particularly for cancer. In this application, the magnetic energy of magnetic nanoparticles is transformed to thermal energy in the presence of an alternating current (AC) magnetic field. With this technique, heat may be applied to tumor tissues with no systemic side effects compared to chemotherapy and radiotherapy. The possibility of treating cancer by artificially induced hyperthermia has led to the development of many different devices designed to heat malignant cells while sparing surrounding healthy tissue [122]. In 1957, the first experimental investigations in the eradication of cancer cells by the heating of magnetic particles in an alternating magnetic field (AMF) were conducted by Gilchrist et al. [123]. In their experiments, various tissue samples were heated with $\gamma-Fe_2O_3$ ranging in size between 20 and 100 nm at 1.2 MHz magnetic field. In the last 50 years, a variety of magnetic nanoparticles along with different energizing methods and delivering techniques at the cancer site have been reported, and now magnetic nanoparticle hyperthermia is accepted as one of the most important methods of secondary treatment to apply along with radiotherapy and chemotherapy.

In a broad sense, magnetic nanoparticle hyperthermia involves dispersing magnetic nanoparticles throughout the target tissue, and subsequently applying an AC magnetic field with sufficient strength and frequency to generate heat from the magnetic nanoparticles. The heat generated can basically cause two types of cell-killing mechanisms based on two different procedures. If a temperature is reached between 42ºC and 45ºC, and is maintained between these values, then cells kill themselves. This killing mechanism is called apoptosis, as seen in hyperthermia treatment. On the other hand, at higher temperatures up to 56ºC, the cell-killing mechanism can be called necrosis, coagulation, or carbonization, depending on temperature. This

treatment is referred to as thermoablation. In terms of ensuring heating around the targeted tissue only (localized hyperthermia), magnetic fluid hyperthermia is more suitable than traditional hyperthermia techniques that can also cause the heating of healthy tissue. The heating capacity of magnetic nanoparticles is quantified through the specific loss power, defined as the amount of heat dissipated in the unit time and mass of magnetic nanoparticles. Many efforts have been devoted in the last 20 years to improve hyperthermia techniques for clinical applications. Development in nanotechnology has contributed to the progress of magnetic fluid hyperthermia. Figure 12 provides a schematic of the localized magnetic hyperthermia treatment on cancer cells.

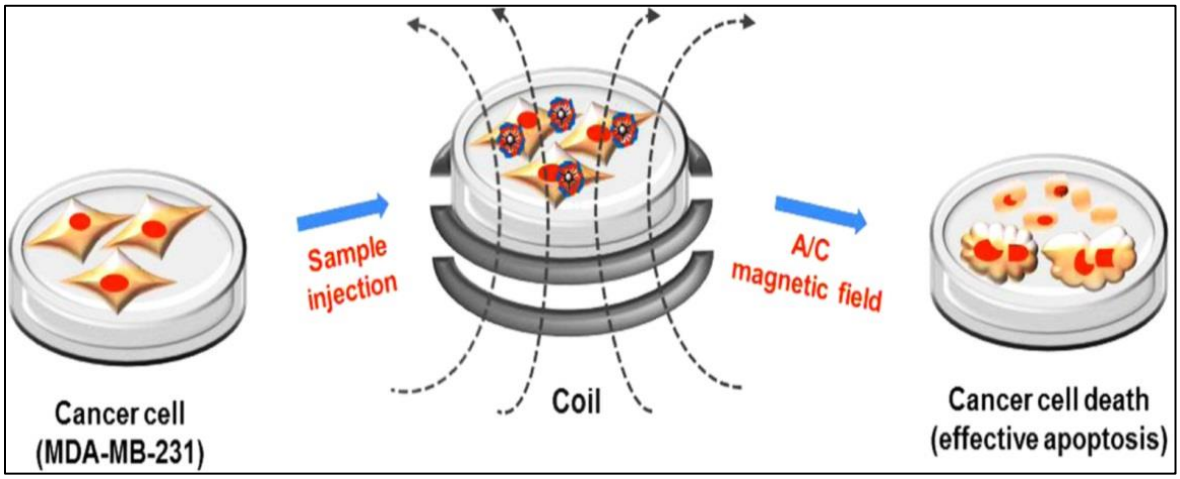

Figure 12. Schematic of localized magnetic hyperthermia treatment on cancer cells [124].

"Classic" hyperthermia induces almost reversible damage to cells and tissues, but as an adjunct therapy, it enhances radiation injury to tumor cells and chemotherapeutic efficiency. Modern clinical hyperthermia trials focus mainly on the optimization of thermal homogeneity at moderate temperatures (42°C–45°C) in the target volume [125]. The essential feature of magnetic fluid hyperthermia is that energy is absorbed from the AC magnetic field and transformed into heat by means of one or a combination of the following mechanisms [126]:

- Generation of eddy currents in a material of low electrical resistivity.
- Loss of hysteresis.

- Reversal of the magnetization inside a magnetic material (Nèel relaxation).
- Rotation of the magnetic material relative to its surroundings (Brownian relaxation).

To explain these terms in detail, first, the structure of a magnetic material should be described. Basically, magnetic nanoparticles can be classified into two groups: multi-domain and single-domain. Figure 13 illustrates the structure of various type of magnetic materials.

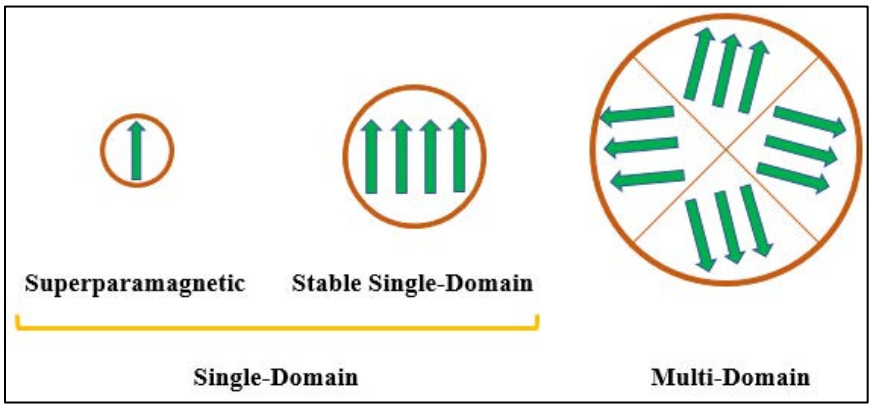

Figure 13. Schematic of magnetic properties of ferromagnetic materials as a function of particle size.

Multi-domain magnetic nanoparticles exhibit ferrimagnetic or ferromagnetic behavior, and for these type of materials, the heating mechanism is based on the loss of hysteresis. That is, when a magnetic field strength is applied to a multi-domain MNP, first, saturation magnetization, which is known as maximum magnetization, is reached. Later on, when the magnetic field is removed, magnetization of the material drops; however, at the magnetic field strength of zero, the material still owns a magnetization in the structure. To eliminate this remaining magnetization in the structure, a negative magnetic field strength must be applied, which eventually results in a hysteresis loop, and the area inside this hysteresis loop gives the hysteresis loss, which is the thermal energy dissipated. Figure 14 shows these hysteresis loops.

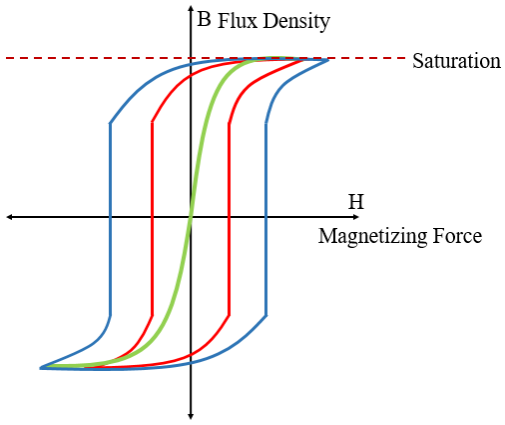

Figure 14. Schematic of hysteresis loops of multi-domain and superparamagnetic materials.

As opposed to multi-domain magnetic materials, single-domain materials basically have a different heat-dissipation mechanism that can be classified under two relaxation groups: Nèel and Brownian. Nèel relaxation is the result of the reorientation of the magnetic moment in the same direction as the applied magnetic field with each field oscillation [127, 128]. The equation to calculate Nèel relaxation time is

$$\tau_N = \tau_0 \exp(KV/k_BT) \tag{15}$$

where τ_N is the Nèel relaxation time, τ_0 is 10^{-9} s, K is the anisotropy constant, V is the volume of the magnetic particle, k_B is the Boltzmann constant, and T is the temperature.

The other loss mechanism, Brownian relaxation, is caused by the rotation of nanoparticles in the surrounding environment. The friction created between the nanoparticle surface and the medium generates heat dissipation. The Brownian relaxation time can be calculated as

$$\tau_B = 3\eta V_H/k_BT \tag{16}$$

where η is the viscosity of the liquid carrier, V_H is the hydrodynamic volume of the particle, k_B is the Boltzmann constant, and T is the temperature.

From equations (15) and (16), it can be said that Nèel relaxation is dependent on nanoparticle size, while Brownian relaxation is dependent on both size and viscosity of the surrounding medium. Accordingly, increasing the viscosity results in a slower motion of nanoparticles. Figure 15 illustrates the loss mechanisms of both Nèel and Brownian relaxations. These mechanisms can be seen together in a material; however, for superparamagnetic materials, which exhibit extremely small particle size, Nèel relaxation is more dominant. As the particle size increases, the strongly viscosity-dependent Brownian relaxation becomes dominant. When these two mechanisms are observed in a magnetic material, relaxation times can be combined, and the overall relaxation time is given by

$$\tau = \tau_B \tau_N / (\tau_B + \tau_N) \tag{17}$$

where τ_B is the Brownian relaxation time, and τ_N is the Nèel relaxation time.

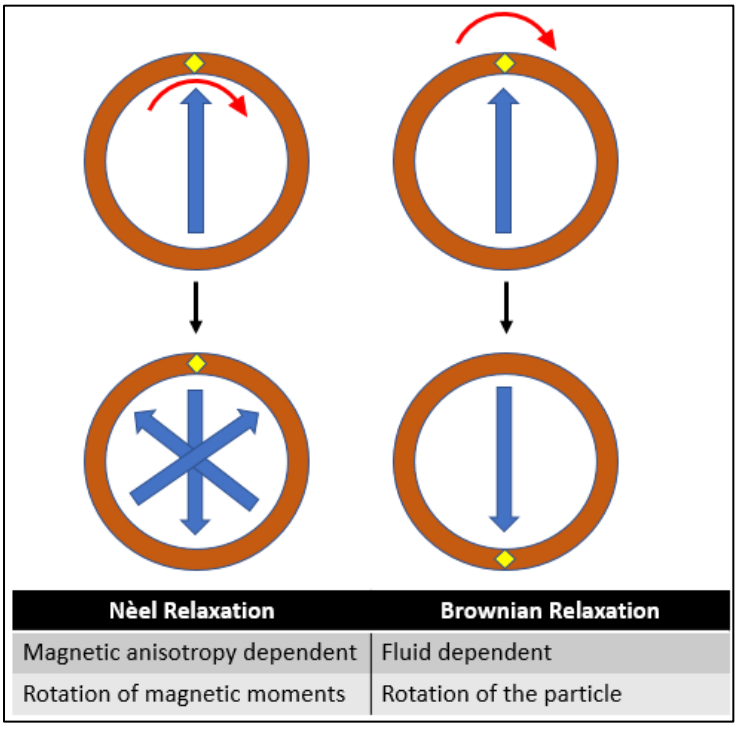

Figure 15. Schematic of Nèel and Brownian relaxation mechanisms.

Relaxation time is important in the sense of determining the amount of heat dissipated because when an alternating magnetic field is applied on a magnetic material, if the oscillating AMF is faster than the relaxation time of the MNPs, then the system causes the release of heat from the MNPs, which results from the delay in the relaxation of the magnetic moment [127].

Power dissipation caused from the delay in relaxation can be calculated by specific loss power, given as

$$SLP = {}^{C}/_{m_p}\, x\, (\Delta t/\Delta t) \tag{18}$$

where C is the heat capacity of sample, m_p is the total amount of magnetic nanoparticles in the material, and $\Delta T/\Delta t$ is the initial slope of the time-dependent heating curve.

Indeed, the heating efficiency can basically be defined via two terms: specific loss power and specific absorption rate (SAR). SLP can be defined as the thermal power per unit mass dissipated by the magnetic material. Even though the term SAR is used interchangeably with the SLP value, they actually describe different concepts in hyperthermia. The term "specific absorption rate," adopted by regulatory agencies, is defined as the rate at which power is absorbed by a volume of dielectric material, such as biological tissue, exposed to radio frequency electromagnetic radiation (or other forms of energy such as ultrasound) [129]. Due to its use in different areas, the use of SLP was chosen in the experimental studies here. Despite the continuing debate, calorimetry is one of the most common methods to estimate the SLP [130-132], because of the adiabatic and mostly quasi-adiabatic nature of the experiments.

CHAPTER 3

EXPERIMENTAL MATERIALS AND METHODS

3.1 Materials

Cold-pressed, 100% pure nigella sativa oil was purchased from Herbal Secrets Company. Medium molecular weight chitosan, polyvinyl alcohol (average molecular weight of 89,000–98,000), 99% hydrolyzed), and Triton X-100 was purchased from Sigma Aldrich, and Span-80 was purchased from TCI America. Sodium bicarbonate was purchased from Fisher Scientific. Magnetic (Fe_3O_4) nanoparticles were purchased from U.S. Nano Company. Deionized water was used in preparation of nanoemulsions and during all tests.

3.2 Methods

3.2.1 Preparation of Nanoemulsions

A probe sonicator was used to prepare the nanoemulsions. Three different oil percentages (10%, 15%, and 20%) were combined with three different surfactant percentages (5, 7.5, and 10%). In the first step, a 10% oil and 5% surfactant mixture was prepared using five different HLB values. These surfactant mixtures with five different HLB were created using two different surfactants in the following ratios: 5:5, 6:4, 7:3, 8:2, and 9:1. After the stabilities of these five nanoemulsions were investigated, it was decided to use ratios 8:2 and 9:1 in further sample preparations for nanoemulsions including 15% and 20% oil. Globule size analysis was conducted using a Zetasizer ZS90 analyzer (Malvern Instruments). Zeta potentials of the samples were determined using the same machine at four different temperatures. Refractive indexes of samples were measured with a Reichert refractometer at 20^{o}C.

3.2.2 Preparation of Magnetic Nanoemulsion Hydrogels

The most stable nanoemulsion defined in the previous experiments was chosen for further gelation studies. This nanoemulsion was comprised of an 8:2 Triton X-100 and Span-80 ratio with a 7.5% surfactant mixture. Later on, a certain amount of magnetite was added into the oil phase containing Span-80, and the mixture was sonicated to disperse the magnetic nanoparticles. Nanoemulsions containing magnetic nanoparticles were prepared using the same procedure used for preparing the nanoemulsions. Then, a 4% chitosan solution prepared in 0.2 M hydrochloric acid (HCl) was mixed with the magnetic nanoemulsions, and homogeneous mixtures were obtained under magnetic stirring, eventually generating the final three Fe_3O_4 concentrations of 8, 16, and 32 mg/ml. Later on, a 2% PVA solution and 1 M sodium bicarbonate solution were mixed in a 1:1 ratio and cooled down to 4^{o}C. Then this cold mixture was added dropwise into the nanoemulsion containing the chitosan hydrogels, and the temperature was increased for gelation. The gelation time and temperature were decided when the hydrogels in the vials showed no more flow. At the end of the process, magnetic nanoemulsion hydrogels (MNHs) were synthesized.

3.2.3 Fourier Transform Infrared Spectroscopy

During infrared (IR) spectroscopy, IR radiation is passed through a sample. While some of the radiation is absorbed by the sample, the remainder passes through the sample, which means that the IR radiation has been transmitted. The resulting spectrum, which shows the molecular absorption and transmission, generates a molecular fingerprint of the sample. By using Fourier transform infrared spectroscopy (FTIR), it is possible to identify unknown materials, determine the quality or consistency of a sample, and ascertain the number of components in a mixture. Attenuated total reflectance (ATR) spectroscopy, one of the FTIR reflectance

techniques, was used to characterize the structure of the manufactured hydrogels. Figure 16 shows the FTIR device.

Figure 16. Fourier transform infrared spectroscopy device used for this study.

3.2.4 Zeta Potential Measurements

Zeta potential is defined as the charge that develops at the interface between a particle and its liquid medium. Derivations indicate that the zeta potential is the double-layer potential, which is close to the particle surface, and one of its applications is the measurement of surface charges of particle surfaces [133]. The liquid layer of a particle in suspension migrating in an electric field moves at the same velocity as the surface-shear surface. This shear surface occurs well within the double layer, likely at a location roughly equivalent to the Stern surface. Even though the precise location of the shear surface is unknown, it is assumed to be within a couple of molecular diameters of the actual particle. This thickness is associated with the zeta potential and defines the ion atmosphere near a surface [134]. The magnitude of the zeta potential can be an indicator of the potential stability of a colloidal system. In the case where particles have relatively large negative or positive zeta potentials (greater than +30 mV and less than –30 mV),

they will repel each other, thus making the colloidal system stable. However, if the particles have low zeta potential (between +30 and –30 mV), then particles tend to coalesce, thus creating instable systems. Figure 17 shows the stability relation depending on zeta potential.

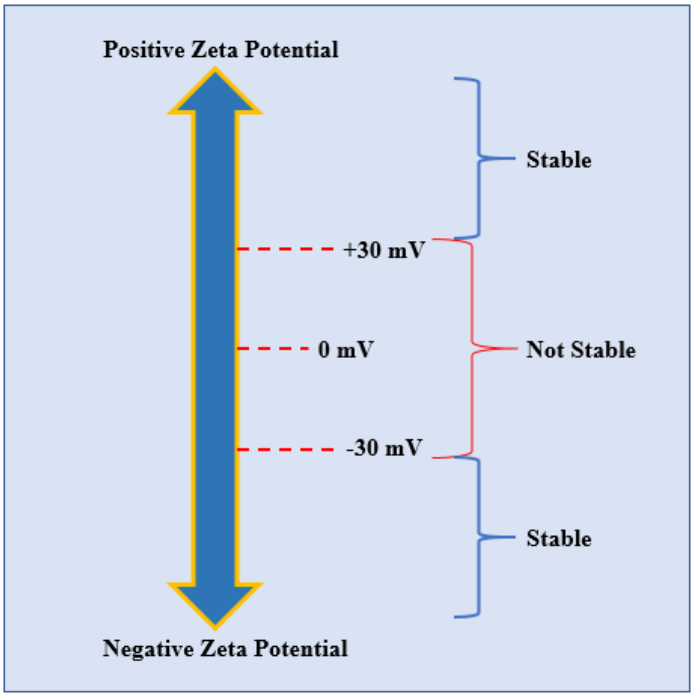

Figure 17. Stability with relation to zeta potential.

Specifications for the Zetasizer ZS90 machine were as follows:

- Size Range: 0.3 nm to 5 µm (diameter) using 90-degree scattering optics
- Accuracy: Better than +/–2% on NIST traceable latex standards
- Repeatability: Better than +/–2% on NIST traceable latex standards
- Minimum Sample Volume: 20 µl
- Measurement Principle: Dynamic light scattering (DLS)
- Results: Mean and standard deviation calculated for size distribution by intensity assuming a log-normal distribution

3.2.5 Dynamic Light Scattering

Dynamic light scattering is an important tool for measuring hydrodynamic size, zeta potential, and the polydispersity index of colloidal solutions, molecules, or nanoparticles. DLS measurements are performed based on the Brownian motion of particles. Once the Brownian motion of particles is characterized, this information is transformed into a hydrodynamic diameter. The hydrodynamic diameter is basically related to physical size of the particle, which involves its diameter as well as the layer created on its surface due to interaction with substances in the solvent such as surfactants or stabilizers. Figure 18 shows a picture of the DLS instrument.

Figure 18. Dynamic light scattering instrument.

Dynamic light scattering measures the intensity of light scattered from a colloidal solution, analyzing the random intensity of the scattered light as a function of time. Basically, coherent light is radiated from a laser and passed through the sample. Parts of the photons are scattered in all directions due to a difference in diffractive index between the solution and the dispersed colloid or dissolved polymer. The scattered photons interfere with each other to display a wave with either larger intensity (constructive interference) or weaker intensity (destructive

interference). Constructive and destructive interferences are dependent on the distance of the scattering centers. Due to the Brownian motion of all colloids in solution, the interference changes over time. When colloids move quickly in a solution, the interference pattern changes rapidly; for slow colloids, the pattern changes more slowly. How fast the colloids move is determined by the signal intensity of the scattered light. This is detected over time, and the gained values are used to generate an intensity autocorrelation function. For very short time intervals, the intensity values are dependent on each other; for longer time intervals, the intensity values are more independent. Sizes that are suitable for analysis range from the lower nanometer to the low micrometer scale. A restriction when measuring very small particles is mainly the very low scattering intensity (which is proportional to the square of the molecular weight). A limitation when measuring very large particles is mainly the slow movement and therefore long measurement time to generate enough data for a statistical analysis.

The DLS measurements were conducted using a Zetasizer Nano ZS (Malvern Instruments, Malvern, UK). Diluted samples were exposed to a helium-neon (HeNe) laser at a wavelength (λ) of 632.8 nm. Measurements were performed at different temperatures using disposable polystyrene cuvettes. Data quality reports obtained by the software (DTS v 5.03) provided information regarding the quality of data collected for the intensity-based size mean, polydispersity index, and zeta potential.

3.2.6 Ultraviolet-Visible Spectroscopy

Ultraviolet-visible (UV-Vis) spectroscopy refers to absorption spectroscopy in the ultraviolet-visible spectral region. This means that it uses light in the visible and adjacent (near-UV and near-infrared [NIR]) ranges. The tests in this study employed the Hitachi-2900 spectrophotometer, which is shown in Figure 19.

Figure 19. UV-Vis spectroscopy device (Hitachi-2900 spectrophotometer).

3.2.7 Swelling Study

Chitosan-based magnetic nanoemulsion hydrogels were prepared and crosslinked with a sodium bicarbonate solution. Gelation was achieved with the increasing temperature, and their swelling characteristics were investigated. The prepared hydrogels were placed in well plates at the same weights and kept in phosphate buffer solution at a pH value of 7.4. Using equation (19), swelling ratios and water content of the hydrogels were calculated at predetermined time periods:

$$\mathrm{SR}(\%) = \frac{(\mathrm{W_s} - \mathrm{W_d})}{\mathrm{W_d}} \mathrm{x100} \tag{19}$$

where W_s is the weight of swollen hydrogels, and W_d is the weight of dry hydrogels.

The equilibrium water content was calculated as

$$\mathrm{WC}(\%) = \frac{(\mathrm{W_e} - \mathrm{W_d})}{\mathrm{W_e}} \mathrm{x100} \tag{20}$$

where W_e and W_d represent the weights of the swollen and dry states at equilibrium, respectively.

Fickian's diffusion law was utilized to investigate the swelling kinetics of hydrogels, and the swelling and diffusion constants were found using equation (21):

$$F = \frac{M_t}{M_\infty} = kt^n \quad (21)$$

3.2.8 Drug-Release Study

For the drug-release study, MNHs containing 24 mg/ml of magnetic nanoparticles, chitosan hydrogels containing only magnetic nanoparticles, and plain chitosan hydrogels were prepared at the same weights and placed in 1 ml of phosphate-buffered saline (PBS) solution (pH = 7.4) at 37°C. At predefined time intervals, the PBS solutions were collected, and a fresh PBS solution was added into the well plates to fully cover the hydrogel samples. Samples were collected for 48 hours, and the concentrations of drugs in the solution were calculated using the UV-Vis spectrometer. First, the calibration curve for 5-Flouracil (5-FU) was plotted, and the model was created as a function of concentration and absorption. Later on, for each sample, the concentration of the drug in the solution was calculated using the equation obtained from the calibration curve. Once the cumulative drug-release results were calculated, data were fit into five different drug-release models, and based on R^2 values, the best-fitting model was determined in order to understand the drug-release characteristics of the samples. The following models were used in the drug-release study:

- Zero-Order
- First-Order
- Higuchi
- Korsmeyer-Peppas
- Hixson-Crowell

3.2.9 Induction Heating System for Hyperthermia Study

Multiple studies [135-137] have used inductor setups for hyperthermia studies. An inductor allows for a first approximation of heating in ferromagnetic materials. Its use in the

heating apparatus setup for this study was similar to the testing measurements done by Jordan et al. [135]. Using this equipment is appealing for the following reasons: efficient power transfer to the ferromagnetic load by the capacitor and inductor in a resonant circuit, selective heating in the ferromagnetic materials over the surrounding media, and the ability to generate repeatable results.

A schematic diagram of the hyperthermia unit based on the induction heating mechanism is shown in Figure 20. The system consists of an AC magnetic field generator, induction coil, and digital thermocouple. Induction heating of the magnetic hydrogel for the hyperthermia application was implemented in a glass vial using an induction heating unit (LH-15A induction heater) with a 3-cm-diameter (three turns) heating coil, as shown here.

Figure 20. Hyperthermia unit based on induction heating, including induction coil and vial with magnetic nanoparticle hydrogel.

To preserve the temperature of the coil at ambient temperature, water circulation was provided in the coil. The glass vial in which hydrogels were generated was placed at the center of

the coil. Samples were heated for 20 minutes with the desired current (110–330 A). The magnetic field for the conducted experiments was calculated as

$$H = {}^{1.257ni}/_{L} \quad (22)$$

where n denotes the number of turns, i is the applied current, and L is the diameter of the turn in centimeters. Calculated values of the magnetic field (H) at 110, 220, and 330 A were 138.27, 276.54, and 414.81 Oe (equivalent to 11.0, 22.0, and 33.0 kA m^{-1}), respectively.

Temperature gradients that exist within the apparatus should additionally be considered, because the coil is more likely to heat due to ohmic losses caused by the alternating current. When power is started, the temperature must always be larger in the coil than in the insulation. Considering that insulation will absorb heat generated by the coil, insulation can have a higher temperature at the points that is closer to the coil until the sample can quickly generate a large amount of heat. Due to the air space between the sample and the insulation, the insulation temperature will likely attain a minimum at the sample rather than at the coil. Moreover, gradients are unlikely to be linear, particularly because of the nonuniform heating within the sample [133].

3.2.10 Statistical Analysis

Statistical analysis was carried out using Design-Expert 7.7 software. Response of the temperature increase corresponding to magnetic nanoparticle amount, magnetic field, and time were performed using general factorial design. All reported *P*-values were statistically significant at $P < 0.05$, $P < 0.01$, and $P < 0.001$.

3.2.11 Specific Loss Power

Specific loss power can be defined as the thermal power per unit mass dissipated by the magnetic material. To calculate the heating efficiency of MNH samples, equation (18), previously given in Chapter 2, was used:

$$SLP = \frac{C}{m_p} x \frac{\Delta T}{\Delta t}$$

where C is the heat capacity of sample, m_p is the total amount of magnetic nanoparticles in the material, and ΔT/Δt is the initial slope of the time-dependent heating curve. To calculate the SLP values, first, heat capacity of the samples was found using the calorimetric technique. Basically, considering that heat flow between two samples will be equal under adiabatic conditions, using equation (19), specific heat capacities of the samples were calculated as

$$Q = mc\Delta T \tag{19}$$

Later on, specific heat capacity was multiplied by the mass of gels to calculate the heat capacity of the samples. Initial heating curves of the samples at three different MFS values were created for 3 min. Finally, SLP results obtained from the calculations were plotted.

CHAPTER 4

RESULTS AND DISCUSSION

4.1 Globule Size Analysis

Globule size analysis over time was initially performed for emulsions including 10% oil and 5% surfactant. Using two different surfactants in five different ratios—5:5, 6:4, 7:3, 8:2, and 9:1—five different emulsions were prepared. Their absorbance at 633 nm, hydrodynamic size, and polydispersity index were measured, and the test results are plotted in Figures 21 to 23, respectively. Over a 70-day period, it was decided to use emulsions with HLBs of 11.6 (8:2 ratio) and 12.58 (9:1 ratio) in further studies because these emulsions showed the least diameter change during this period.

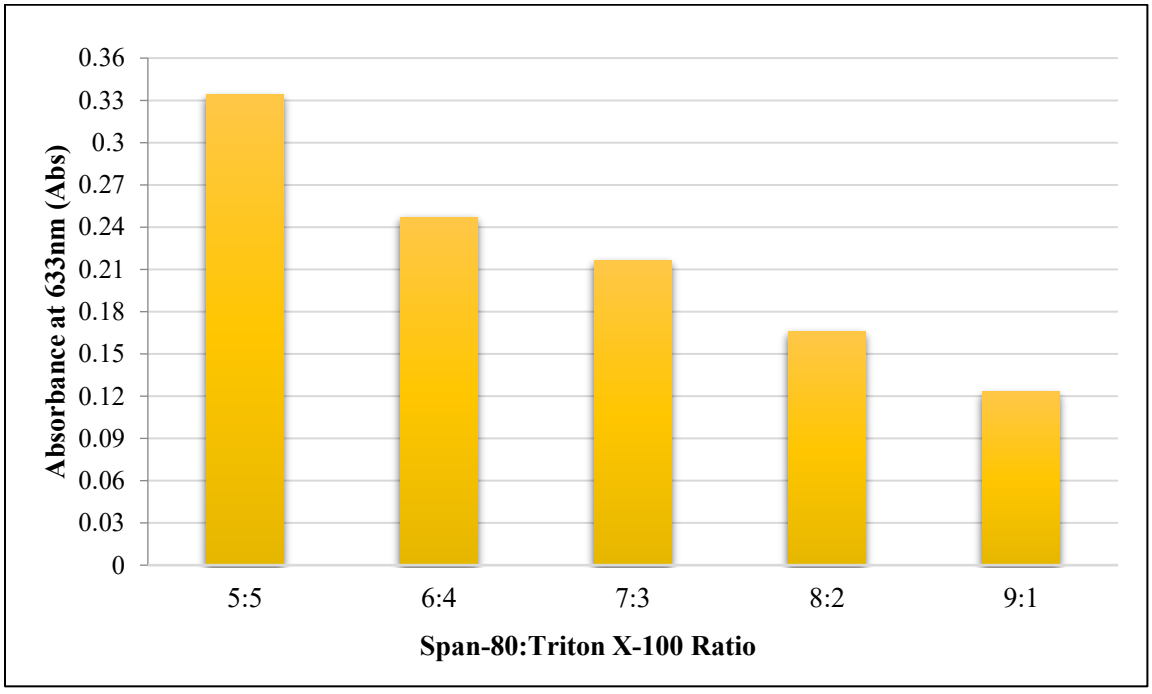

Figure 21. UV-Vis spectrometry results of nanoemulsions prepared at five different HLB values collected at 633 nm.

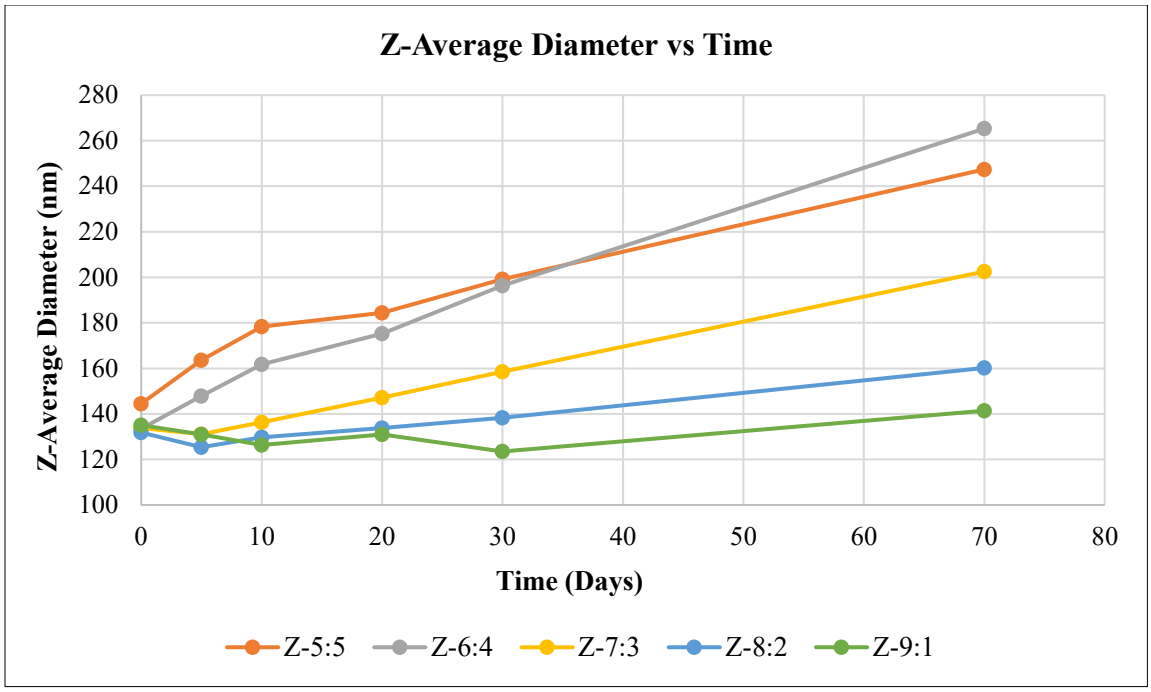

Figure 22. Z-average diameter versus time for emulsions including 10% oil and 5% surfactant.

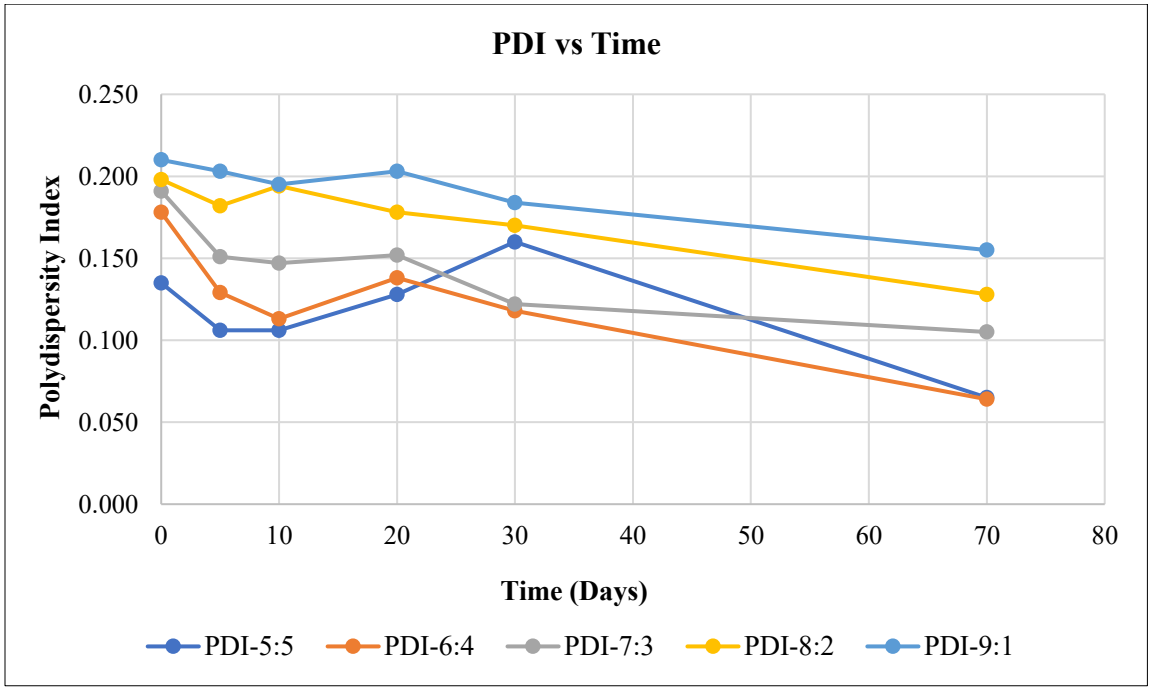

Figure 23. PDI versus time for emulsions including 10% oil and 5% surfactant.

As shown in Figure 23, there is a drop in PDI by time. This was associated with the globule size change at equilibrium, which resulted from small micelles combining with larger micelles and providing more homogeneous size distribution by time.

Figure 24 shows the Z-average diameter of nanoemulsions as a function of HLB value over a 70-day period, and Figure 25 shows the PDI of samples as a function of HLB collected over a 70-day period.

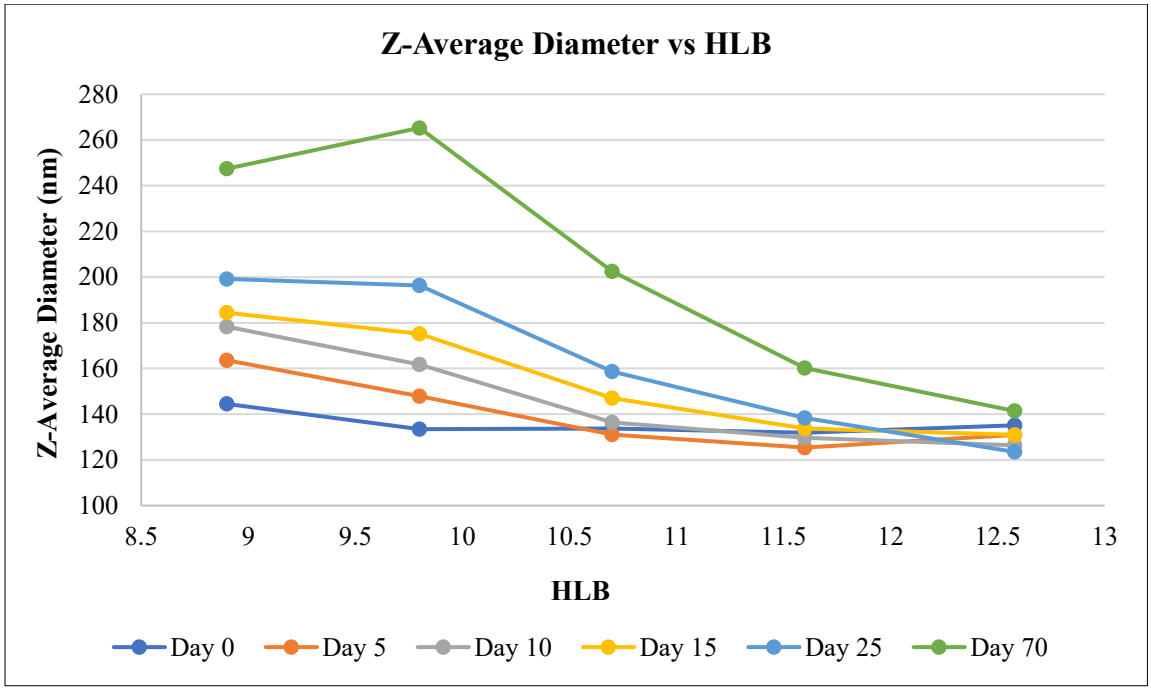

Figure 24. Z-average diameter versus HLB of samples collected over 70-day period.

From the first step in this study, HLB values of 11.6 (8:2) and 12.58 (9:1) were chosen to use in further investigations. The nanoemulsion including 10% oil and 5% of surfactant with an HLB of 12.58 (9:1) shows a small amount of separation, less than 2%. Even though it was planned to eliminate this HLB, it was included in order to investigate the effect of surfactant amount and oil amount on separation for this HLB value, since it provided the nanoemulsion with the smallest hydrodynamic size.

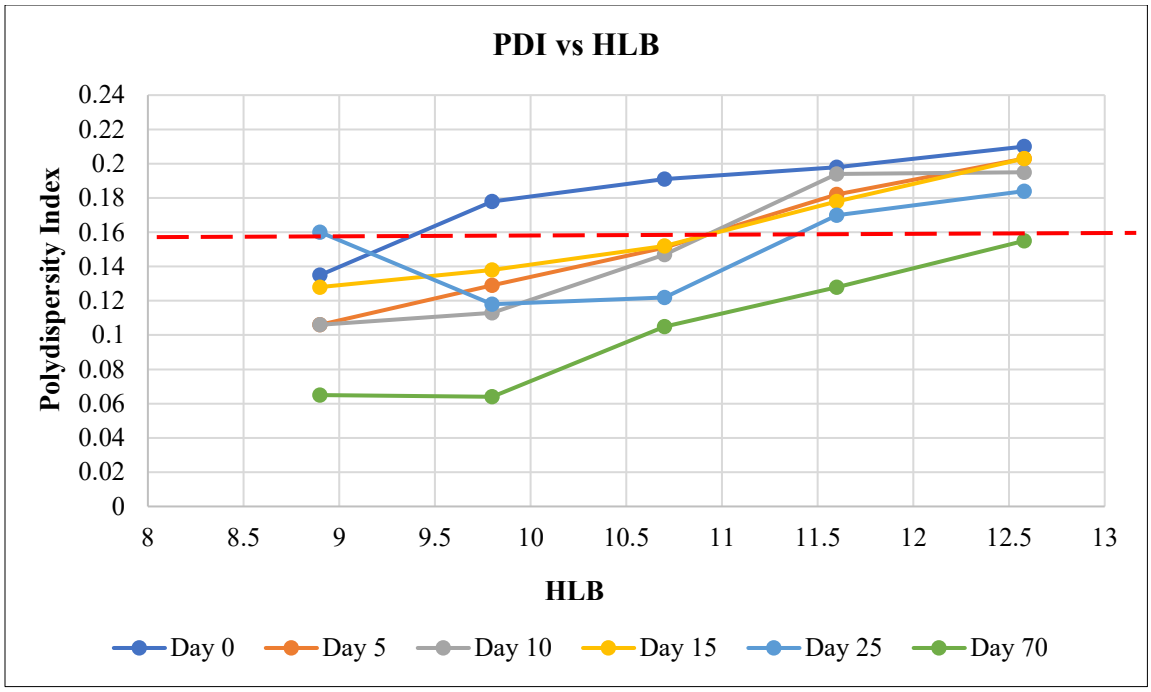

Figure 25. PDI versus HLB of samples collected over 70-day period.

Test results obtained using these two HLB values along with three different oil-and-surfactant percentages were plotted, as shown in Figures 26 to 28.

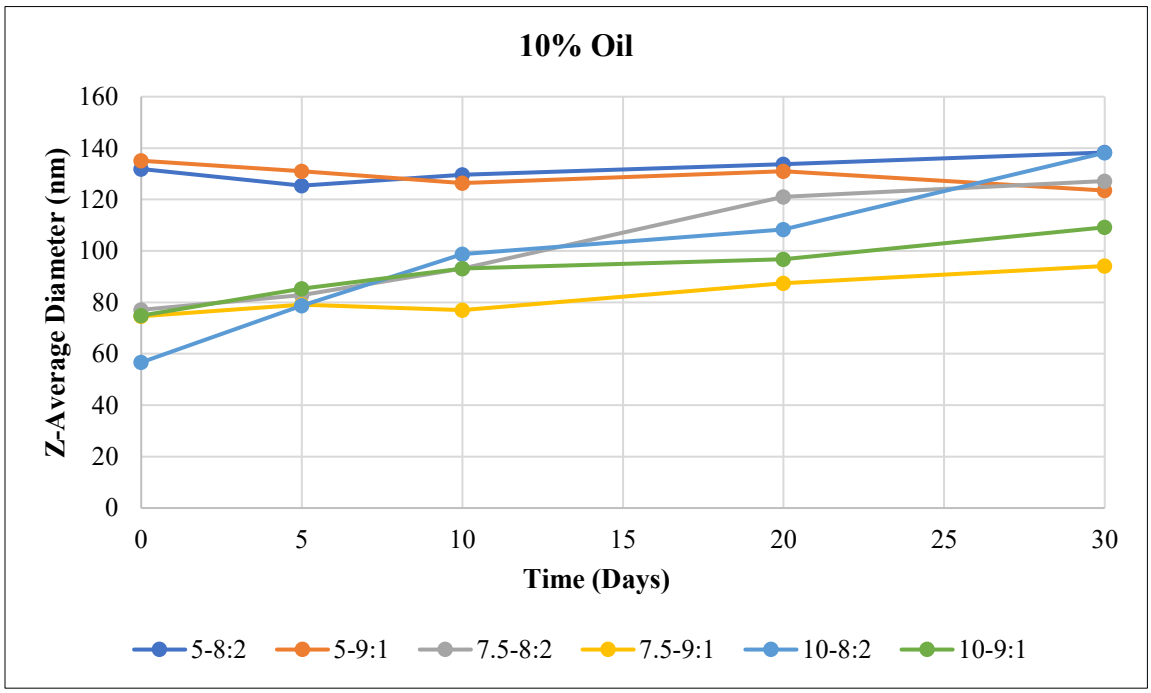

Figure 26. Z-average diameter change during 30 days for emulsions including 10% oil.

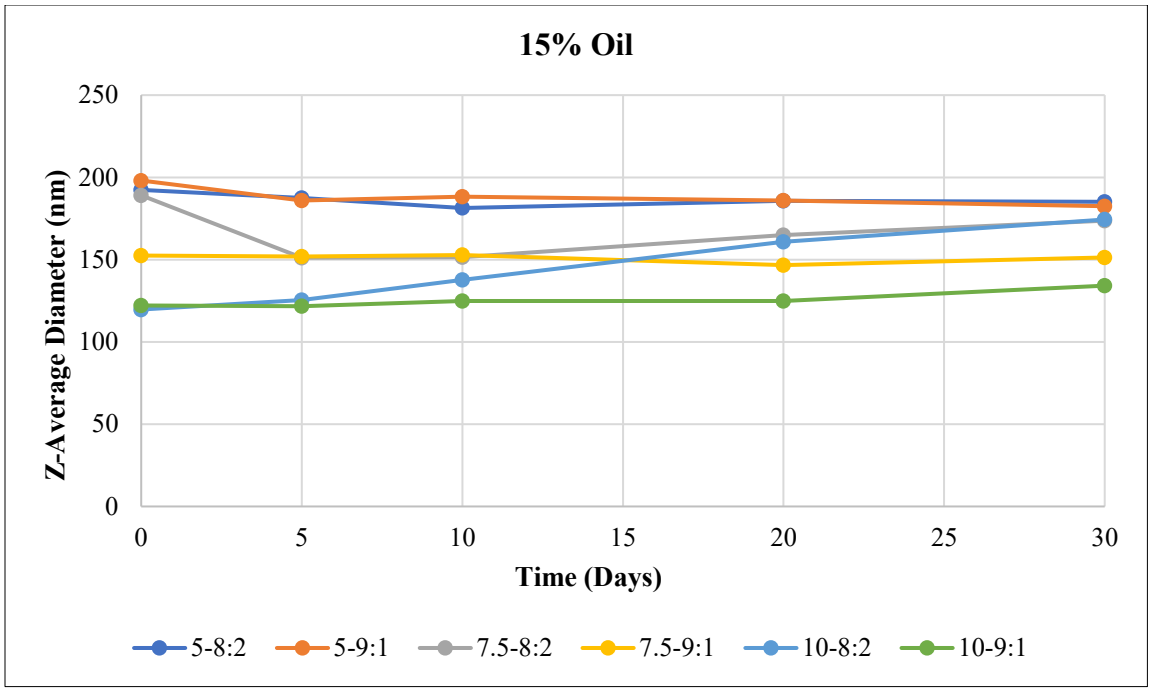

Figure 27. Z-average diameter change during 30 days for emulsions including 15% oil.

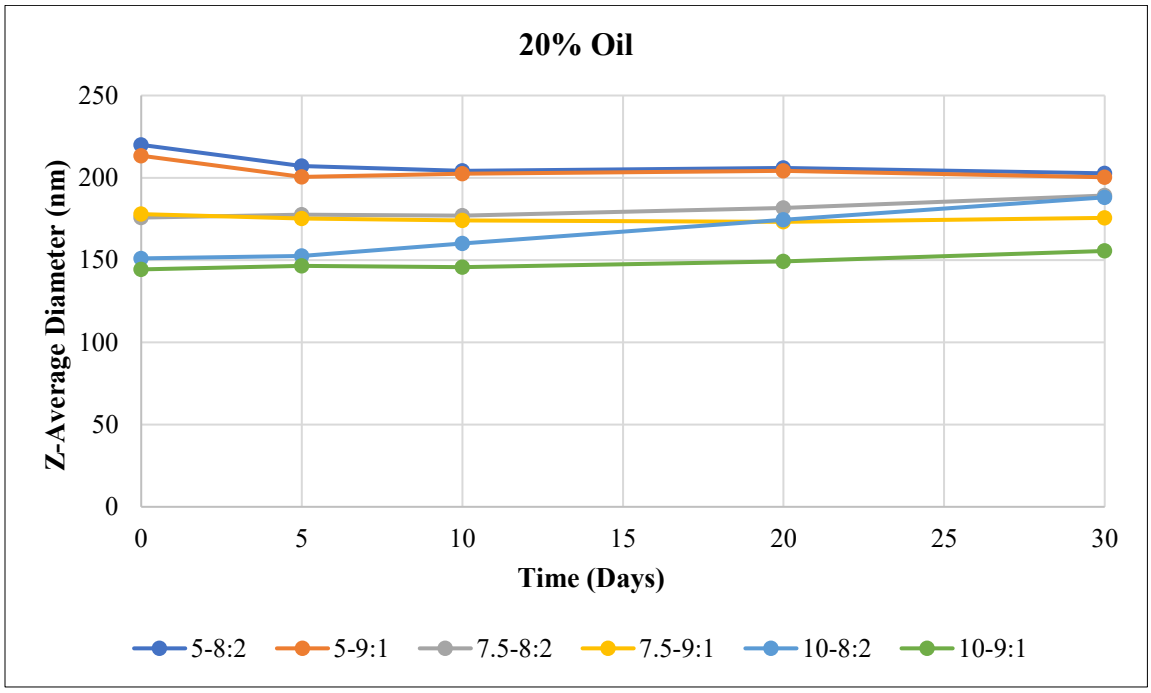

Figure 28. Z-average diameter change during 30 days for emulsions including 20% oil.

It is obvious from these figures that with the increasing oil percentage, the average diameter increased, as expected. While a 5% surfactant percentage provided the highest diameter, the emulsion containing 10% surfactant resulted in the smallest-diameter nanoemulsions. In addition, it was observed that with increasing oil percentages, the change in diameter over time was less compared to the emulsions with lower oil percentages. In addition, as can be seen in all three graphs, it is obvious that emulsions with 10% surfactant and 8:2 ratio of surfactants (HLB: 11.6) exhibited the highest diameter increase over time. Overall, these plots indicate that increasing the surfactant percentage increased the instability at all oil percentage levels. This was associated with a depletion in flocculation due to the osmotic pressure increment via increasing surfactant concentration. However, this increment was seen to be less with increasing oil percentage.

During the 30-day period, in addition to measuring the average diameter, samples were also inspected to see whether any separation occurred in the emulsion. It was observed that, at all oil and surfactant levels, emulsions with an HLB value of 12.58 (9:1 ratio) exhibited a separation of less than two percent, except the emulsion with 15% oil and 7.5% surfactant (data not shown here). This suggests that the stability of an emulsion is not only a matter of HLB because no separation was observed in the emulsions with 15% oil and 7.5% surfactant. The amount of oil, surfactant, water, and HLB should be considered together for achieving better nanoemulsions.

4.2 Zeta Potential Analysis

The zeta potential of samples was collected using a Zetasizer machine. Test results are listed in Tables 5 to 7, which show the zeta potential of samples at four different temperatures.

TABLE 5

ZETA POTENTIAL OF EMULSIONS INCLUDING 10% OIL AT FOUR DIFFERENT TEMPERATURES AFTER 30 DAYS (MEAN ± SD, N = 5)

	10% Oil					
	5% Surfactant		**7.5% Surfactant**		**10% Surfactant**	
Temp. (°C)	**8:2**	**9:1**	**8:2**	**9:1**	**8:2**	**9:1**
25	– 19.1 ± 0.3	–7.27 ± 1.4	–25.3 ± 1.3	–23.9 ± 2.1	–23.3 ± 1.5	–9.59 ± 0.3
37	–17.8 ± 0.1	–7.11 ± 1.1	–22.4 ± 1.1	–20 ± 1.1	–21.5 ±1.5	–9.02 ± 0.6
40	–16.5 ± 0.1	–7.2 ± 0.5	–21.3 ± 0.6	–19.2 ± 1.3	–19.4 ±0.5	–9.16 ± 0.5
50	–14.7 ± 0.8	–6.72 ± 0.3	–21 ± 1.17	–17.1 ± 0.6	–18.7 ±0.4	–9.01 ± 0.9

TABLE 6

ZETA POTENTIAL OF EMULSIONS INCLUDING 15% OIL AT FOUR DIFFERENT TEMPERATURES AFTER 30 DAYS (MEAN ± SD, N = 5)

	15% Oil					
	5% Surfactant		**7.5% Surfactant**		**10% Surfactant**	
Temp. (°C)	**8:2**	**9:1**	**8:2**	**9:1**	**8:2**	**9:1**
25	–31.8 ± 0.6	–30.8 ± 0.6	–33.9 ± 0.6	–26 ± 0.4	–24.3 ± 0.9	–21.5 ± 0.5
37	–29.1 ± 1.2	–26.3 ± 0.4	–29.8 ± 1.1	–23.4 ± 0.3	–22 ± 0.7	–18.6 ± 0.4
40	–29 ± 0.5	–26.1 ±0.6	–29.5 ± 0.4	–23.6 ± 0.1	–21.9 ± 0.4	–18 ± 0.3
50	–27.4 ± 0.6	–24.9 ± 0.4	–28.6 ± 0.2	–23 ± 0.9	–20.1 ± 0.5	–17 ± 0.6

TABLE 7

ZETA POTENTIAL OF EMULSIONS INCLUDING 20% OIL AT FOUR DIFFERENT TEMPERATURES AFTER 30 DAYS (MEAN ± SD, N = 5)

	20% Oil					
	5% Surfactant		**7.5% Surfactant**		**10% Surfactant**	
Temp. (°C)	**8:2**	**9:1**	**8:2**	**9:1**	**8:2**	**9:1**
25	–39.8 ± 0.6	–32.1 ± 0.7	–35.8 ± 0.4	–32.5 ± 0.4	–32.9 ± 1.3	–21.2 ± 0.9
37	–32.9 ± 0.4	–28.8 ± 0.6	–33.4 ± 0.2	–28.6 ± 0.5	–28.3 ± 0.3	–19.8 ± 1.2
40	–33.1 ± 0.3	–28.9 ± 0.5	–33.6 ± 0.8	–28.2 ± 0.6	–28.7 ± 0.2	–20.2 ± 0.6
50	–32.6 ± 0.7	–27.6 ± 0.5	–33 ± 0.6	–27.5 ± 0.4	–27.4 ± 0.5	–19.1 ± 0.7

Overall, it was observed that the zeta potential slightly dropped with increasing temperature, and increasing surfactant percentages pulled the zeta potential down. Test results clearly indicate that the surfactant ratio of 8:2 exhibited higher zeta potential compared to that of 9:1. In addition, a higher oil percentage resulted in a greater zeta potential. Since the zeta potential values that are greater than +25 mV and less than –25 mV exhibit good stability, samples in this range with minimum particle size can be considered for drug delivery applications. Considering the average diameter and zeta potential results together, it was concluded that emulsions with 7.5% surfactant and an HLB value of 11.6 is the best combination for the present studies. This emulsion provided the smaller diameter with lowest zeta potential, and without any phase separation.

4.3 Polydispersity Index Analysis

Selected samples from the Z-average diameter and zeta potential measurements were compared in terms of their polydispersity index. Test results provided in Table 8 indicate that

almost all PDI values are low, which were expected to be less than 0.2. Moreover, it was observed that there is a decrement in the PDI over 30 days. This was associated with globule size tending to reach equilibrium over time after the rebinding of smaller globules onto larger globules.

TABLE 8

POLYDISPERSITY INDEX OF SAMPLES FOR ONE MONTH (MEAN ± SD, N = 5)

7.5% Surfactant with HLB 11.6			
Day	**10% Oil**	**15% Oil**	**20% Oil**
0	0.260 ± 0.009	0.195 ± 0.020	0.205 ± 0.029
5	0.144 ± 0.022	0.192 ± 0.016	0.181 ± 0.033
10	0.139 ± 0.016	0.162 ± 0.016	0.155 ± 0.024
20	0.165 ± 0.023	0.147 ± 0.040	0.128 ± 0.020
30	0.082 ± 0.009	0.113 ± 0.024	0.121 ± 0.018

These samples did not exhibit any increment in PDI under various temperatures. Test results for samples after 30 days were collected at four different temperatures—25, 37, 40, and 50ºC. Results indicate that temperature did not cause the PDI value to go higher, around 0.2. This suggests that selected emulsions own good dispersity characteristics in the temperature range of 25ºC –50ºC. Table 9 shows the polydispersity index of samples at four different temperatures.

As shown in Figure 29, particle size readings did not show substantial changes at different temperatures, indicating that samples were stable between 25ºC and 50ºC. Results suggest that emulsions can be good candidates for drug delivery applications in terms of maintaining their size at body temperature.

TABLE 9

POLYDISPERSITY INDEX OF SAMPLES AT FOUR DIFFERENT TEMPERATURES
(MEAN ± SD, N = 5)

7.5% Surfactant with HLB 11.6			
Temp. (°C)	**10% Oil**	**15% Oil**	**20% Oil**
25	0.082 ± 0.009	0.113 ± 0.024	0.121 ± 0.018
37	0.055 ± 0.028	0.105 ± 0.028	0.120 ± 0.006
40	0.073 ± 0.014	0.095 ± 0.012	0.104 ± 0.027
50	0.094 ± 0.013	0.126 ± 0.011	0.100 ± 0.023

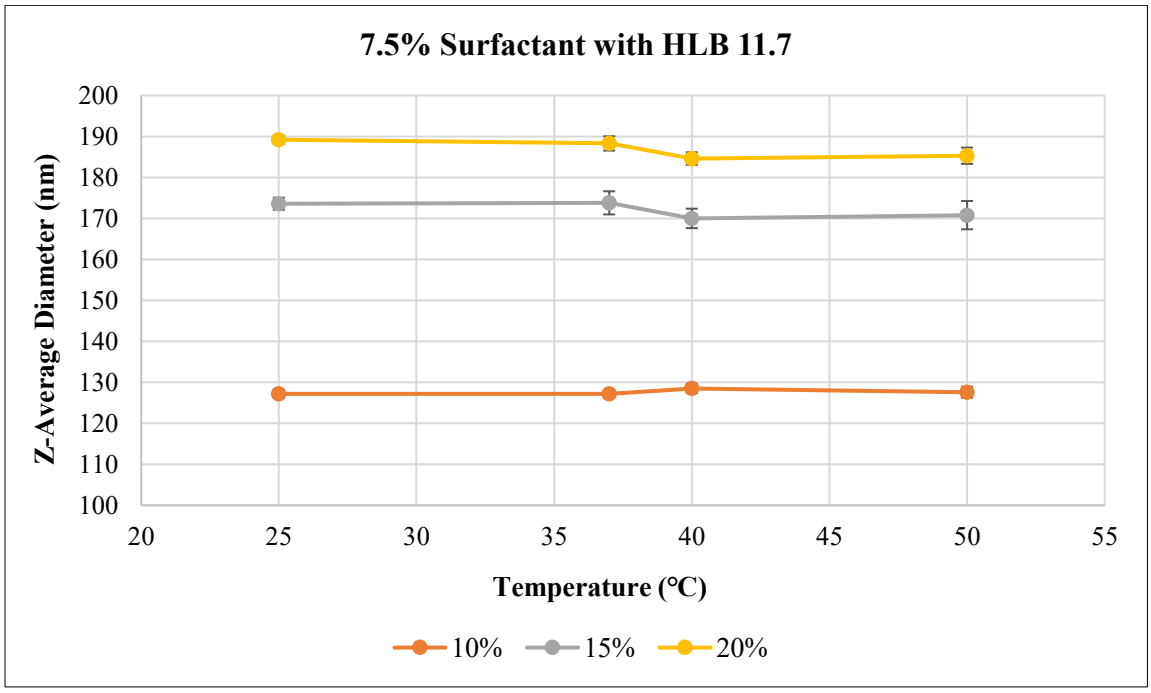

Figure 29. Z-average diameter of selected samples corresponding to four different temperatures.

4.4 Refractive Index Analysis

Refractive index measurements showed that the selected nanoemulsions were isotropic in nature. All results collected from three samples exhibited a refractive index close to the refractive index of water at 1.33. These results are shown in the Table 10. The reason behind the slight increment in refractive index corresponding to increasing amount of oil may be due to the decreasing water content in the environment.

TABLE 10

REFRACTIVE INDEX OF SELECTED FORMULATIONS (MEAN ± SD: 0.001, N = 3)

7.5% Surfactant with HLB of 11.6		
10% Oil	15% Oil	20% Oil
1.359	1.367	1.374

4.5 Rheological Analysis

Rheology studies suggested that nanoemulsions with a small amount of oil exhibited lower viscosity, and with an increasing amount of oil, they exhibited increased viscosity. Moreover, temperature was seen to affect the viscosity properties of the samples. At room temperature, viscosities were seen to be constant at all shear rates; however, increasing the temperature to 37ºC resulted in viscosity higher at a shear rate range of 1 to 100 s^{-1}. After this point, viscosities were seen to be constant with increasing shear rate and slightly higher than that of samples at room temperature (25ºC). Figures 30 to 32 show viscosity versus shear rate of nanoemulsions containing 10%, 15%, and 20% of the oil phase at two different temperature values of 25ºC and 37ºC after one day, 15 days, and 30 days of nanoemulsion preparation, respectively.

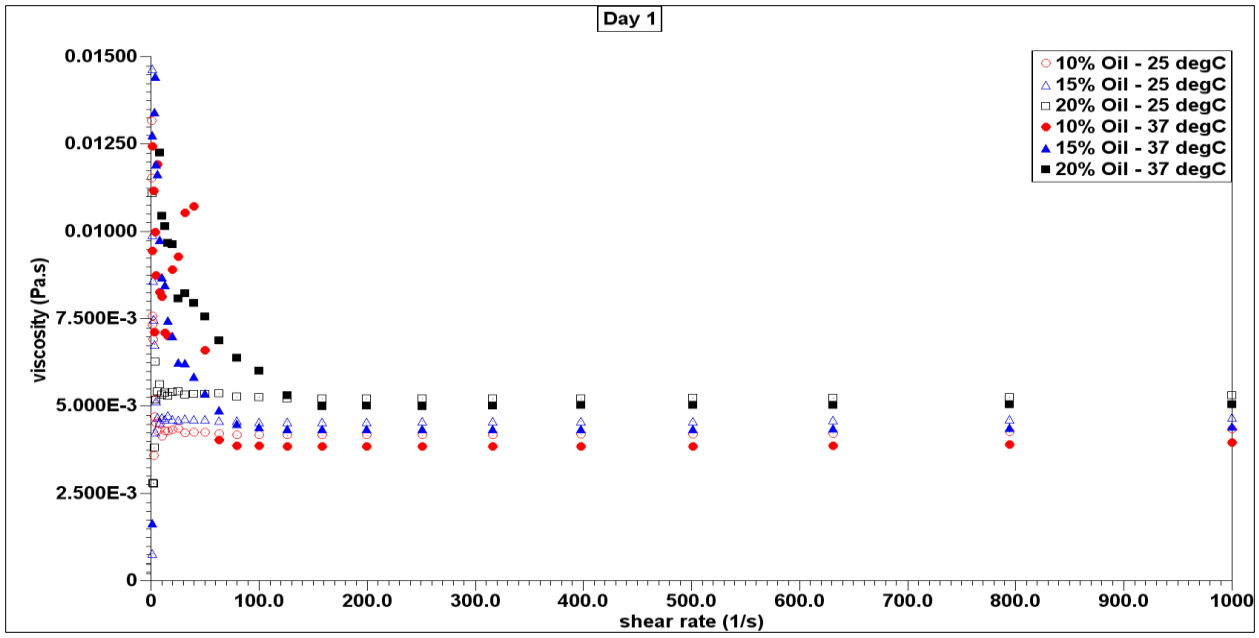

Figure 30. Viscosity as a function of shear rate of nanoemulsions containing 10%, 15%, and 20% oil phase at two different temperature values of 25°C and 37°C and one day after nanoemulsion preparation.

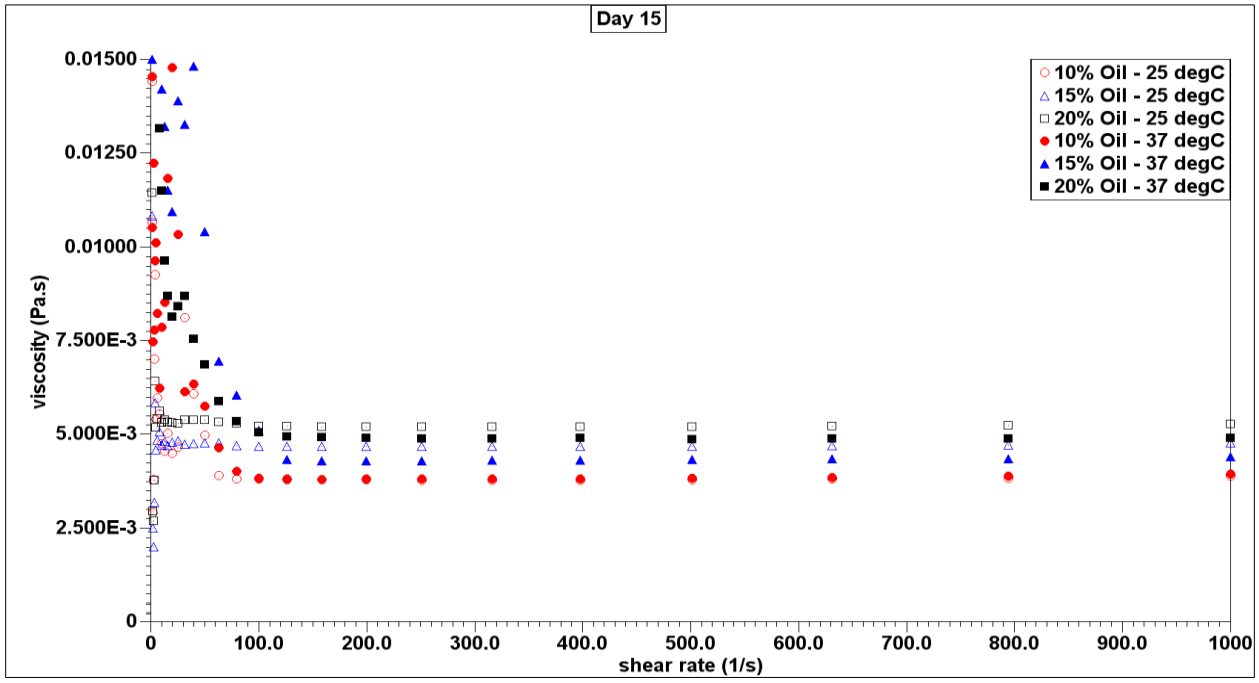

Figure 31. Viscosity as a function of shear rate of nanoemulsions containing 10%, 15%, and 20% oil phase at two different temperature values of 25°C and 37°C and 15 days after nanoemulsion preparation.

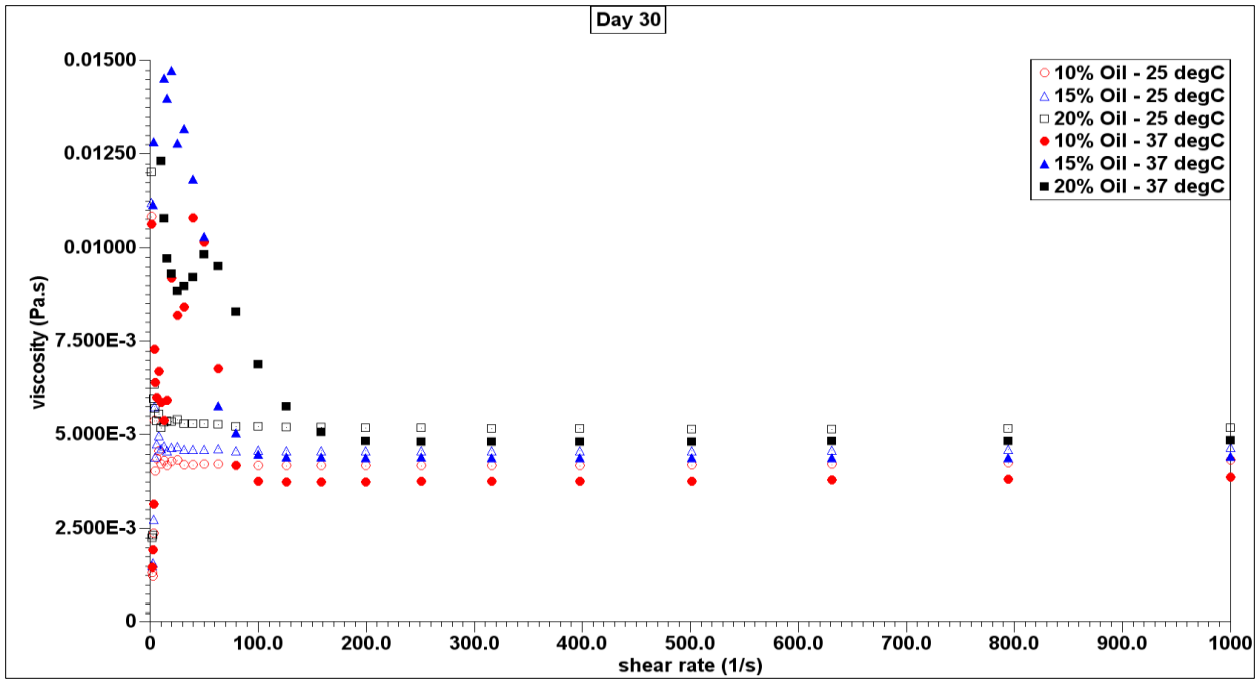

Figure 32. Viscosity as a function of shear rate of nanoemulsions containing 10%, 15%, and 20% oil phase at two different temperature values of 25°C and 37°C and 30 days after nanoemulsion preparation.

Viscosity changes for the 30-day period were investigated by plotting the viscosity-shear rate graph at the 1st, 15th, and 30th day for all three samples containing three different oil percentages at two different temperatures. As indicated in the results shown in Figures 33 to 35, the viscosity of the samples did not change during one month for both temperature values. In addition, samples at 37°C kept a higher viscosity than the samples at 25°C. Also, the temperature effect on viscosity difference is slightly observable at a low oil percentage of 10%; however, with increasing oil percentage, curves in the graph tend to overlap, indicating closer viscosity values at two different temperature values for a greater amount of oil in the system.

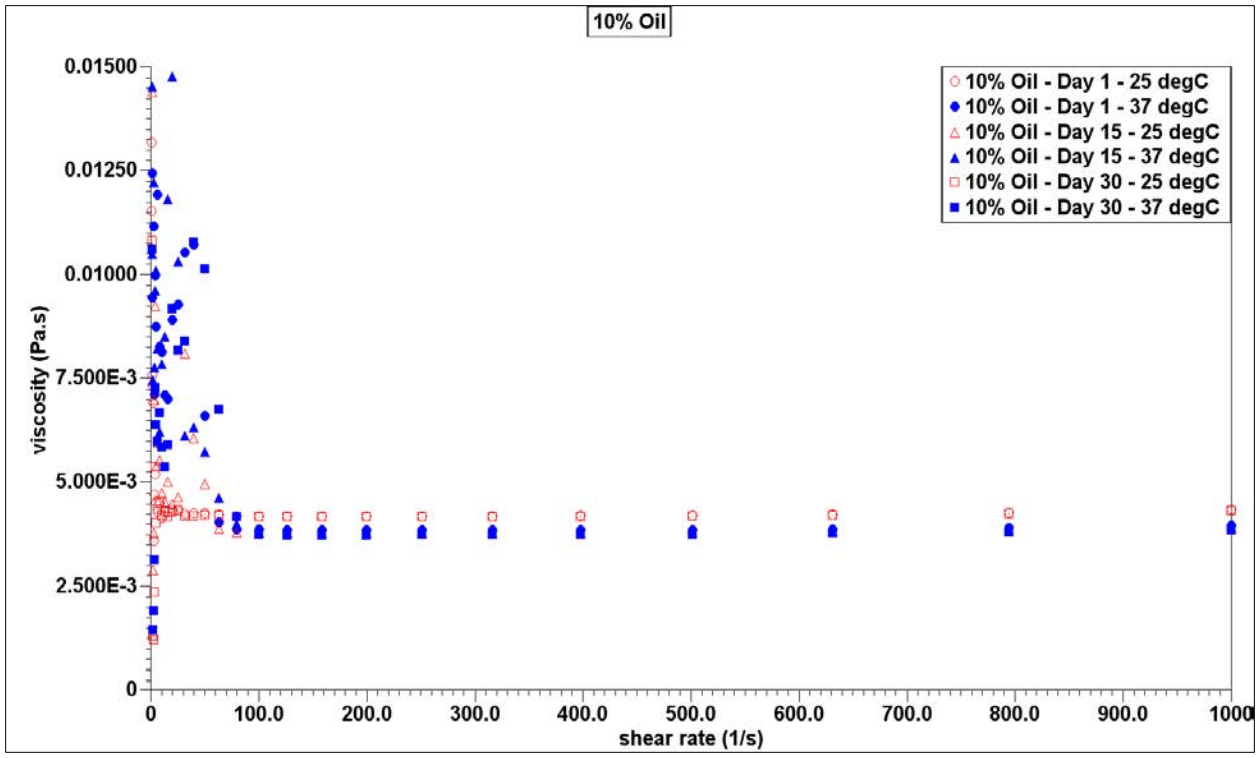

Figure 33. Viscosity results as a function of shear rate of nanoemulsions containing 10% oil phase at two different temperature values of 25℃ and 37℃ at days 1, 15, and 30.

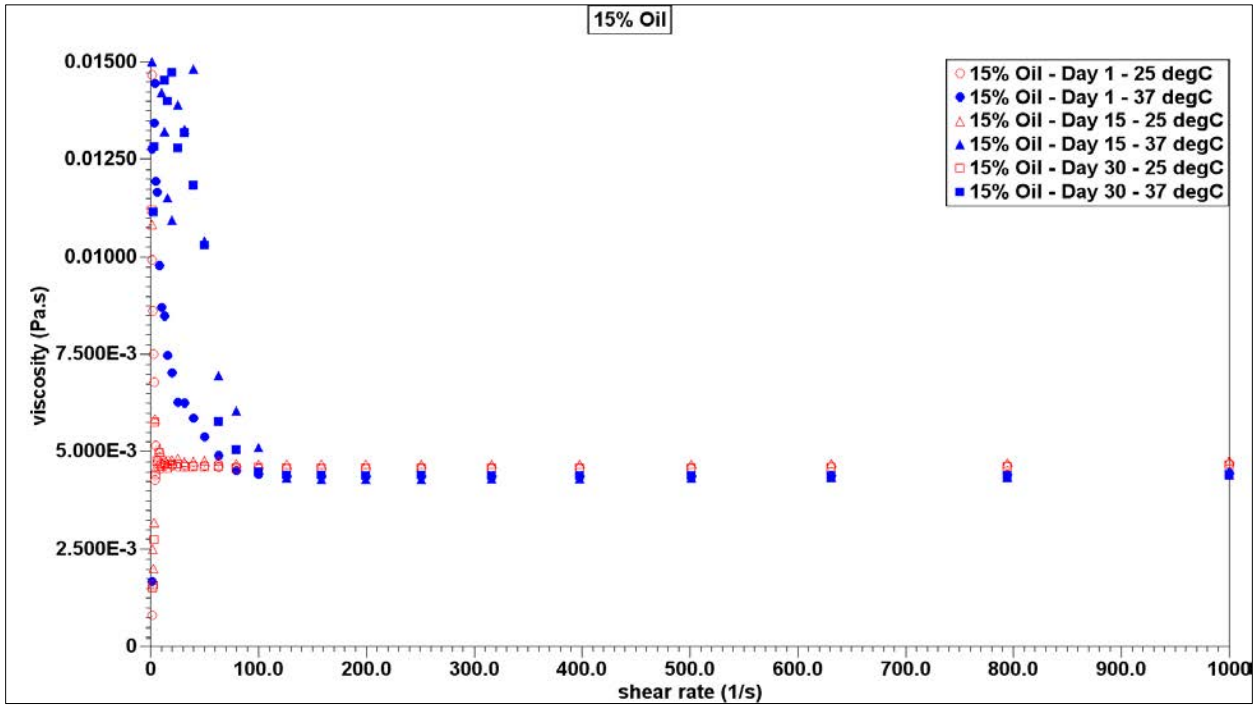

Figure 34. Viscosity results as a function of shear rate of nanoemulsions containing 15% oil phase at two different temperature values of 25℃ and 37℃ at days 1, 15, and 30.

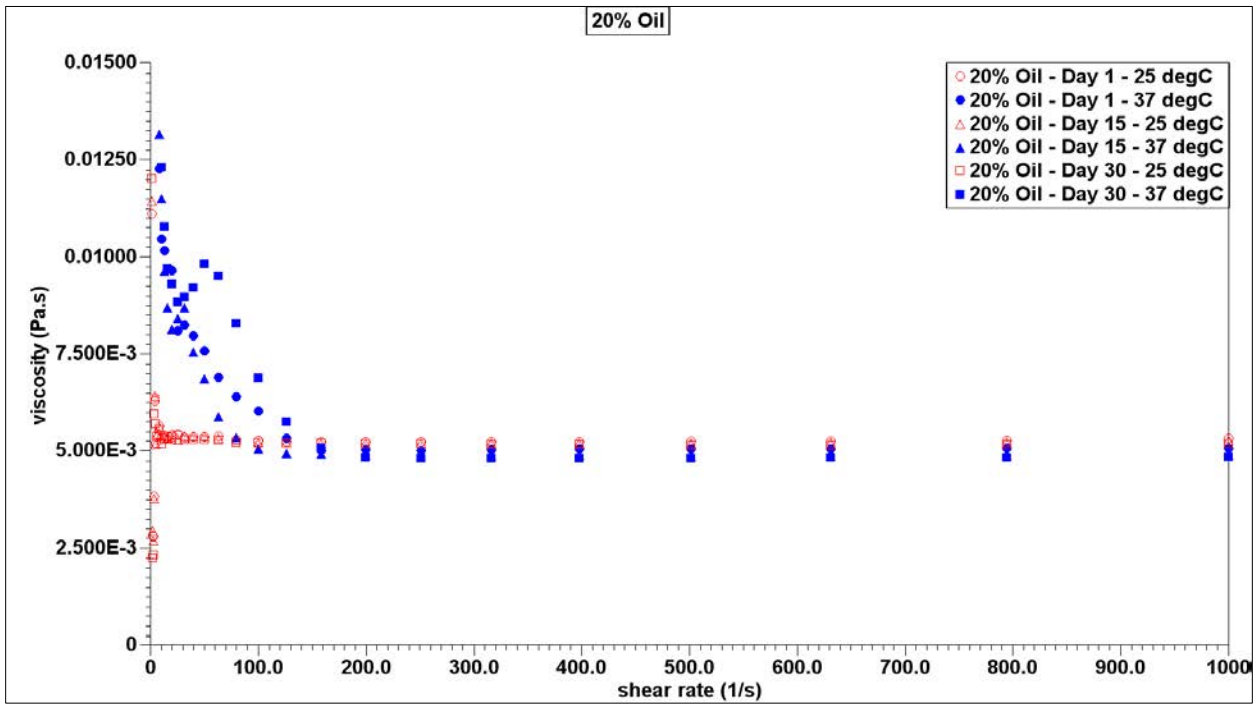

Figure 35. Viscosity results as a function of shear rate of nanoemulsions containing 20% oil phase at two different temperature values of 25℃ and 37℃ at days 1, 15, and 30.

4.6 Fourier Transform Infrared Spectroscopy Study

As shown in results of the FTIR study in Figure 36, the broad and intense band at around 3420 cm^{-1} belongs to an overlap between O–H and N–H stretching vibration, while pristine chitosan powder indicates a shallow peak, where peak depth increased upon preparing the chitosan solution and magnetic nanoparticle hydrogel. The two peaks existing at wavelengths of 2923 and 2879 cm^{-1} are attributed to the C–H stretching vibration of $–CH_2$ and $–CH_3$ aliphatic groups, respectively [138, 139]. The peaks at 2364 and 2337 cm^{-1} are assigned to the amino protonation of the $–NH_2$ and $–NHCOCH_3$ groups. As seen from this graph, upon the preparation of chitosan solution with HCl acid, the depth of these two peaks drastically increased, indicating generated protonated groups in the structure with the addition of HCl. Also, upon formation of the MNP hydrogel, these two peaks disappeared, which is due to the change in pH with the

addition of sodium bicarbonate. The peaks at 1649 and 1558 cm^{-1} refer to the C=O stretching vibration of the acetyl group and the C=O stretching vibration of the amine group (NH_2), respectively. The peaks at 1150, 1032, and 1375 cm^{-1} are related to C–O–C stretching vibration and C–H symmetric bending vibration, separately. The broad peak at 1070 indicates C–O stretching vibration in the chitosan spectrum. It was observed that C–H out-of-plane bending vibration and N–H wagging vibration occurred at ca. 898 and 660 cm^{-1} [140].

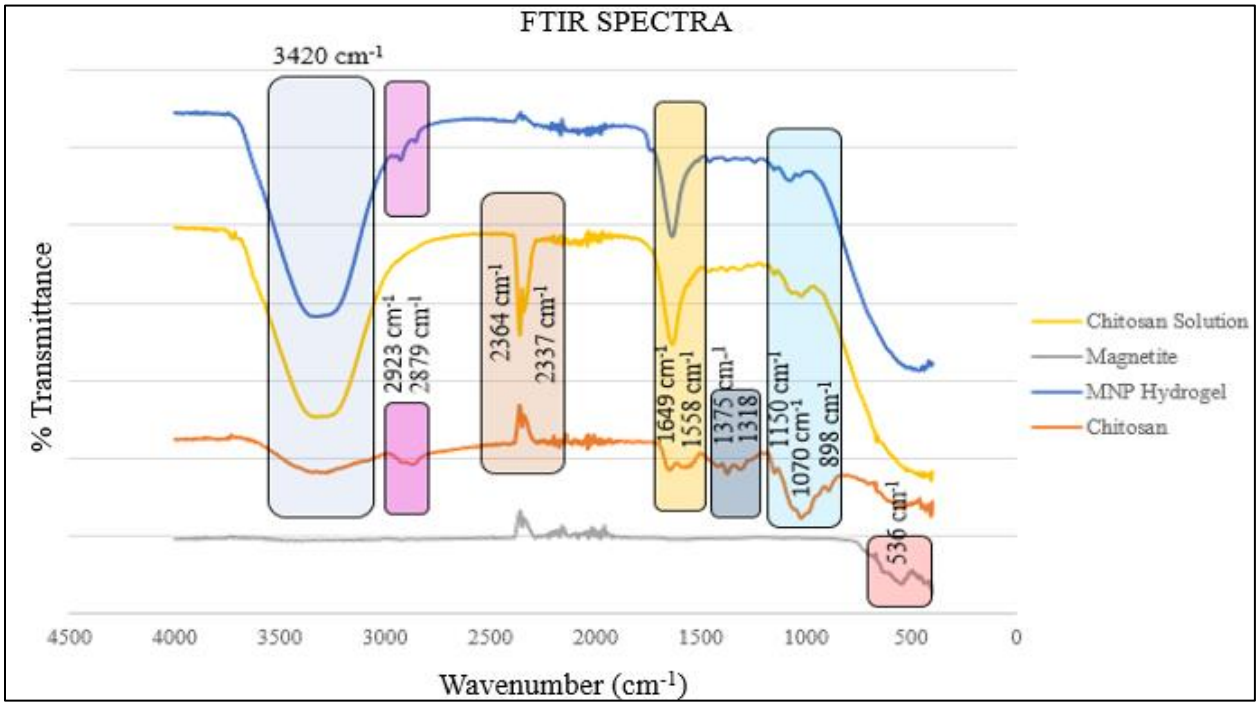

Figure 36. FTIR spectra of chitosan, chitosan solution, magnetite, and magnetic nanoparticle hydrogel.

4.7 Swelling Study and Kinetics

Swelling behaviors of the three hydrogels containing three different magnetic nanoparticle concentrations—8, 16, and 32 mg/ml—were plotted, based on the average of three trials. The swelling kinetics and time-dependent swelling behaviors of chitosan hydrogels in a PBS solution (pH 7.4) at 37ºC were investigated, and results from the experiments are shown in Figures 37 and 38. These graphs clearly indicate that swelling percentages and water content of

the hydrogels decrease with increasing MNP concentration. In addition, at greater MNP percentages, hydrogels did not exhibit much change in the swelling ratio with time. This was associated with the MNPs acting as a crosslinker agent, better proving the intense network in the structure, which eventually decreases the amount of water absorbed into it.

Also, equilibrium swelling ratio and equilibrium water content, which are the maximum reachable swelling ratio and water content, were found to be reached after eight hours. After that time, no further swelling or water content increment was observed, indicating that equilibrium swelling and water content were reached.

Using Fickian diffusion law, diffusion and swelling coefficients were determined, thus providing information about the nature of water absorption into the hydrogel matrix. These results are shown in Table 11.

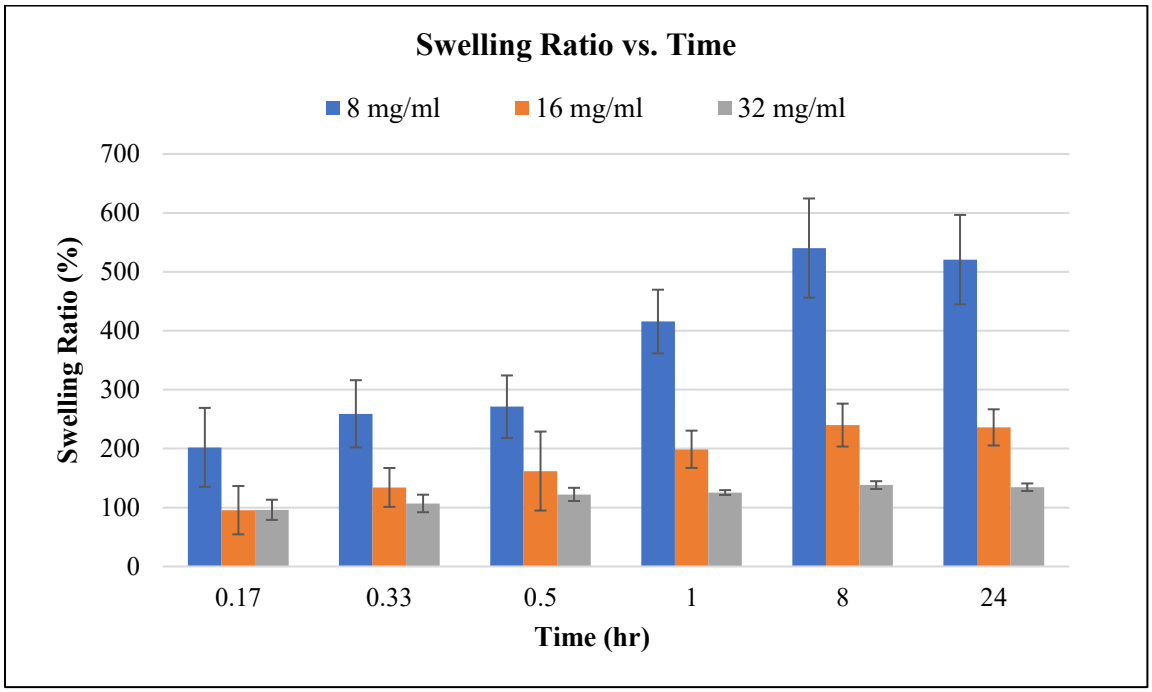

Figure 37. Swelling ratio of hydrogels with magnetite concentrations of 8, l6, and 32 mg/ml collected after 1, 8, and 24 hours.

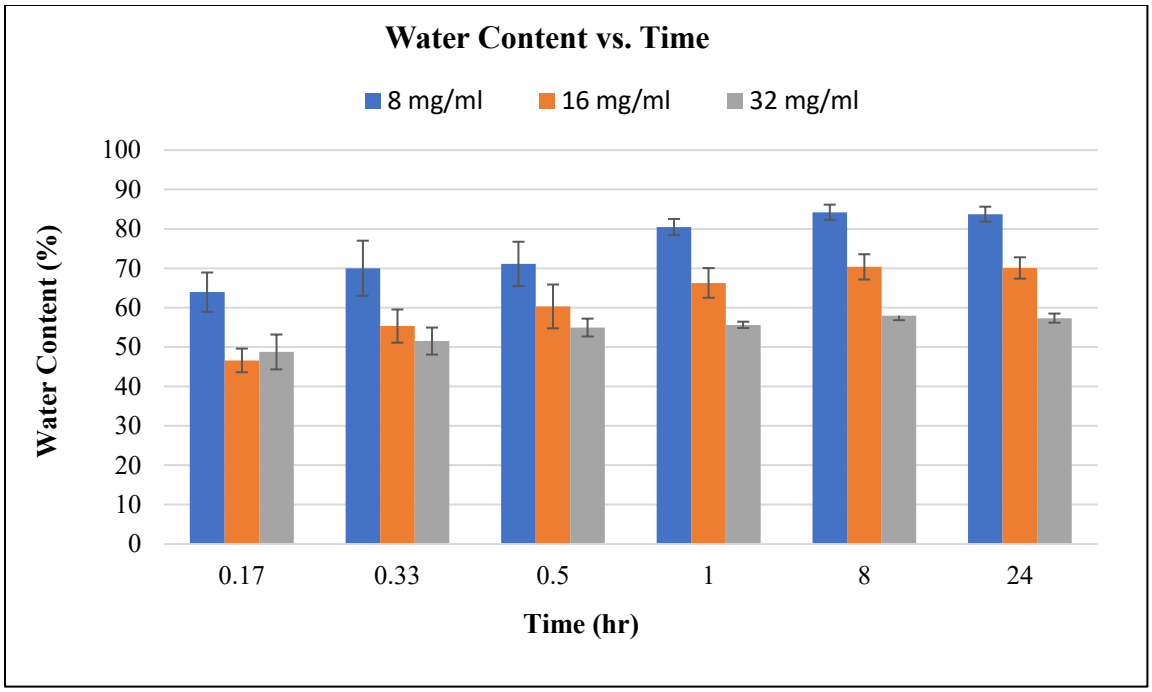

Figure 38. Water content of hydrogels with magnetite concentrations of 8, 16, and 32 mg/ml collected after 1, 8, and 24 hours.

TABLE 11

DIFFUSION AND SWELLING COEFFICIENTS OF MAGNETIC NANOEMULSION HYDROGELS SAMPLES CANTAINING 8, 16, AND 32 mg/ml OF MAGNETIC NANOPARTICLES

Sample	Diffusion Exponent (n)	Diffusion Constant (k)
MNH-8 mg/ml	0.3582	0.1639
MNH-16 mg/ml	0.4895	0.1290
MNH-32 mg/ml	0.1539	0.4884

4.8 Drug-Release Study and Kinetics

The drug-release study was completed in 48 hours, and the collected samples were run in the UV-Vis spectrometer to calculate the released drug concentrations. For this purpose, first, the calibration curve for 5-FU was created, and the results are shown in Figure 39. Later, these

results were used to calculate the cumulative drug release (CDR), and the results, which are plotted in Figure 40 were fit into five different drug-release models. Plots created for these five models are shown in the Appendix (Figures A1 to A15). Based on the highest R^2 values, the best-fitting models were determined and shown in Table 12.

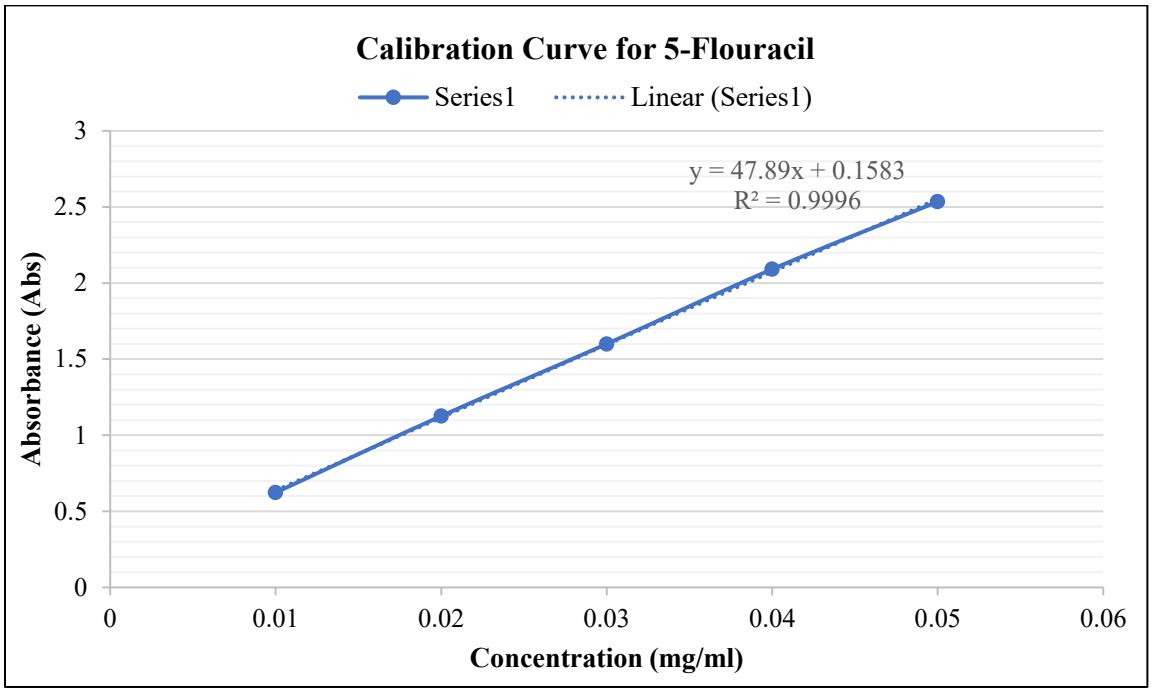

Figure 39. Calibration curve for 5-Flouracil.

According to the drug-release kinetics study, it was concluded that adding magnetic nanoparticles into plain chitosan hydrogels caused a drop in the CDR percentage. This was attributed to the more compact structure formation of the MNPs, which acted as a barrier against drug release. When decreasing the water uptake percentages with increasing MNP percentages was considered (Figure 38), this can be associated to the diffusion rate of the medium into the hydrogel structure, which eventually caused less CDR. On the other hand, it was observed that in the case of loading the drug into magnetic nanoemulsion hydrogel, the CDR percentage increased, which was attributed to the hydrophilic nature of the drug (5-FU). While at the end of two days the CDR was approximately at 35% and 30% for plain chitosan hydrogel and magnetic

nanoparticle-incorporated chitosan hydrogel, respectively, this number was 46% for MNHs. Another observation from the release test was relative to saturation of drugs in the structure. For plain chitosan hydrogels and magnetic nanoparticle-incorporated chitosan hydrogel, a plateau starting from the 8th hour was observed, after which no increase was observed in the CDR percentage. However, for the MNH samples, drug release was seen to be continuous. CDR percentage values were seen to be increasing at the end of each time period, indicating a continuation in drug release.

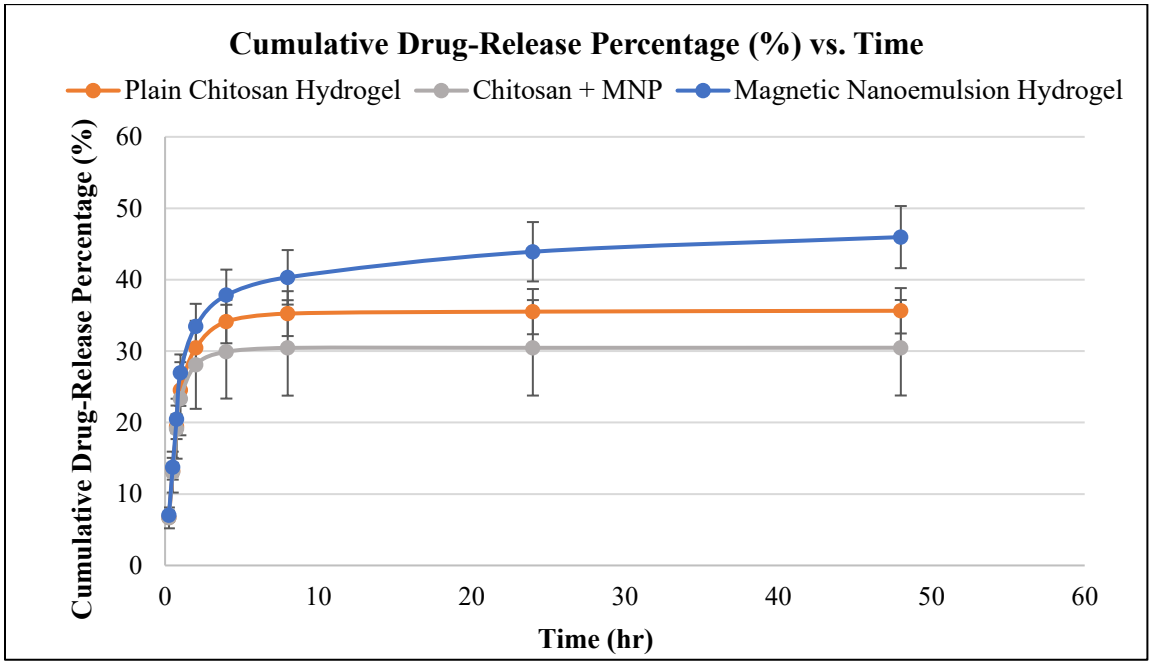

Figure 40. Cumulative drug-release percentages from plain chitosan hydrogel, chitosan hydrogel incorporated with magnetic nanoparticles, and magnetic nanoemulsion hydrogels.

For the quantification of drug-release behavior from hydrogel structures, CDR study results were fitted into five different drug-release models. Based on these results, the best-fitting model was determined to be the Higuchi release model. From this model, R^2 values obtained were 0.9257, 0.8839, and 0.9224 for MNHs, chitosan hydrogels incorporated with MNPs, and plain chitosan hydrogels, respectively.

TABLE 12

R^2 VALUES OF CUMULATIVE RELEASE PERCENTAGES FITTED INTO FIVE DIFFERENT DRUG-RELEASE MODELS

Drug-Release Models	**R^2 Values**		
	Magnetic Nanoemulsion Hydrogel	**Chitosan Hydrogel + Magnetic Nanoparticles**	**Plain Chitosan Hydrogel**
Zero-Order	0.7430	0.6557	0.7277
First-Order	0.7852	0.6862	0.7662
Higuchi	0.9257	0.8839	0.9224
Korsmeyer-Peppas	0.8912	0.8473	0.8850
Hixson-Crowell	0.7714	0.6761	0.7536

4.8 Hyperthermia Study Analysis

Hyperthermia studies were conducted at three different magnetic field strengths and three different magnetic nanoparticle concentrations for 20 minutes. Temperature values collected every 5 minutes for 20 minutes were plotted, and the results are shown in Figures 41 to 43. These graphs indicate that increasing the magnetic field strength and increasing the magnetic nanoparticle concentration resulted in an observable increment in sample temperature.

Results collected from samples with a magnetic nanoparticle concentration of 8 mg/ml showed that this concentration was not enough to reach the temperature required for hyperthermia at all chosen MFSs. Moreover, the results also indicated that increasing the MFS from 22 kA/m to 33 kA/m did not cause a remarkable change in the temperature increment of the samples. These results suggest that there might be a maximum MFS to be applied on a material with a certain magnetic nanoparticles concentration, beyond which applying a further magnetic field would not affect the results.

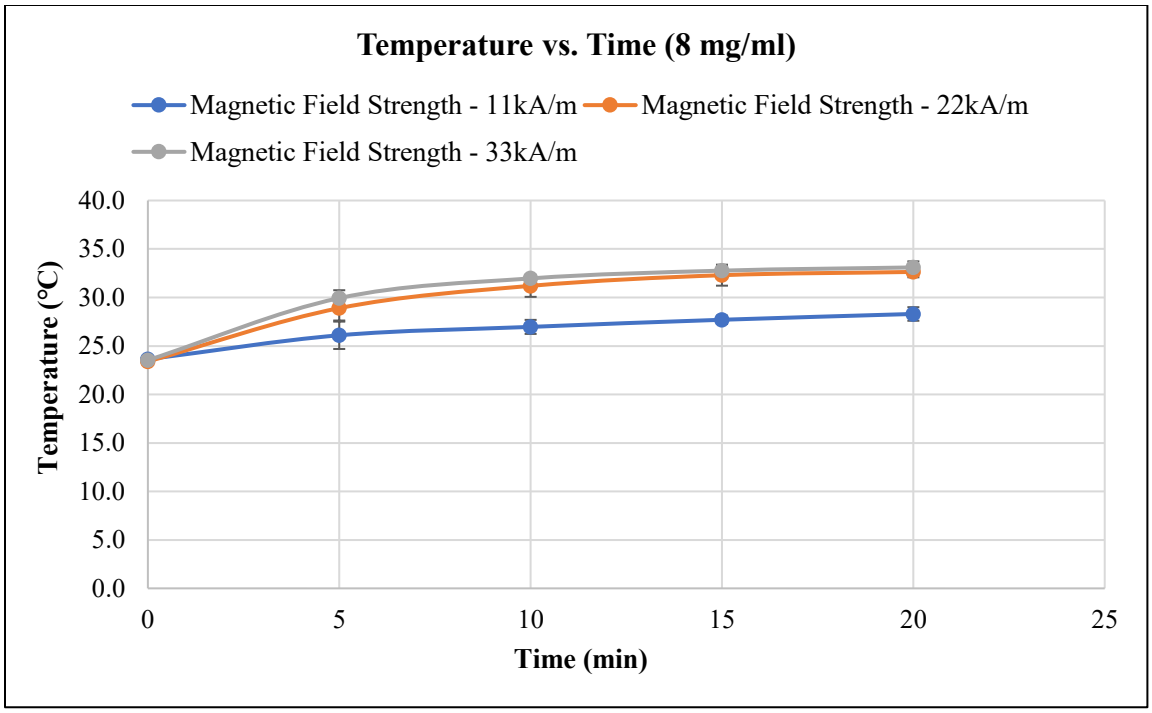

Figure 41. Temperature data collected during 20 minutes from samples with magnetic nanoparticle concentration of 8 mg/ml at three different magnetic field strengths of 11, 22, and 33 kA/m.

When the concentration of magnetic nanoparticles was increased to 16 and 32 mg/ml, all samples exhibited an increase in temperature values. For samples with a 16 mg/ml MNP concentration, the MFS of 11 kA/m was seen to be not very effective in the temperature increment, compared to the 8 mg/ml sample. At greater MFS values of 22 and 33 kA/m, the temperature was seen to increase more significantly.

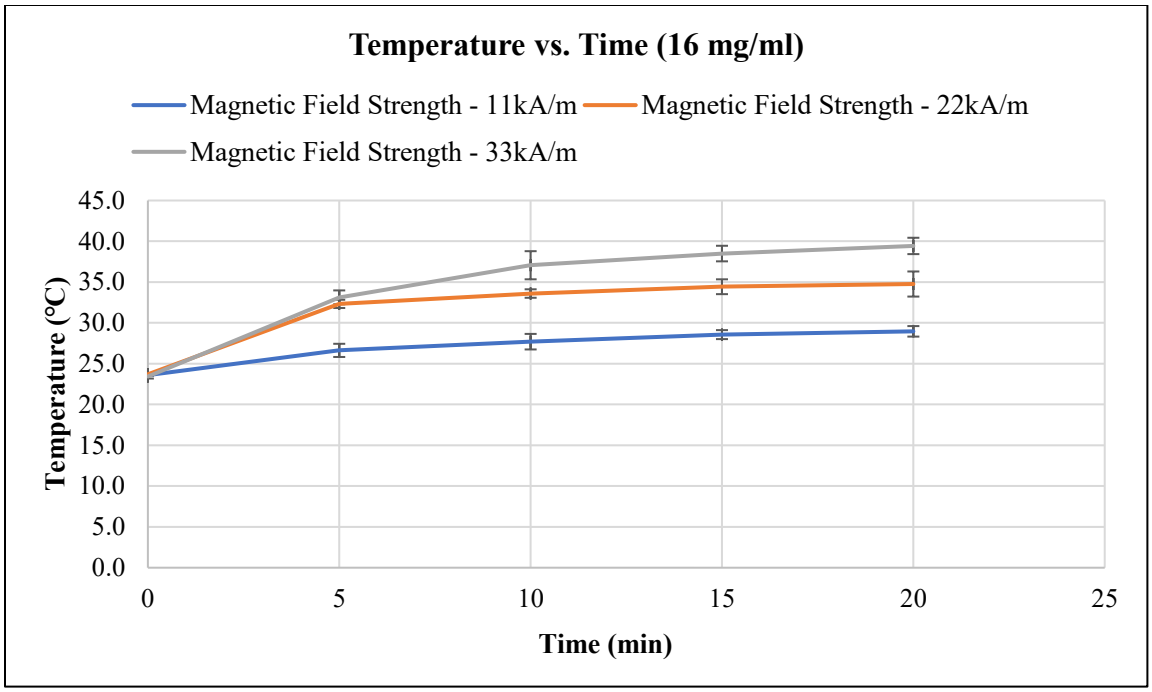

Figure 42. Temperature data collected during 20 minutes from samples with magnetic nanoparticle concentration of 16 mg/ml at three different magnetic field strengths of 11, 22, and 33 kA/m.

This study aimed to reach the hyperthermia temperature, which falls between 42℃ and 45℃. This target was achieved at a magnetic nanoparticle concentration of 32 mg/ml at the MFS of 22 kA/m and higher. Even though the temperature increased to 40℃ at an MNP concentration of 16 mg/ml and MFS of 33 kA/m, the increment did not reach 42℃. This result suggests that there could be a way to achieve a hyperthermia temperature range with a lower magnetic nanoparticle concentration by adjusting either the magnetic field strength or time. On the other hand, a longer period of time would be necessary to reach the targeted temperature, while it requires only 5 minutes to reach the hyperthermia temperature.

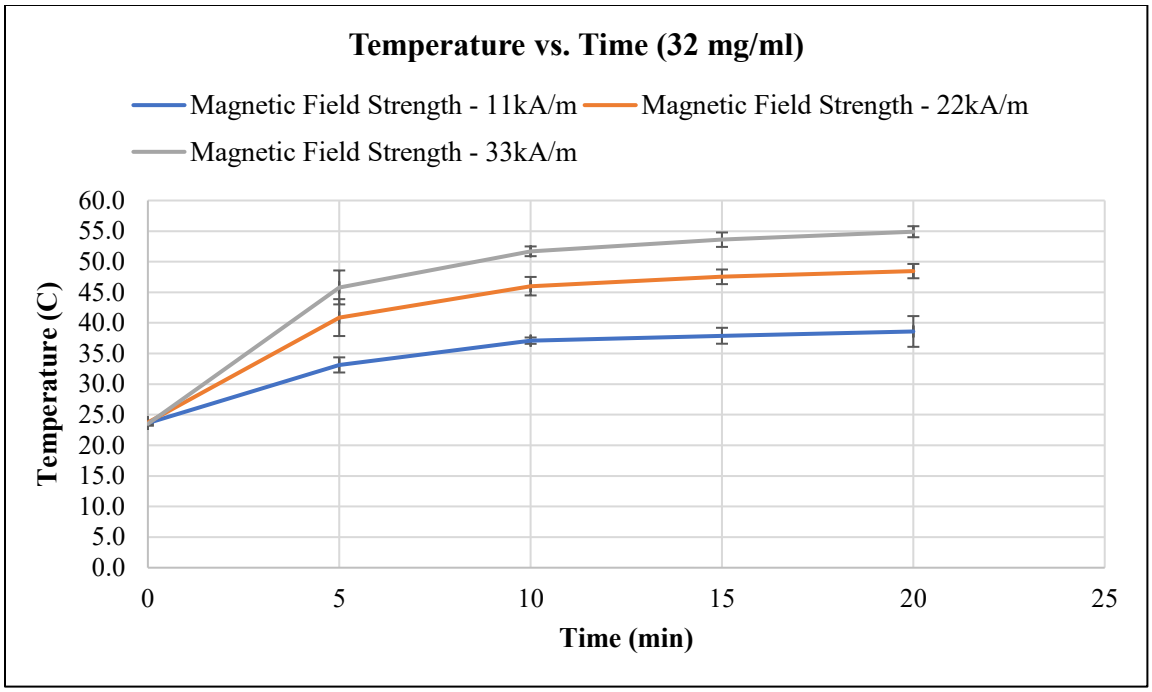

Figure 43. Temperature data collected during 20 minutes from samples with magnetic nanoparticle concentration of 32 mg/ml at three different magnetic field strengths of 11, 22, and 33 kA/m.

4.8 Statistical Analysis

An analysis of variance (ANOVA) table of the model was obtained using Design-Expert 7.0 software, and the results are shown in Table 13. As can be seen, the overall model is significant, with a *P*-value less than 0.0001. Moreover, all other main factors and two factor interactions were seen to be significant, with a *P*-value less than 0.0001 and 0.05. Also, R^2 and Adjusted-R^2 values of 0.9823 and 0.9774, respectively, indicate that the model is strong (Table 14). The "Lack of Fit F-value" of 0.57 implies that the lack of fit is not significant relative to the pure error, which is the indicator of whether that model can fit. The three-factor interaction was seen to be not significant, with a *P*-value of 0.8578. When this is compared to the cutoff value for significance, which is 0.05 in statistics, because of the high *P*-value, which is greater than 0.05, the ABC interaction was not included in the model. In addition, the effect of BC interaction

(interaction between MFS and concentration) on temperature at the maximized time of the 20th minute is plotted in Figure 44.

TABLE 13

ANOVA TABLE OF MODEL

Source	Sum of Squares	df	Mean Square	F Value	*P*-Value Prob > F	
Model	6683.18	23	290.57	202.62	< 0.0001	**significant**
A-Time	350.72	3	116.91	81.52	< 0.0001	
B-MFS	1686.67	2	843.33	588.08	< 0.0001	
C-Concentration	4251.74	2	2125.87	1482.43	< 0.0001	
AB	22.47	6	3.75	2.61	0.0227	
AC	60.5	6	10.08	7.03	< 0.0001	
BC	311.09	4	77.77	54.23	< 0.0001	
Residual	120.46	84	1.43			
Lack of Fit	10.48	12	0.87	0.57	0.8578	**not significant**
Pure Error	109.98	72	1.53			
Cor Total	6803.64	107				

TABLE 14

STATICTICAL RESULTS FROM ANALYSIS OF VARIANCE

Standard Deviation	1.2	**R-Squared**	0.9823
Mean	35.91	**Adj R-Squared**	0.9774
C.V%	3.34	**Pred R-Squared**	0.9707

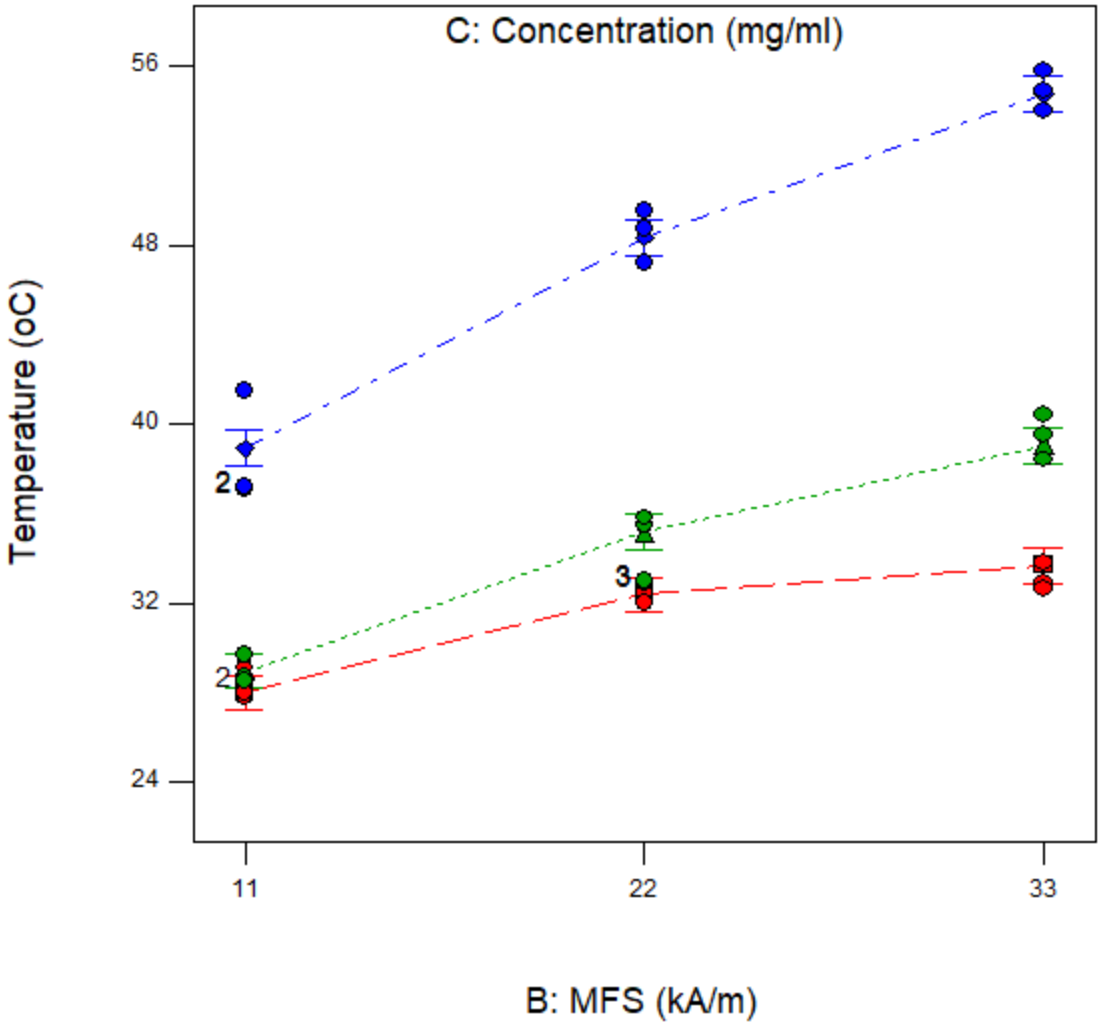

Figure 44. Plot showing interaction between three different MFS values and three different concentrations of 8 (red), 16 (green), and 32 (blue) mg/ml at maximized time of 20th minute.

Results more clearly indicate that at a low magnetic field strength of 11 kA/m, increasing the concentration from 8 to 16 mg/ml did not show a significant effect in temperature rise. When the concentration was increased to 32 mg/ml, there was a significant rise in temperature. On the other hand, at higher MFS values of 22 and 33 kA/m, the concentration increment was seen to have a more significant effect on temperature rise as a function of concentration. While the

maximum temperature reached at 8 and 16 mg/ml concentration levels did not show a significant difference at 11 kA/m, the increase in MFS increment to 22 and 33 kA/m allowed for the observation of concentration effect on temperature by exhibiting a significant difference at the maximum temperature reached. Moreover, when concentration was increased to 32 mg/ml, results showed a dramatic rise in temperature at the MFS of 33 kA/m. Overall, at higher MFS values, the effect of concentration on temperature rise was seen to be more significant.

Model diagnostics is another important procedure that should be completed. These procedures make it possible to check whether the assumptions of the regression model are valid and if there is any violation. Resulting diagnostics plots, such as normal plot, externally studentized residuals plot, and difference in fits (DFFITS), help decide whether subsequent inference results are trustable. These diagnostics plots are provided in the Appendix in Figures A16 to A19. In the second step of statistical analysis, an ANOVA table was created for continuous factors (numerical factors), in order to conduct an optimization study on the data collected. Based on the fit summary, models were compared, and among them, the quadratic model was chosen due to the significant *P*-value for this model with a value of less than 0.0001 and not being significant for "lack of fit" with a value of 0.54, which is greater than 0.05 (Table 15).

TABLE 15

FIT SUMMARY FOR SEQUENTIAL MODEL AND LACK OF FIT TEST

	Sequential Model	**Lack of Fit Test**
Source	Quadratic vs 2FI	Quadratic
F-Value	41.83	0.95
***P*-Value Prob > F**	< 0.0001	0.54

Three-dimensional (3D) surface graphs involving temperature, time, and magnetic field strength are provided in Figures 45 to 47. When the third factor is maximized, the effect of the other two-factor interactions on temperature are shown in these graphs. The twist generated on the 3D surface indicates that there is not just one factor interaction, but rather a significant interaction between two factors. This suggest handling the change of the level of factors corresponding to the other factors. Figure 45 indicates the temperature change corresponding to both time and magnetic field strength. As shown, at a chosen MFS, time caused a logarithmic increment in the temperature. Also, temperature tends to reach a plateau over time. This behavior is more obvious at lower MFS values. With increasing MFS, temperature was seen to increase by time, and the sample was less likely to reach a plateau during induction heating.

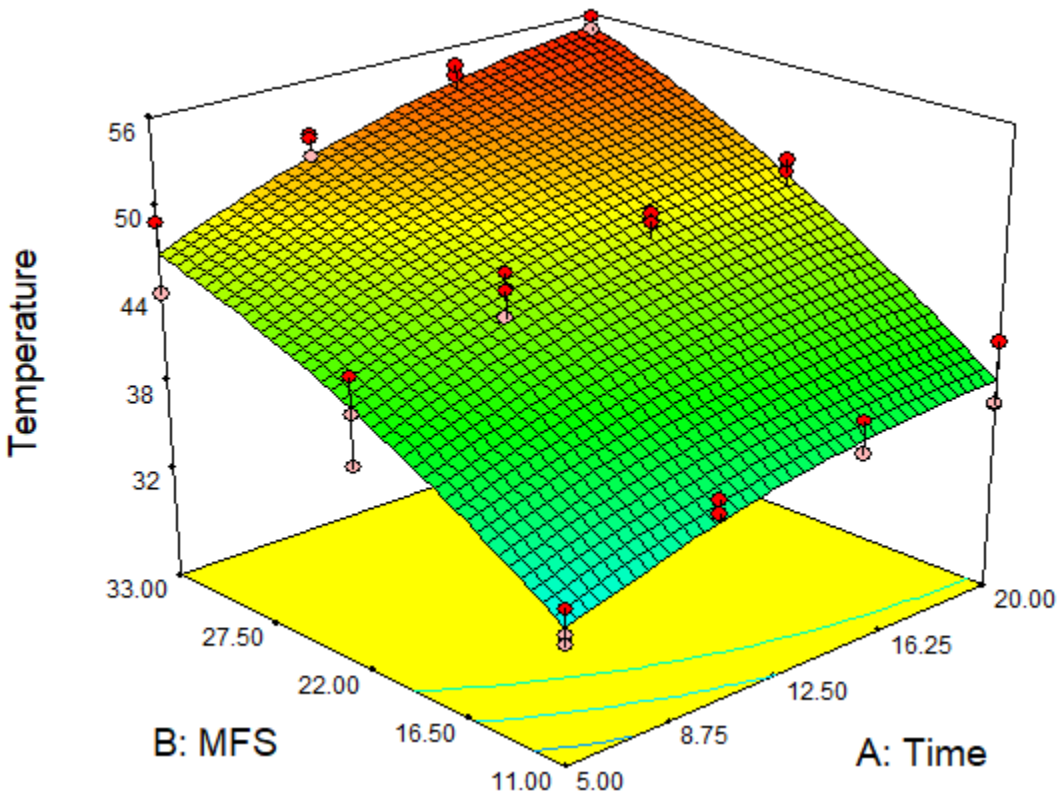

Figure 45. Temperature-time-MFS graph at maximized magnetic nanoparticle concentration of 32 mg/ml.

Figure 46 shows the temperature response of materials corresponding to time and concentration at a maximized MFS value of 33 kA/m. This graph is similar to the previous graph of temperature, time, and MFS. At a lower concentration of magnetic nanoparticles, the temperature increase was slow, plateauing at around the 15th minute and samples not showing a further temperature increment. With an increasing MNP concentration, materials showed drastic rise in temperature with time.

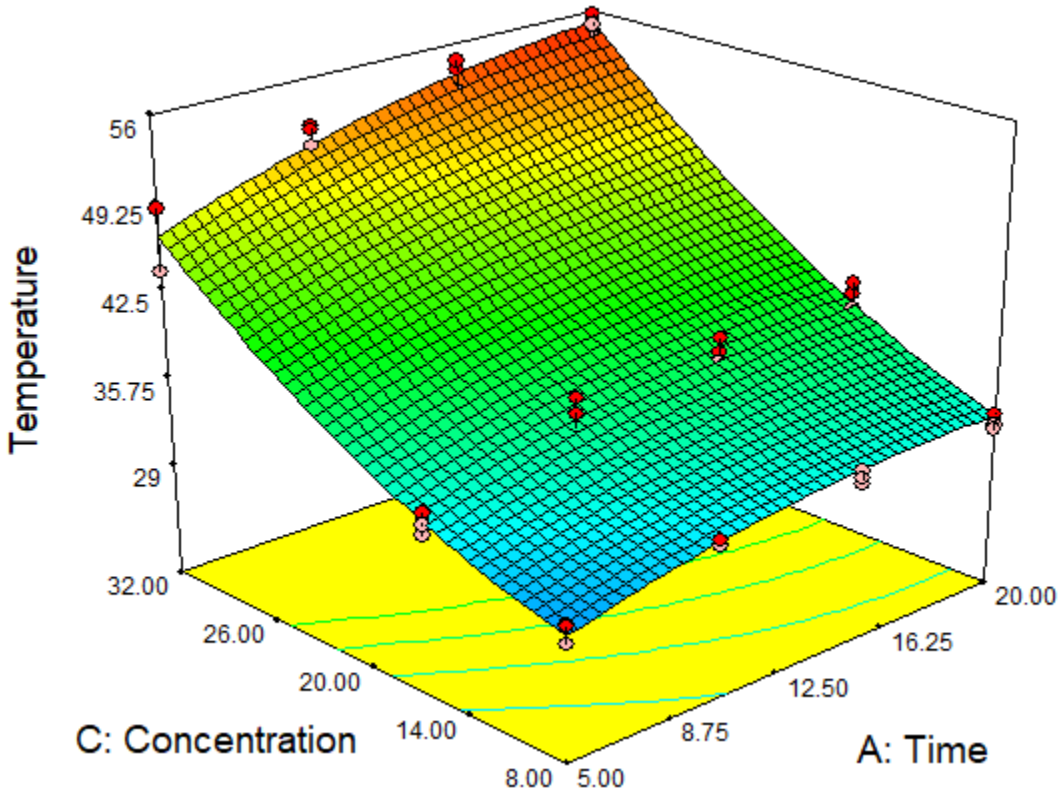

Figure 46. Temperature-time-concentration graph at maximized MFS of 33 kA/m.

The temperature-MFS-concentration graph shown in Figure 47 indicates that at a chosen concentration level, the temperature exhibited a logarithmic increase with increasing MFS. However, at a fixed MFS value, while the concentration increased, the temperature also increased in an exponential manner.

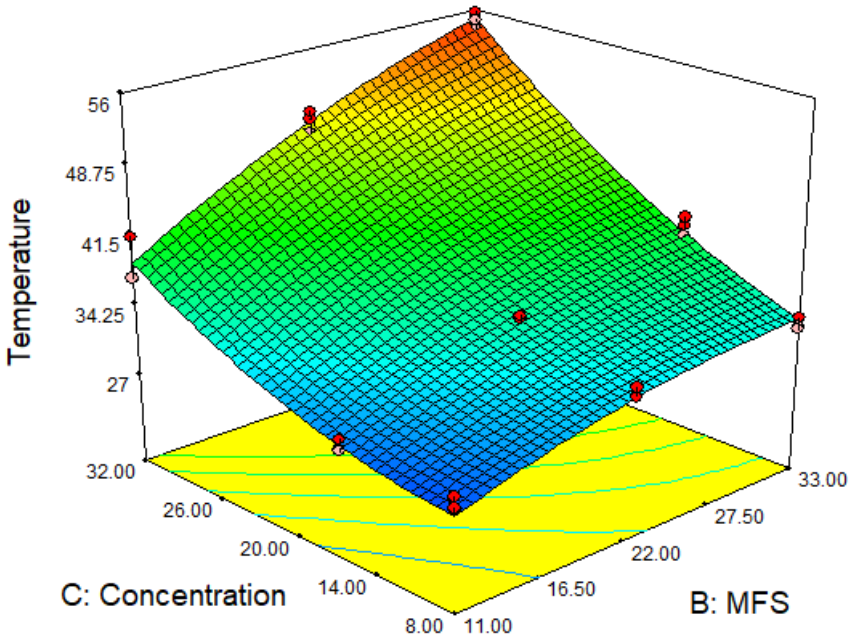

Figure 47. Temperature-MFS-concentration graph at maximized time of 20 minutes.

A cube diagram for temperature responses for a combination of corresponding factors is shown in Figure 48. As can be seen, when the concentration, time, and MFS are maximized, the samples exhibit better heating properties.

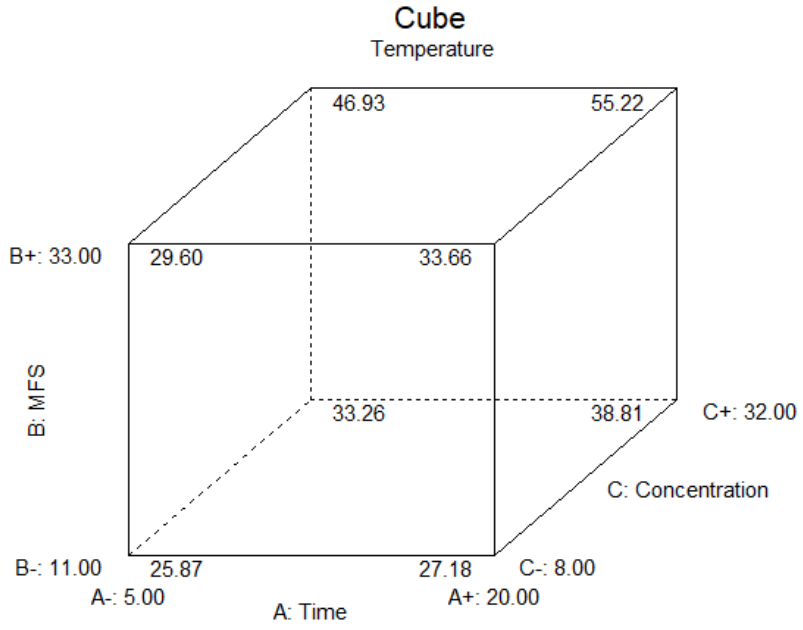

Figure 48. Cube diagram of temperature response corresponding to factors of concentration, time, and magnetic field strength.

Due to possible restrictions during a hyperthermia study, such as AC field application time, heating amount, and lower magnetic field requirement, an optimization study for the test was conducted to find possible solutions for a certain temperature range. Because hyperthermia requires a temperature range between 42°C and 45°C, the targeted temperature in the optimization study was chosen to be in this same range. Other factors set in the range included the lowest and highest levels chosen for each factor. The optimization study yielded 30 solutions, which are listed in Table 16. Considering that samples did not exhibit a significant temperature increment after the 20th minute, this information can help decide which combination of time, MFS, and concentration would be the best solution to provide a hyperthermia temperature range at the 20th minute, which will assure the least temperature increment after 20 minutes, in order for controlling the hyperthermia operation in a safe range.

TABLE 16

THIRTY POSSIBLE SOLUTIONS FROM OPTIMIZATION STUDY

Number	Time (min)	MFS (kA/m)	Concentration (mg/ml)	Temperature (ºC)	Desirability
1	19.46	30.74	22.22	43.4479	1
2	10.06	19.36	31.91	43.1759	1
3	13.68	32.93	24.67	44.9573	1
4	11.94	23.55	26.47	42.0168	1
5	14.65	30.68	21.87	42.1156	1
6	13.64	31.08	23.13	42.9797	1
7	12.55	16.92	31.81	42.421	1
8	14.87	31.25	21.89	42.3614	1
9	9.06	30.02	24.97	42.0173	1
10	14.43	18.36	30.61	43.1739	1
11	9.36	22.83	31.5	44.7436	1

TABLE 16 (continued)

Number	Time (min)	MFS (kA/m)	Concentration (mg/ml)	Temperature (°C)	Desirability
12	17.21	25.01	24.98	43.1552	1
13	11.04	32.83	22.86	42.0345	1
14	7.95	32.62	27.13	44.0834	1
15	18.86	27.91	23.04	43.0546	1
16	14.58	21.33	29.81	44.6324	1
17	14.23	29.86	23.09	42.7729	1
18	19.01	26.82	22.58	42.2003	1
19	15.87	30.94	22.68	43.2618	1
20	6.76	24.31	31.32	43.7156	1
21	10.27	32.5	23.78	42.3632	1
22	18.86	21.93	27.58	43.9372	1
23	18.54	29.95	24.03	44.7363	1
24	14.27	23.82	26.32	42.9328	1
25	6.74	22.4	30.86	42.161	1
26	19.14	29.18	21.35	42.0976	1
27	19.47	19.54	28.59	43.2612	1
28	16.15	30.49	21.34	42.0208	1
29	10.79	29.72	27.2	44.9476	1
30	15.29	23.17	25.48	42.1672	1

As mentioned previously, reaching the temperature range of hyperthermia at the 20th minute of time is desired so that temperature can be controlled, and the risk of exceeding the maximum hyperthermia temperature of 45℃ can be minimized. One out of the 30 solutions provided from the optimization study is shown in Figure 49 as an example. As can be seen, at the 18.29th minute, the temperature falls between 42℃ and 45℃. From the perspective of both time

and the targeted temperature values, this graph can suggest one of the best solutions to be used in further studies.

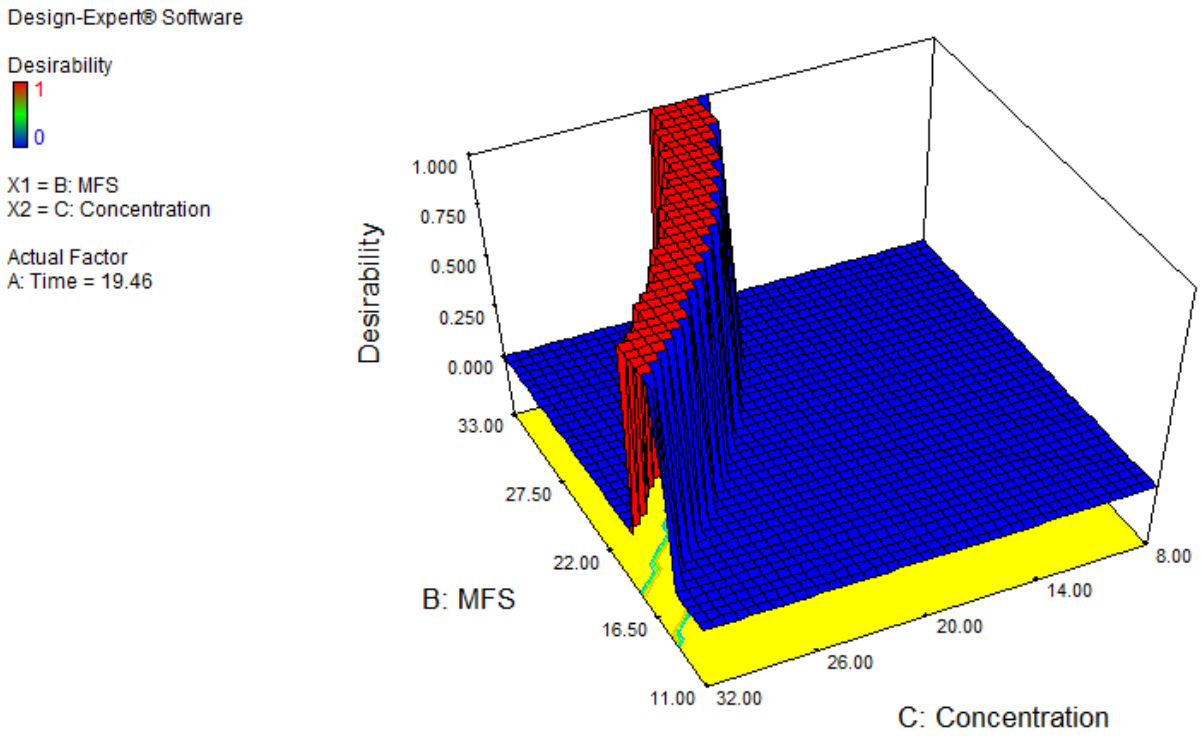

Figure 49. One solution obtained from optimization study for finding possible solutions providing temperature range between targeted values of 42℃ and 45℃.

In the next step, confirmation of the optimization study was completed. The goal here was to confirm the predicted solutions obtained in order to reach a targeted hyperthermia temperature between the ranges of the other three factors. For this purpose, a new design was generated using the optimization tool. In this new study, instead of continuing the experiment with the previous concentration values, and changing only the MFS, a new sample containing 24 mg/ml of magnetic nanoparticle was fabricated. In the optimization tool, the temperature value of 42ºC was targeted. The target concentration was chosen as 24 mg/ml, and the goal was to reach this temperature around the 20th minute. This design was created in the software, and the possible solutions are given in Table 17.

TABLE 17

EIGHTEEN POSSIBLE SOLUTIONS FROM OPTIMIZATION STUDY

Number	Time (min)	MFS (kA/m)	Concentration (mg/ml)	Temperature (°C)	Desirability
1	12.35	27.57	24	41.9999	1
2	19.2	23.92	24	42	1
3	9.51	31.97	24	42	1
4	14.72	25.58	24	42	1
5	11.41	28.7	24	41.9999	1
6	18.53	24.04	24	42	1
7	11.31	28.83	24	42	1
8	18.82	23.98	24	42	1
9	18.2	24.11	24	42	1
10	9.15	32.87	24	42	1
11	19.99	23.84	24	42	1
12	15.16	25.31	24	42	1
13	10.26	30.47	24	42	1
14	8.55	33	24.39	42	0.976
15	20	26.09	22.66	42.0001	0.957
16	20	22.2	25.11	42	0.928
17	20	28.82	21.32	41.9999	0.913
18	15.48	21.54	26.37	41.9999	0.839

Based on the solutions provided in Table 17, solution 11 was chosen. Magnetic nanoemulsion hydrogel samples including 24 mg/ml of MNP were placed in a coil, and a magnetic field strength of 24 kA/m was applied. At the end of 20 minutes, the final temperatures were recorded. The results acquired from three samples are given in Table 18.

TABLE 18

FINAL TEMPERATURES REACHED AT 20th MINUTE FOR HYDROGEL SAMPLES CONTAINING 24 MG/ML OF MAGNETIC NANOPARTICLES

First Sample	Second Sample	Third Sample
42.4	42.5	41.9
Average = 42.3 (sd = ± 0.32)		

When the experimental results were compared to the predicted result under the given criteria, it was observed that the results matched each other. While solution 11 gave a temperature value of 42ºC, the average of the experimental results was 42.3ºC, with a standard deviation of ± 0.32. The reason for the small difference between the experimental and predicted values could be the slight difference in the magnetic field strength. While the solution provided an MFS value of 23.84 kA/m, the MFS value that was set for the experiment was 24 kA/m. On the other hand, when the standard deviation value of ± 0.32 is compared to the standard deviation value provided by the design study, which is ± 1.22, the temperature of 42.3ºC is acceptable and supports the possible solutions acquired from ANOVA.

4.9 Specific Loss Power Analysis

Specific loss power calculations were conducted on magnetic nanoparticle-incorporated hydrogels with three different nanoparticle concentrations—8, 16, and 32 mg/ml. First, the initial slopes of heating curves were created (Figures 50 to 52). Later on, the specific heat capacity of the samples was calculated (Figure 53) and multiplied by the mass of the gels to obtain the heat capacity of the samples. Finally, SLPs were calculated using equation (18), and these results are shown in Figure 54. According to the graph in Figure 54, it can be said that the specific loss power, that is, the heat dissipation power of the samples, was seen to be indepentent of the

magnetic nanoparticle concentration. Even though, higher temperature values were obtained during the hyperthermia study with the increasing magnetic nanoparticle concentration. The magnetic nanoparticle concentration did not exhibit a proportinal increment effect on SLP. A significant increment in the SLP value was seen to be the result of an increment in the magnetic field strength. As the magnetic field strength increased from 11 kA/m to 22 and 33 kA/m, an obvious increment was observed in each type of material.

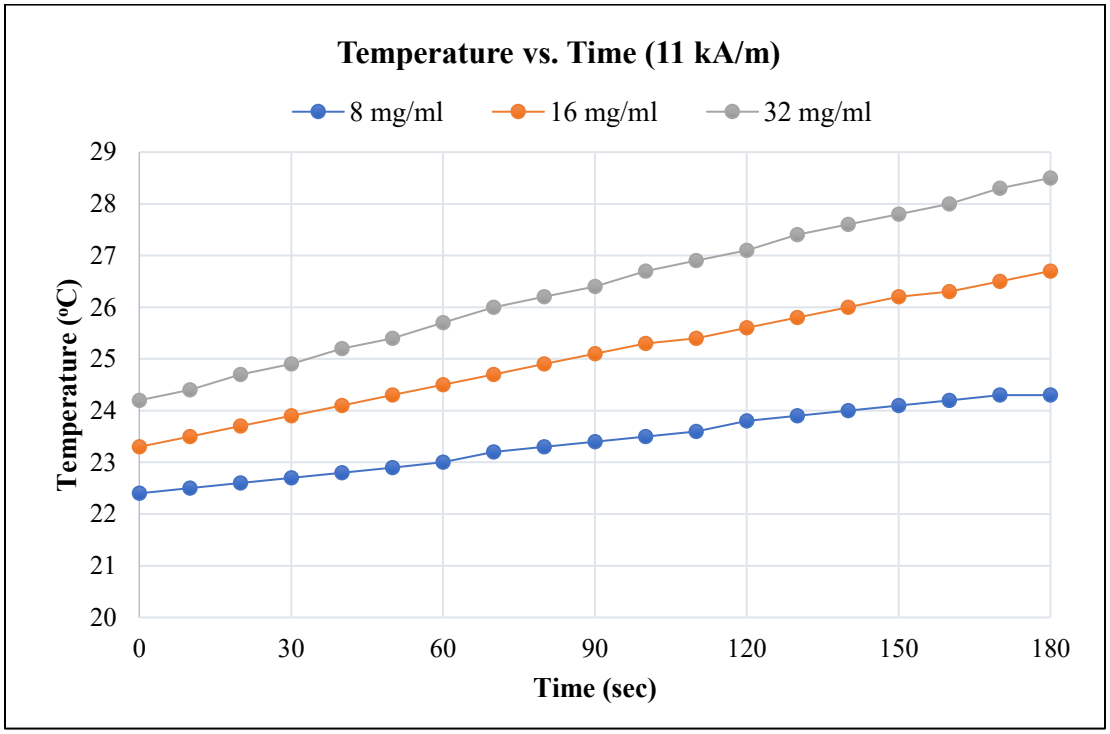

Figure 50. Initial heating curve of magnetic nanoemulsion hydrogels containing 8, 16, and 32 mg/ml of magnetic nanoparticles under magnetic field strength of 11 kA/m.

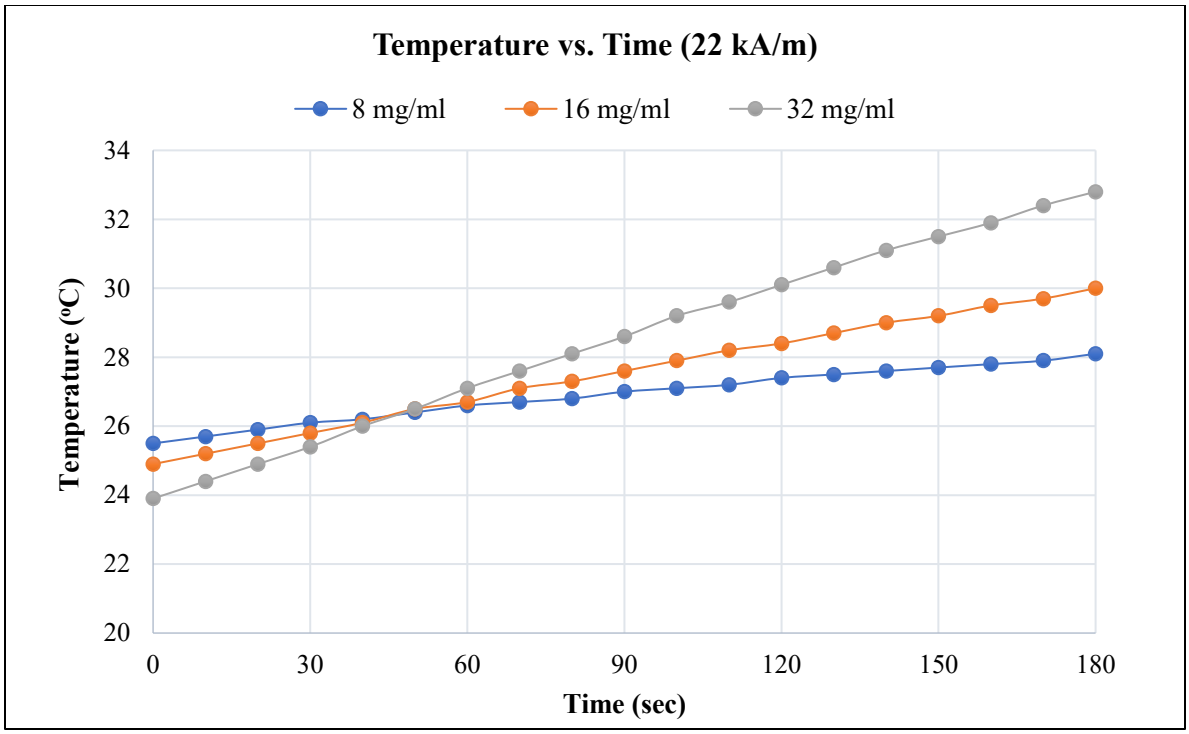

Figure 51. Initial heating curve of magnetic nanoemulsion hydrogels containing 8, 16, and 32 mg/ml of magnetic nanoparticles under magnetic field strength of 22 kA/m.

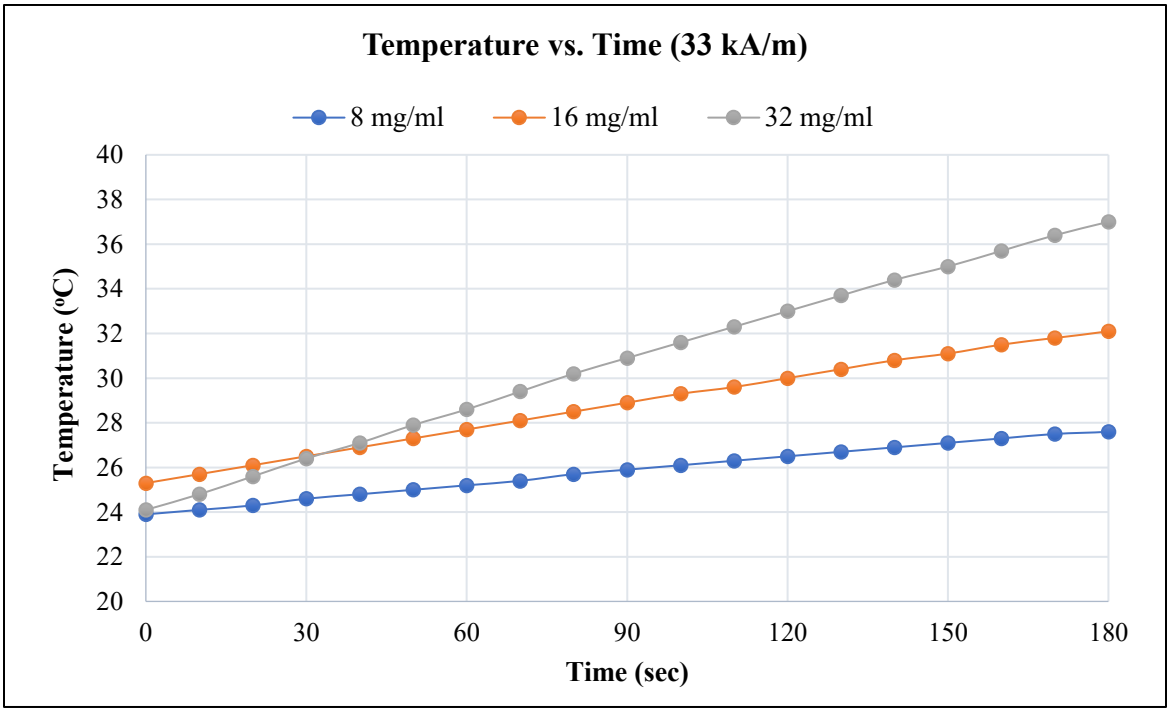

Figure 52. Initial heating curve of magnetic nanoemulsion hydrogels containing 8, 16, and 32 mg/ml of magnetic nanoparticles under magnetic field strength of 33 kA/m.

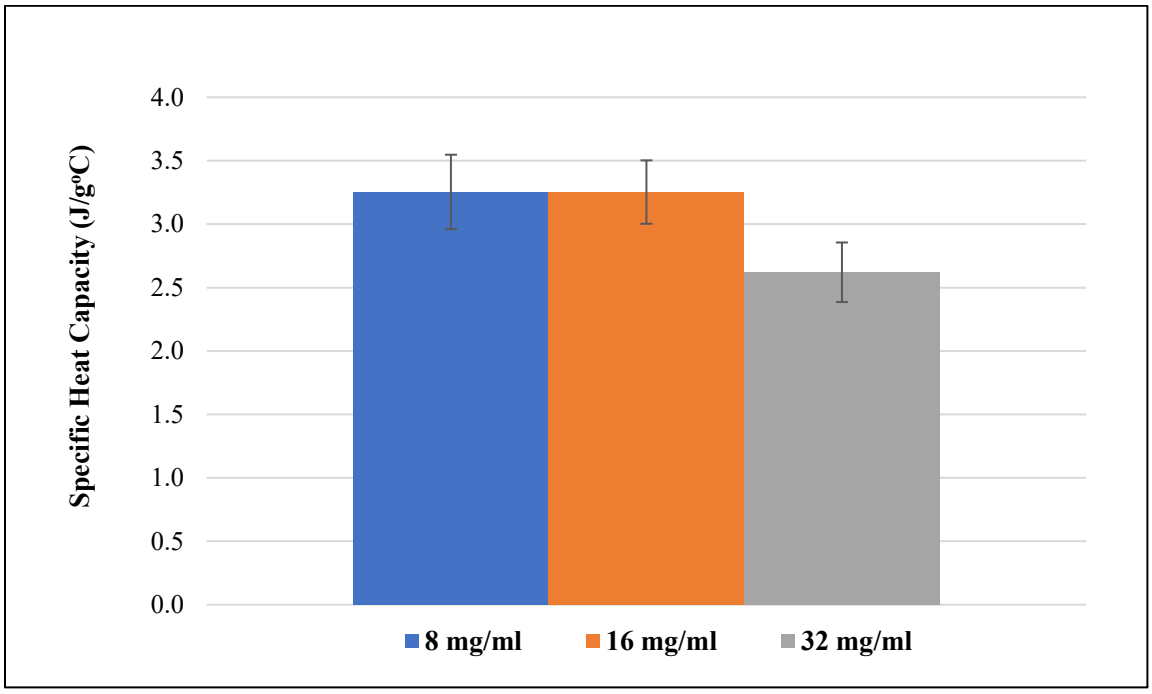

Figure 53. Specific heat capacity of samples containing 8, 16, and 32 mg/ml of magnetic nanoparticles.

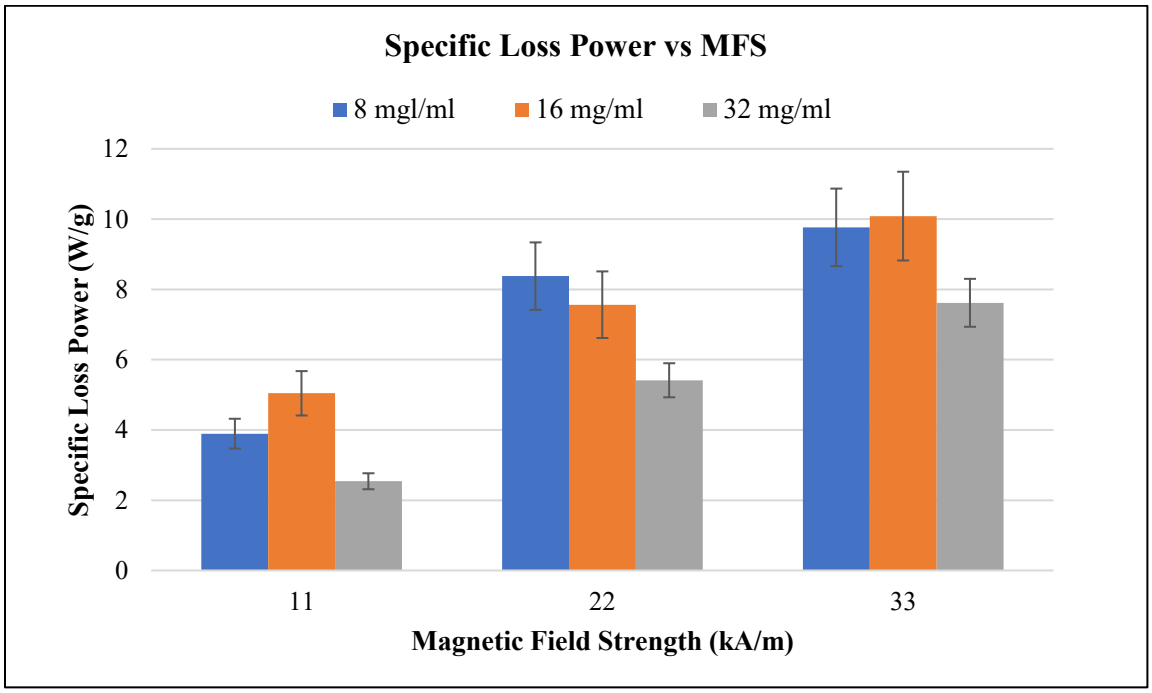

Figure 54. Specific loss power of samples containing 8, 16, and 32 mg/ml of magnetic nanoparticle under magnetic field strengths of 11, 22, and 33 kA/m.

CHAPTER 5

CONCLUSION

The effect of hydrophilic-lipophilic balance, oil percentage, and surfactant percentage on the globule size and zeta potential of nanoemulsions were investigated for a 30-day period. The average diameter, zeta potential, and polydispersity index were defined for different temperature ranges. Test results provided insight into the roles and importance of oil, surfactant amount, and HLB. It was concluded that in addition to HLB, oil and surfactant percentages greatly affect the stability of an emulsion. A surfactant amount of 7.5% with an 11.6 HLB value was found to be the best candidate for future studies. Also, it was concluded that these samples did not show significant change in their particle size and polydispersity index corresponding to temperature. Zeta potential studies demonstrated that with increasing temperature, the zeta potential decreased. Overall, test results proved that the selected black seed oil emulsions can be a good candidate for further studies and for drug delivery applications. All characteristic peaks belonging to chemicals and samples used were obtained for each sample in the Fourier transform infrared spectroscopy study. Rheology studies showed that the chosen nanoemulsions exhibited stable viscosity behavior over a one-month period for tests that were conducted at both room temperature and body temperature. The swelling behavior for hydrogels was seen to be diffusion controlled. This was explained by the n number, which was less than 0.5. The study of drug-release kinetics suggested that for quantification of the drug-release amount, the best model to use was the Higuchi release model. However, even though this model provided the highest R^2 values, these values should be improved and become close to 1 for better control of the drug release. This can be achieved with alternating the crosslinking percentage in the polymer structure, swelling ratio, and swelling rate.

Hyperthermia studies clearly indicated the effects of time, concentration, and magnetic field strength on the heating ability of the samples. Results suggested that after 20 minutes, the temperature increase was not significant, and only when the magnetic nanoparticle concentration was 32 mg/ml and the magnetic field strength was 33 kA/m that the targeted hyperthermia temperature was reached. However, since the temperature increase was so drastic, a quick statistical analysis and optimization study were performed. Statistical analysis supported these effects, and the optimization study provided a possible experimental setup that could be applied during a hyperthermia study considering time and minimum magnetic nanoparticle concentration preferences during the hyperthermia studies. Moreover, one of the possible solutions created for the confirmation of the optimization study suggested that the model is strong and that hyperthermia test results can be controlled by adjusting time, concentration, and magnetic field strength, which are crucial in terms of effective hyperthermia in cancer treatment without causing necrosis during biological studies.

CHAPTER 6

FUTURE DIRECTIONS

Suggestions for future work in this area are listed below:

- Rheology studies need to be performed to observe precisely the gelling points of the hydrogels and to determine their mechanical properties.
- *In-vitro* degradation and *in-vitro* release cytotoxicity studies could be performed to ascertain both the drug-release properties and the possible toxicity of the samples.
- *In-vivo* studies need to be conducted in order to see the real efficiency of the system in the body.
- A certain cancer drug could be employed to load into the oil phase, thereby completing both the drug solubility of the oil-in-water nanoemulsion system and the drug-release study.
- Mechanical properties of the hydrogel could be investigated and enhanced to provide long-lasting release properties and a more controlled drug release.
- A histology study involving organs, such as the liver and lung, need to be carried out to observe the effect of chemotherapeutics on them. This would also help to discern if targeted delivery is successful in limiting the diffusion of chemotherapeutics away from the tumor region.

REFERENCES

REFERENCES

[1] N. Csaba, M. Garcia-Fuentes, and M. J. Alonso, "Nanoparticles for nasal vaccination," *Advanced Drug Delivery Reviews*, vol. 61, pp. 140-157, 2009.

[2] A. Mistry, S. Stolnik, and L. Illum, "Nanoparticles for direct nose-to-brain delivery of drugs," *International Journal of Pharmaceutics*, vol. 379, pp. 146-157, 2009.

[3] F. Liu, J. Yang, L. Huang, and D. Liu, "Effect of non-ionic surfactants on the formation of DNA/emulsion complexes and emulsion-mediated gene transfer," *Pharmaceutical Research*, vol. 13, pp. 1642-1646, 1996.

[4] S. W. Yi, T. Y. Yune, T. W. Kim, H. Chung, Y. W. Choi, I. C. Kwon, *et al.*, "A cationic lipid emulsion/DNA complex as a physically stable and serum-resistant gene delivery system," *Pharmaceutical Research*, vol. 17, pp. 314-320, 2000.

[5] F. A. Araújo, R. G. Kelmann, B. V. Araújo, R. B. Finatto, H. F. Teixeira, and L. S. Koester, "Development and characterization of parenteral nanoemulsions containing thalidomide," *European Journal of Pharmaceutical Sciences*, vol. 42, pp. 238-245, 2011.

[6] T. P. U. Ravi and T. Padma, "Nanoemulsions for drug delivery through different routes," *Research in Biotechnology*, vol. 2, pp. 1-13, 2011.

[7] D. W. Osborne, A. J. Ward, and K. J. O'Neill, "Microemulsions as topical drug delivery vehicles: In-vitro transdermal studies of a model hydrophilic drug," *Journal of Pharmacy and Pharmacology*, vol. 43, pp. 450-454, 1991.

[8] J. Kemken, A. Ziegler, and B. W. Müller, "Influence of supersaturation on the pharmacodynamic effect of bupranolol after dermal administration using microemulsions as vehicle," *Pharmaceutical Research*, vol. 9, pp. 554-558, 1992.

[9] A. Usta and R. Asmatulu, "Synthesis and Analysis of Electrically Sensitive Hydrogels for Advanced Drug Delivery Systems," presented at the ASME International Mechanical Engineering Congress and Exposition, Houston, TX, 2015.

[10] L. Saeednia, A. Usta, and R. Asmatulu, "Preparation and Characterization of Drug-loaded Thermosensitive Hydrogels," presented at the ASME International Mechanical Engineering Congress and Exposition, San Diego, CA, 2013.

[11] A. Usta, L. Saeednia, S. Pyarasani, and R. Asmatulu, "Antibacterial Hydrogels Reinforced by Electrospun PVC Nanofibers for Biomedical Applications," presented at the SAMPE Fall Technical Conference, Wichita, KS, 2013.

[12] A. Usta and R. Asmatulu, "Synthesis and Anaysis of Electrically Sensitive Hydrogels Incorporated with Cancer Drugs," *Journal of Pharmaceutics & Drug Delivery Research*, vol. 5, iss. 2, 8 pp., 2016.

[13] S. Mahdi Jafari, Y. He, and B. Bhandari, "Nano-Emulsion Production by Sonication and Microfluidization—A Comparison," *International Journal of Food Properties*, vol. 9, pp. 475-485, 2006.

[14] A. Jemal, F. Bray, M. M. Center, J. Ferlay, E. Ward, and D. Forman, "Global cancer statistics," *CA: A Cancer Journal for Clinicians*, vol. 61, pp. 69-90, 2011.

[15] T. J. Wilt, R. MacDonald, I. Rutks, T. A. Shamliyan, B. C. Taylor, and R. L. Kane, "Systematic review: Comparative effectiveness and harms of treatments for clinically localized prostate cancer," *Annals of Internal Medicine*, vol. 148, pp. 435-448, 2008.

[16] R. Misra, S. Acharya, and S. K. Sahoo, "Cancer nanotechnology: Application of nanotechnology in cancer therapy," *Drug Discovery Today*, vol. 15, pp. 842-850, 2010.

[17] G. Atlanta, "Cancer Facts and Figures 2012," *American Cancer Society*, 2012.

[18] The Oral Cancer Foundation, "Surgery," 2018, URL: https:// oralcancerfoundation. org/ treatment/surgery/, [July 1, 2018].

[19] E. C. Halperin, L. W. Brady, D. E. Wazer, and C. A. Perez, *Perez & Brady's Principles and Practice of Radiation Oncology*, Lippincott Williams & Wilkins, 2013.

[20] Medline Plus, "Radiation therapy," 2018, URL: https://medlineplus.gov/ ency/article/ 001918.htm, [July 2, 2018].

[21] B. E. Henderson, R. K. Ross, and M. C. Pike, "Hormonal chemoprevention of cancer in women," *Science-New York Then Washington*, vol. 259, pp. 633-633, 1993.

[22] R. S. Thakur, "Lung cancer/cancer of lungs," March 22, 2016, URL: http://www.medindia.net/patients/patientinfo/lung-cancer.htm, [July 2, 2018].

[23] A. Jordan, R. Scholz, P. Wust, H. Fähling, and R. Felix, "Magnetic fluid hyperthermia (MFH): Cancer treatment with AC magnetic field induced excitation of biocompatible superparamagnetic nanoparticles," *Journal of Magnetism and Magnetic Materials*, vol. 201, pp. 413-419, 1999.

[24] P. Wust, B. Hildebrandt, G. Sreenivasa, B. Rau, J. Gellermann, H. Riess, *et al.*, "Hyperthermia in combined treatment of cancer," *The Lancet Oncology*, vol. 3, pp. 487-497, 2002.

[25] J. van der Zee, "Heating the patient: A promising approach?," *Annals of Oncology: Official Journal of the European Society for Medical Oncology*, vol. 13, pp. 1173-1184, 2002.

[26] B. Hildebrandt, P. Wust, O. Ahlers, A. Dieing, G. Sreenivasa, T. Kerner, *et al.*, "The cellular and molecular basis of hyperthermia," *Critical Reviews in Oncology/Hematology*, vol. 43, pp. 33-56, 2002.

[27] R. K. Jain, "Normalization of tumor vasculature: An emerging concept in antiangiogenic therapy," *Science*, vol. 307, pp. 58-62, 2005.

[28] C. W. Song, "Effect of Local hyperthermia on blood flow and microenvironment: A review," *Cancer Research*, vol. 44, pp. 4721s-4730s, 1984.

[29] American Cancer Sociey, "What is breast cancer?" 2016, URL: https:// www. cancer. org/ cancer/breast-cancer/about/what-is-breast-cancer.html, [Nov 14, 2017].

[30] American Cancer Society, "Cancer facts & figures 2016," American Cancer Society, Atlanta, GA, 2016.

[31] National Cancer Institute, "Breast cancer treatment (PDQ®)–Patient version," URL: https://www.cancer.gov/types/breast/patient/breast-treatment-pdq, [Nov 21, 2017].

[32] M. A. Augustin and Y. Hemar, "Nano- and micro-structured assemblies for encapsulation of food ingredients," *Chemical Society Reviews*, vol. 38, pp. 902-912, 2009.

[33] A. Nazir, K. Schroën, and R. Boom, "Premix emulsification: A review," *Journal of Membrane Science*, vol. 362, pp. 1-11, 2010.

[34] A. A. M. Sharif, A. M. Astaraki, P. A. Azar, S. A. Khorrami, and S. Moradi, "The effect of NaCl and Na2SO4 concentration in aqueous phase on the phase inversion temperature O/W nanoemulsions," *Arabian Journal of Chemistry*, vol. 5, pp. 41-44, 2012.

[35] C. Solans, P. Izquierdo, J. Nolla, N. Azemar, and M. J. Garcia-Celma, "Nano-emulsions," *Current Opinion in Colloid & Interface Science*, vol. 10, pp. 102-110, 2005.

[36] N. Rodríguez-Burneo, M. Busquets, and J. Estelrich, "Magnetic nanoemulsions: Comparison between nanoemulsions formed by ultrasonication and by spontaneous emulsification," *Nanomaterials*, vol. 7, no. 7, 2017, doi: 10.3390/nano7070190

[37] G. Kumar and A. Divya, "Nanoemulsion based targeting in cancer therapeutics," *Journal of Medical Chemistry*, vol. 5, pp. 272-284, 2015.

[38] M. El-Dakhakhny, "Studies on the chemical constitution of Egyptian Nigella Sativa L. seeds. The essential oil," *Planta Medica*, vol. 11, no. 4, pp. 465-470, 1963.

[39] M. A. El-Mahdy, Q. Zhu, Q.-E. Wang, G. Wani, and A. A. Wani, "Thymoquinone induces apoptosis through activation of caspase-8 and mitochondrial events in p53-null myeloblastic leukemia HL-60 cells," *International Journal of Cancer*, vol. 117, pp. 409-417, 2005.

[40] H. Gali-Muhtasib, M. Diab-Assaf, C. Boltze, J. Al-Hmaira, R. Hartig, A. Roessner, *et al.*, "Thymoquinone extracted from black seed triggers apoptotic cell death in human colorectal cancer cells via a p53-dependent mechanism," *International Journal of Oncology*, vol. 25, pp. 857-866, 2004.

[41] I. O. Farah and R. A. Begum, "Effect of Nigella sativa (N. sativa L.) and oxidative stress on the survival pattern of MCF-7 breast cancer cells," *Biomedical Sciences Instrumentation*, vol. 39, pp. 359-364, 2003.

[42] O. A. Ghosheh, A. A. Houdi, and P. A. Crooks, "High performance liquid chromatographic analysis of the pharmacologically active quinones and related compounds in the oil of the black seed (Nigella sativa L.)," *Journal of Pharmaceutical and Biomedical Analysis*, vol. 19, pp. 757-762, 1999.

[43] A. Haq, P. I. Lobo, M. Al-Tufail, N. R. Rama, and S. T. Al-Sedairy, "Immunomodulatory effect of Nigella sativa proteins fractionated by ion exchange chromatography," *International Journal of Immunopharmacology*, vol. 21, pp. 283-295, 1999.

[44] P. S. Koka, D. Mondal, A. B. A. Mageed, and K. Agrawal, "Paradoxical effects of thymoquinone in prostate cancer cells: Induction of reactive oxygen species," *The FASEB Journal*, vol. 23, pp. 761-768, 2009.

[45] E.-S. A. Arafa, Q. Zhu, Z. I. Shah, G. Wani, B. M. Barakat, I. Racoma, *et al.*, "Thymoquinone up-regulates PTEN expression and induces apoptosis in doxorubicin-resistant human breast cancer cells," *Mutation Research/Fundamental and Molecular Mechanisms of Mutagenesis*, vol. 706, pp. 28-35, 2011.

[46] C. Lovelyn and A. Attama, "Current state of nanoemulsions in drug delivery," *Journal of Biomaterialsand Nanobiotechnology*, vol. 02, pp. 626-639, 2011.

[47] N. Anton and T. F. Vandamme, "The universality of low-energy nano-emulsification," *International Journal of Pharmaceutics*, vol. 377, pp. 142-147, 2009.

[48] L.-C. Peng, C.-H. Liu, C.-C. Kwan, and K.-F. Huang, "Optimization of water-in-oil nanoemulsions by mixed surfactants," *Colloids and Surfaces A: Physicochemical and Engineering Aspects*, vol. 370, pp. 136-142, 2010.

[49] N. Anton and T. F. Vandamme, "Nano-emulsions and micro-emulsions: Clarifications of the critical differences," *Pharmaceutical Research*, vol. 28, pp. 978-985, 2011.

[50] A. Gupta, H. B. Eral, T. A. Hatton, and P. S. Doyle, "Nanoemulsions: Formation, properties and applications," *Soft Matter*, vol. 12, pp. 2826-2841, 2016.

[51] A. Nasr, A. Gardouh, H. Ghonaim, E. Abdelghany, and M. Ghorab, "Effect of oils, surfactants and cosurfactants on phase behavior and physicochemical properties of self-nanoemulsifying drug delivery system (SNEDDS) for Irbesartan and Olmesartan," *International Journal of Applied Pharmaceutics*, vol. 8, pp. 13-24, 2016.

[52] S. A. Chime, F. C. Kenechukwu, and A. A. Attama, "Nanoemulsions—Advances in formulation, characterization and applications in drug delivery," in *Application of Nanotechnology in Drug Delivery*, Ch. 3, A. D. Sezer, Ed., Rijeka: InTech, 2014.

[53] A. B. Jodar-Reyes, A. Martin-Rodriguez, and J. L. Ortega-Vinuesa, "Effect of the ionic surfactant concentration on the stabilization/destabilization of polystyrene colloidal particles," *Journal of Colloid and Interface Science*, vol. 298, pp. 248-257, 2006.

[54] T. R. Kommuru, B. Gurley, M. A. Khan, and I. K. Reddy, "Self-emulsifying drug delivery systems (SEDDS) of coenzyme Q10: Formulation development and bioavailability assessment," *International Journal of Pharmaceutics*, vol. 212, pp. 233-246, 2001.

[55] A. Azeem, M. Rizwan, F. J. Ahmad, Z. Iqbal, R. K. Khar, M. Aqil, *et al.*, "Nanoemulsion components screening and selection: A technical note," *American Association of Pharmeceutical Scientists PharmSciTech*, vol. 10, pp. 69-76, 2009.

[56] H. K. Syed and K. K. Peh, "Identification of phases of various oil, surfactant/ co-surfactants and water system by ternary phase diagram," *Acta Poloniae Pharmaceutica*, vol. 71, pp. 301-309, 2014.

[57] S. M. Jafari, E. Assadpoor, Y. He, and B. Bhandari, "Re-coalescence of emulsion droplets during high-energy emulsification," *Food Hydrocolloids*, vol. 22, pp. 1191-1202, 2008.

[58] N. Grampurohit, P. Ravikumar, and R. Mallya, "Microemulsions for topical use: A review," *Indian Journal of Pharmaceutical Education*, vol. 45, pp. 100-107, 2011.

[59] K. Kawakami, T. Yoshikawa, T. Hayashi, Y. Nishihara, and K. Masuda, "Microemulsion formulation for enhanced absorption of poorly soluble drugs," *Journal of Controlled Release*, vol. 81, pp. 75-82, 2002.

[60] M. Rosety-Rodriguez, F. J. Ordonez, S. Roldan, J. M. Rosety, M. Rosety, A. Ribelles, *et al.*, "Acute effects of sodium dodecyl sulphate on the survival and on morpho-histochemical characteristics of the trunk kidney of juvenile turbot Scophthalmus maximus L," *European Journal of Histochemistry: EJH*, vol. 46, pp. 179-184, 2002.

[61] L. A. Gould, A. B. Lansley, M. B. Brown, B. E. N. Forbes, and G. P. Martin, "Mitigation of surfactant erythrocyte toxicity by egg phosphatidylcholine," *Journal of Pharmacy and Pharmacology*, vol. 52, pp. 1203-1209, 2000.

[62] R. L. Grant and D. Acosta, "Prolonged adverse effects of benzalkonium chloride and sodium dodecyl sulfate in a primary culture system of rabbit corneal epithelial cells," *Toxicological Sciences*, vol. 33, pp. 71-82, 1996.

[63] D. Myers, Surfaces, interfaces, and colloids—Principles and applications, 2nd ed., vol. 3, New York: VCH Publishers, 1991.

[64] R. Singh, G. A. Husseini, and W. G. Pitt, "Phase transitions of nanoemulsions using ultrasound: Experimental observations," *Ultrasonic Sonochemistry*, vol. 19, pp. 1120-1125, 2012.

[65] S. I. Karakashev, E. D. Manev, R. Tsekov, and A. V. Nguyen, "Effect of ionic surfactants on drainage and equilibrium thickness of emulsion films," *Journal of Colloid and Interface Science*, vol. 318, pp. 358-364, 2008.

[66] P. J. Wilde, "Interfaces: Their role in foam and emulsion behaviour," *Current Opinion in Colloid & Interface Science*, vol. 5, pp. 176-181, 2000.

[67] I. B. Ivanov and P. A. Kralchevsky, "Stability of emulsions under equilibrium and dynamic conditions," *Colloids and Surfaces A: Physicochemical and Engineering Aspects*, vol. 128, pp. 155-175, 1997.

[68] H. C. Hamaker, "The London-van der Waals attraction between spherical particles," *Physica*, vol. 4, pp. 1058-1072, 1937.

[69] T. F. Tadros, "Emulsion formation, stability, and rheology," in *Emulsion Formation and Stability*, Wiley-VCH Verlag GmbH & Co. KGaA, 2013, pp. 1-75.

[70] K. Rahn-Chique, A. M. Puertas, M. S. Romero-Cano, C. Rojas, and G. Urbina-Villalba, "Nanoemulsion stability: Experimental evaluation of the flocculation rate from turbidity measurements," *Advances in Colloid and Interface Science*, vol. 178, pp. 1-20, 2012.

[71] "Repulsion—Electrocratic," 2011, URL: http://soft-matter.seas.harvard.edu/index.Php/Repulsion_-_Electrocratic, [July 20, 2018].

[72] A. S. Dunn, "Polymeric stabilization of colloidal dispersions," *British Polymer Journal*, vol. 18, pp. 278-278, 1986.

[73] P. Walstra, "Principles of emulsion formation," *Chemical Engineering Science*, vol. 48, pp. 333-349, 1993.

[74] G. Narsimhan and P. Goel, "Drop coalescence during emulsion formation in a high-pressure homogenizer for tetradecane-in-water emulsion stabilized by sodium dodecyl sulfate," *Journal of Colloid and Interface Science*, vol. 238, pp. 420-432, 2001.

[75] S. Tcholakova, N. D. Denkov, and T. Danner, "Role of surfactant type and concentration for the mean drop size during emulsification in turbulent flow," *Langmuir*, vol. 20, pp. 7444-7458, 2004.

[76] T. G. Mason, J. N. Wilking, K. Meleson, C. B. Chang, and S. M. Graves, "Nanoemulsions: Formation, structure, and physical properties," *Journal of Physics: Condensed Matter*, vol. 18, p. R635, 2006.

[77] J. Mewis and N. J. Wagner, *Colloidal Suspension Rheology*, Cambridge University Press, 2012.

[78] C. Wagner, "Theory of precipitate change by redissolution," *Zeitschrift fur Elektrochemie*, vol. 65, pp. 581-591, 1961.

[79] I. M. Lifshitz and V. V. Slyozov, "The kinetics of precipitation from supersaturated solid solutions," *Journal of Physics and Chemistry of Solids*, vol. 19, pp. 35-50, 1961.

[80] S. Kotta, A. W. Khan, K. Pramod, S. H. Ansari, R. K. Sharma, and J. Ali, "Exploring oral nanoemulsions for bioavailability enhancement of poorly water-soluble drugs," *Expert Opinion on Drug Delivery*, vol. 9, pp. 585-598, 2012.

[81] S. Ganta and M. Amiji, "Coadministration of Paclitaxel and curcumin in nanoemulsion formulations to overcome multidrug resistance in tumor cells," *Molecular Pharmaceutics*, vol. 6, pp. 928-939, 2009.

[82] G. M. Eccleston, "Microemulsions," in *Encyclopedia of Pharmaceutical Technology*, vol. 9, J. Swarbrick and J. C. Boylan, Ed., New York, Basel, and Hong Kong: Marcel Dekker Inc., 1994, pp. 375-421.

[83] R. G. Lawrence MJ, "Microemulsion-based media as novel drug delivery systems," *Advanced Drug Delivery*, vol. 45, pp. 89-121, 2000.

[84] T. Tadros, P. Izquierdo, J. Esquena, and C. Solans, "Formation and stability of nano-emulsions," *Advances in Colloid and Interface Science.*, vol. 108, pp. 303-318, 2004.

[85] A. Servant, C. Bussy, K. Al-Jamal, and K. Kostarelos, "Design, engineering and structural integrity of electro-responsive carbon nanotube-based hydrogels for pulsatile drug release," *Journal of Materials Chemistry B*, vol. 1, pp. 4593-4600, 2013.

[86] K. R. Kamath and K. Park, "Biodegradable hydrogels in drug-delivery," *Advanced Drug Delivery Reviews*, vol. 11, pp. 59-84, 1993.

[87] K. Park, K. R. Kamath, and H. Park, "Biodegradable hydrogels for delivery of protein drugs," *Abstracts of Papers American Chemical Society*, vol. 205, pp. 474-Poly, 1993.

[88] Y. Qiu and K. Park, "Environment-sensitive hydrogels for drug delivery," *Advanced Drug Delivery Reviews*, vol. 64, pp. 49-60, 2012.

[89] A. Usta and R. Asmatulu, "Hydrogels in various biomedical applications," in *Polymer Science: Research Advances*, *Practical Applications and Educational Aspects*, A. M.-V. A. Solano, Ed., Badajoz, Spain: Formatex Research Center, 2016, pp. 248-257.

[90] N. A. Peppas, P. Bures, W. Leobandung, and H. Ichikawa, "Hydrogels in pharmaceutical formulations," *European Journal of Pharmaceutics and Biopharmaceutics*, vol. 50, pp. 27-46, 2000.

[91] S. W. Kim, Y. H. Bae, and T. Okano, "Hydrogels—Swelling, drug loading, and release," *Pharmaceutical Research.*, vol. 9, pp. 283-290, 1992.

[92] S. K. Bajpai, "Swelling studies on hydrogel networks—A review," *Journal of Scientific and Industrial Research India*, vol. 60, pp. 451-462, 2001.

[93] I. C. Kwon, Y. H. Bae, and S. W. Kim, "Electrically Erodible polymer gel for controlled release of drugs," *Nature*, vol. 354, pp. 291-293, 1991.

[94] R. Kishi and Y. Osada, "Reversible volume change of microparticles in an electric field," *Journal of the Chemical Society*, *Faraday Transactions 1: Physical Chemistry in Condensed Phases*, vol. 85, pp. 655-662, 1989.

[95] Y. Qiu and K. Park, "Environment-sensitive hydrogels for drug delivery," *Advanced Drug Delivery Reviews*, vol. 53, pp. 321-339, 2001.

[96] H. Priya James, R. John, A. Alex, and K. R. Anoop, "Smart polymers for the controlled delivery of drugs—A concise overview," *Acta Pharmaceutica Sinica B*, vol. 4, pp. 120-127, 2014.

[97] E. Ruel-Gariepy and J. C. Leroux, "In situ-forming hydrogels—Review of temperature-sensitive systems," *European Journal of Pharmaceutics and Biopharmaceutics*, vol. 58, pp. 409-426, 2004.

[98] D. Schmaljohann, "Thermo- and pH-responsive polymers in drug delivery," *Advanced Drug Delivery Reviews*, vol. 58, pp. 1655-1670, 2006.

[99] G. A. Soares, F. M. Carbinatto, B. S. Cury, and R. C. Evangelista, "Effect of drying technique on some physical properties of cross-linked high amylose/pectin mixtures," *Drug Development and Industrial Pharmacy*, vol. 39, pp. 284-289, 2013.

[100] P. Sriamornsak, N. Thirawong, Y. Weerapol, J. Nunthanid, and S. Sungthongjeen, "Swelling and erosion of pectin matrix tablets and their impact on drug release behavior," *European Journal of Pharmaceutics and Biopharmaceutics*, vol. 67, pp. 211-219, 2007.

[101] B. Cury, A. Castro, S. I. Klein, and R. C. Evangelista, "Modeling a system of phosphated cross-linked high amylose for controlled drug release. Part 2: Physical parameters, cross-linking degrees and drug delivery relationships," *International Journal of Pharmaceutics*, vol. 371, pp. 8-15, 2009.

[102] M. Gierszewska-Drużyńska and J. Ostrowska-Czubenko, "Mechanism of water diffusion into noncrosslinked and ionically crosslinked chitosan membranes," *Progress on Chemistry and Application of Chitin and Its Derivatives*, vol. 17, pp. 59-66, 2012.

[103] K. Ranga Rao, K. P. Devi, and P. Buri, "Cellulose matrices for zero-order release of soluble drugs," *Drug Development and Industrial Pharmacy*, vol. 14, pp. 2299-2320, 1988.

[104] A. R. Khare and N. A. Peppas, "Swelling/deswelling of anionic copolymer gels," *Biomaterials*, vol. 16, pp. 559-567, 1995.

[105] K. Ramteke, P. Dighe, A. Kharat, and S. Patil, "Mathematical models of drug dissolution: A review," *Scholars Academic Journal of Pharmacy*, vol. 3, pp. 388-396, 2014.

[106] R. Kiessling, A. Gröunberg, J. Ivanyi, K. Soderstroum, M. Ferm, S. Kleinau, *et al.*, "Role of hsp60 during autoimmune and bacterial inflammation," *Immunological Reviews*, vol. 121, pp. 91-111, 1991.

[107] M. Falk and R. Issels, "Hyperthermia in oncology," *International Journal of Hyperthermia*, vol. 17, pp. 1-18, 2001.

[108] J. L. Roti Roti, "Cellular responses to hyperthermia (40–46 C): Cell killing and molecular events," *International Journal of Hyperthermia*, vol. 24, pp. 3-15, 2008.

[109] C. C. Berry and A. S. Curtis, "Functionalisation of magnetic nanoparticles for applications in biomedicine," *Journal of Physics D: Applied Physics*, vol. 36, p. R198, 2003.

[110] R. Gordon, J. Hines, and D. Gordon, "Intracellular hyperthermia a biophysical approach to cancer treatment via intracellular temperature and biophysical alterations," *Medical Hypothesis*, vol. 5, pp. 83-102, 1979.

[111] J. C. Bischof and X. He, "Thermal stability of proteins," *Annals of the New York Academy of Sciences*, vol. 1066, pp. 12-33, 2006.

[112] X. Yang, J. Du, and Y. Liu, "Advances in hyperthermia technology," in *Conference Proceedings of IEEE Engineering in Medicine and Biology Society*, vol. 7, pp. 6766-6769, 2005.

[113] A. J. Cole, V. C. Yang, and A. E. David, "Cancer theranostics: The rise of targeted magnetic nanoparticles," *Trends in Biotechnology*, vol. 29, pp. 323-332, 2011.

[114] N. Nasongkla, E. Bey, J. Ren, H. Ai, C. Khemtong, J. S. Guthi, *et al.*, "Multifunctional polymeric micelles as cancer-targeted, MRI-ultrasensitive drug delivery systems," *Nano Letters*, vol. 6, pp. 2427-2430, 2006.

[115] S. Mornet, S. Vasseur, F. Grasset, and E. Duguet, "Magnetic nanoparticle design for medical diagnosis and therapy," *Journal of Materials Chemistry*, vol. 14, pp. 2161-2175, 2004.

[116] I. Hilger, W. Andrä, R. Hergt, R. Hiergeist, H. Schubert, and W. A. Kaiser, "Electromagnetic heating of breast tumors in interventional radiology: In vitro and in vivo studies in human cadavers and mice," *Radiology*, vol. 218, pp. 570-575, 2001.

[117] K. G. Hofer, "Hyperthermia and cancer," *European Cells and Materials*, vol. 3, pp. 67-69, 2002.

[118] K. Maier-Hauff, F. Ulrich, D. Nestler, H. Niehoff, P. Wust, B. Thiesen, *et al.*, "Efficacy and safety of intratumoral thermotherapy using magnetic iron-oxide nanoparticles combined with external beam radiotherapy on patients with recurrent glioblastoma multiforme," *Journal of Neuro-oncology*, vol. 103, pp. 317-324, 2011.

[119] M. Johannsen, B. Thiesen, A. Jordan, K. Taymoorian, U. Gneveckow, N. Waldöfner, *et al.*, "Magnetic fluid hyperthermia (MFH) reduces prostate cancer growth in the orthotopic Dunning R3327 rat model," *The Prostate*, vol. 64, pp. 283-292, 2005.

[120] I. A. Brezovich, "Low frequency hyperthermia: Capacitive and ferromagnetic thermoseed methods," *Medical Physics Monograph*, vol. 16, pp. 82-111, 1988.

[121] S. Jha, P. K. Sharma, and R. Malviya, "Hyperthermia: Role and risk factor for cancer treatment," *Achievements in the Life Sciences*, vol. 10, pp. 161-167, 2016.

[122] Q. A. Pankhurst, J. Connolly, S. Jones, and J. Dobson, "Applications of magnetic nanoparticles in biomedicine," *Journal of Physics D: Applied Physics*, vol. 36, p. R167, 2003.

[123] R. Gilchrist, R. Medal, W. D. Shorey, R. C. Hanselman, J. C. Parrott, and C. B. Taylor, "Selective inductive heating of lymph nodes," *Annals of Surgery*, vol. 146, no. 4, pp. 596-606, 1957.

[124] O. Yunok, L. Nohyun, K. Hyun Wook, and O. Junghwan, "In vitro study on apoptotic cell death by effective magnetic hyperthermia with chitosan-coated $MnFe_2O_4$," *Nanotechnology*, vol. 27, no. 11, p. 115101, 2016.

[125] L. C. Kennedy, L. R. Bickford, N. A. Lewinski, A. J. Coughlin, Y. Hu, E. S. Day, *et al.*, "A new era for cancer treatment: Gold-nanoparticle-mediated thermal therapies," *Small*, vol. 7, no. 2, pp. 169-183, 2011.

[126] R. A. Frimpong and J. Z. Hilt, "Magnetic nanoparticles in biomedicine: Synthesis, functionalization and applications," *Nanomedicine*, vol. 5, pp. 1401-1414, 2010.

[127] M. Suto, Y. Hirota, H. Mamiya, A. Fujita, R. Kasuya, K. Tohji, *et al.*, "Heat dissipation mechanism of magnetite nanoparticles in magnetic fluid hyperthermia," *Journal of Magnetism and Magnetic Materials*, vol. 321, pp. 1493-1496, 2009.

[128] R. Kötitz, W. Weitschies, L. Trahms, and W. Semmler, "Investigation of Brownian and Neel relaxation in magnetic fluids," *Journal of Magnetism and Magnetic Materials*, vol. 201, pp. 102-104, 1999.

[129] R. E. Fields, "Evaluating compliance with FCC guidelines for human exposure to radiofrequency electromagnetic fields," *OET Bulletin*, vol. 65, p. 10, 1997.

[130] I. Andreu and E. Natividad, "Accuracy of available methods for quantifying the heat power generation of nanoparticles for magnetic hyperthermia," *International Journal of Hyperthermia*, vol. 29, pp. 739-751, 2013.

[131] D. F. Coral, P. Mendoza Zélis, M. E. de Sousa, D. Muraca, V. Lassalle, P. Nicolás, *et al.*, "Quasi-static magnetic measurements to predict specific absorption rates in magnetic fluid hyperthermia experiments," *Journal of Applied Physics*, vol. 115, p. 043907, 2014.

[132] E. Garaio, J. M. Collantes, J. A. Garcia, F. Plazaola, S. Mornet, F. Couillaud, *et al.*, "A wide-frequency range AC magnetometer to measure the specific absorption rate in nanoparticles for magnetic hyperthermia," *Journal of Magnetism and Magnetic Materials*, vol. 368, pp. 432-437, 2014.

[133] S. S. Al-Hayek, "Experimantal and theoretcal study of magnetic hyperthermia," Ph.D dissertation, Department of Mechanical Engineering, Florida State University, Tallahassee, 2007.

[134] P. C. Hiemenz and R. Rajagopalan, *Principles of Colloid and Surface Chemistry*, *Revised and Expanded*, vol. 14, CRC Press, 1997.

[135] A. Jordan, P. Wust, H. Fähling, W. John, A. Hinz, and R. Felix, "Inductive heating of ferrimagnetic particles and magnetic fluids: Physical evaluation of their potential for hyperthermia," *International Journal of Hyperthermia*, vol. 25, pp. 499-511, 2009.

[136] B.H. Park, B. S. Koo, Y. K. Kim, and M. K. Kim, "The induction of hyperthermia in rabbit liver by means of duplex stainless steel thermoseeds," *Korean Journal of Radiology*, vol. 3, pp. 98-104, 2002.

[137] N. A. Brusentsov, V. Gogosov, T. Brusentsova, A. Sergeev, N. Jurchenko, A. A. Kuznetsov, *et al.*, "Evaluation of ferromagnetic fluids and suspensions for the site-specific radiofrequency-induced hyperthermia of MX11 sarcoma cells in vitro," *Journal of Magnetism and Magnetic Materials*, vol. 225, pp. 113-117, 2001.

[138] Y.-S. Ho and G. McKay, "Pseudo-second order model for sorption processes," *Process Biochemistry*, vol. 34, pp. 451-465, 1999.

[139] T. B. Mostafa and A. S. Darwish, "An approach toward construction of tuned chitosan/polyaniline/metal hybrid nanocomposites for treatment of meat industry wastewater," *Chemical Engineering Journal*, vol. 243, pp. 326-339, 2014.

[140] A. Sarı, M. Tuzen, and M. Soylak, "Adsorption of Pb (II) and Cr (III) from aqueous solution on Celtek clay," *Journal of Hazardous Materials*, vol. 144, pp. 41-46, 2007.

APPENDIX

APPENDIX

ADDITIONAL AND COMPLEMENTARY DATA

Figures A1 to A5 represent the release of 5-FU from magnetic nanoemulsion hydrogels containing 24 mg/ml of magnetic nanoparticles using five different release models: zero-order, first-order, Higuchi, Korsmeyer-Peppas, and Hixson-Crowell. Figures A6 to A10 represent the release of 5-FU from chitosan hydrogels containing 24 mg/ml of MNPs using the same five release models, and Figures A11 to A15 represent the release of 5-FU from plain chitosan hydrogels using the same five release models. Figures A16 to A19 provide plots of the model diagnostics.

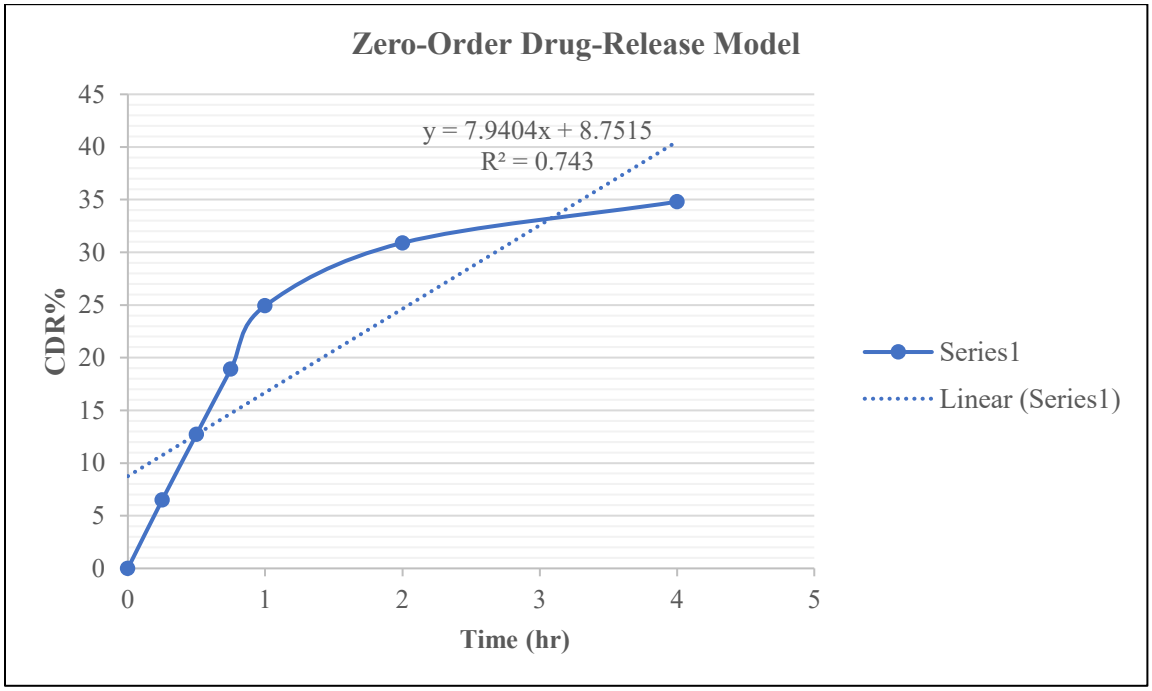

Figure A1. Release of 5-FU from MNHs containing 24 mg/ml magnetic nanoparticles using zero-order drug-release model.

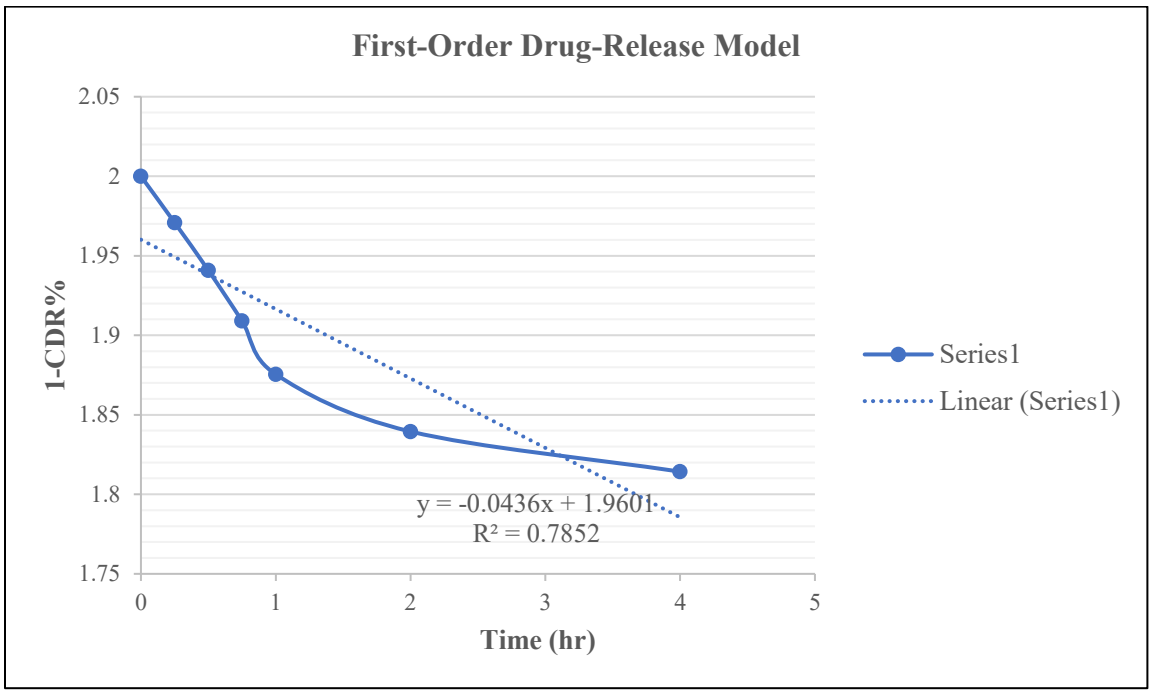

Figure A2. Release of 5-FU from MNHs containing 24 mg/ml magnetic nanoparticles using first-order drug-release model.

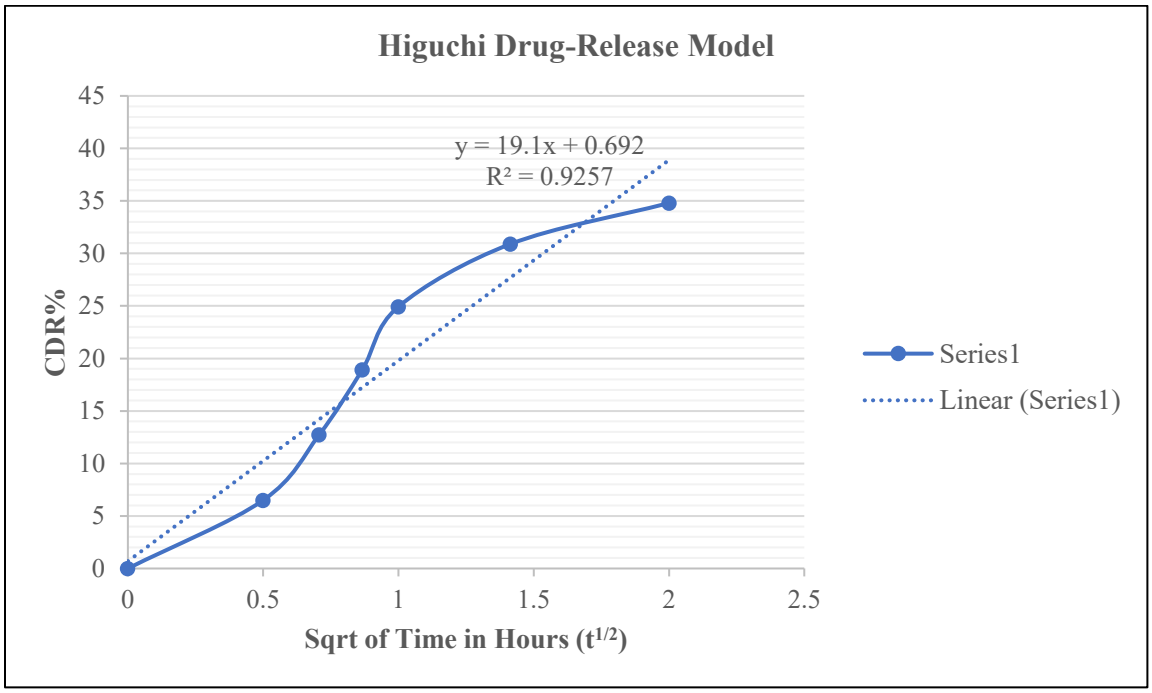

Figure A3. Release of 5-FU from MNHs containing 24 mg/ml magnetic nanoparticles using Higuchi drug-release model.

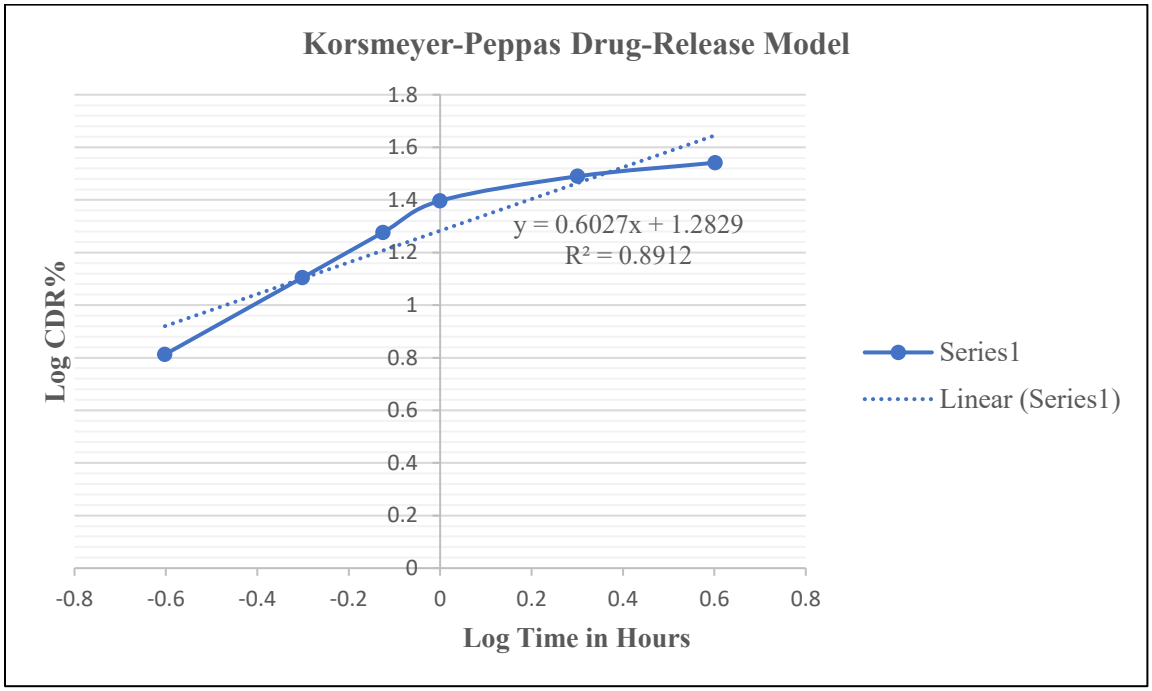

Figure A4. Release of 5-FU from MNHs containing 24 mg/ml magnetic nanoparticles using Korsmeyer-Peppas drug-release model

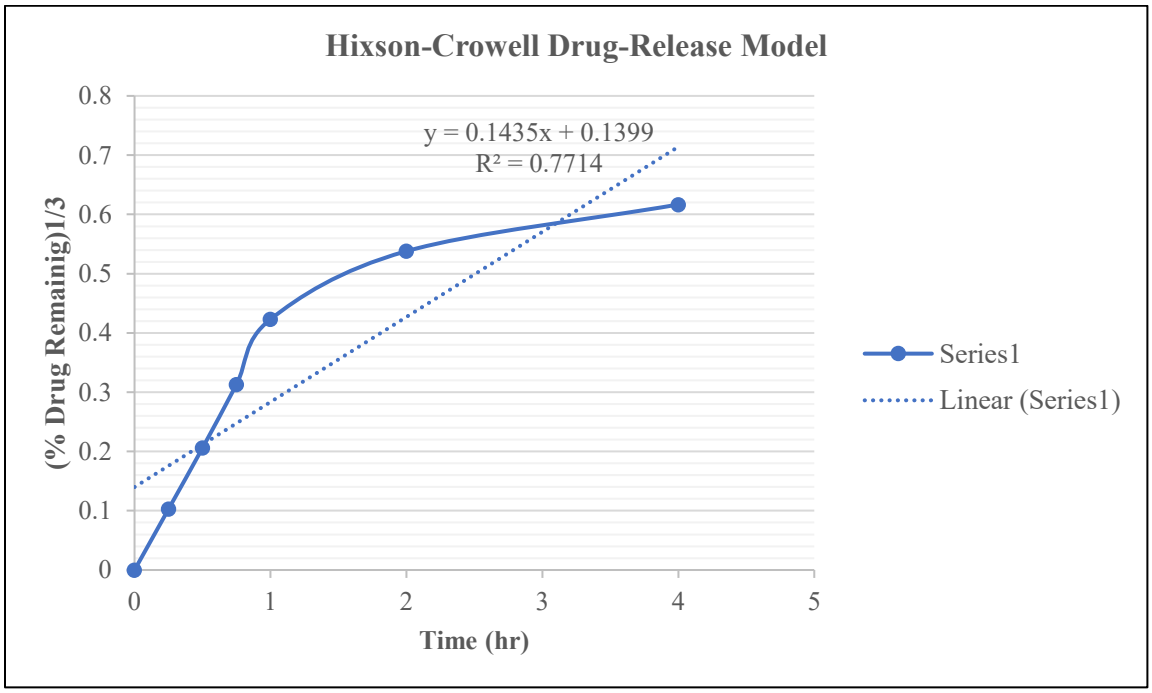

Figure A5. Release of 5-FU from MNHs containing 24 mg/ml magnetic nanoparticles using Hixson-Crowell drug-release model.

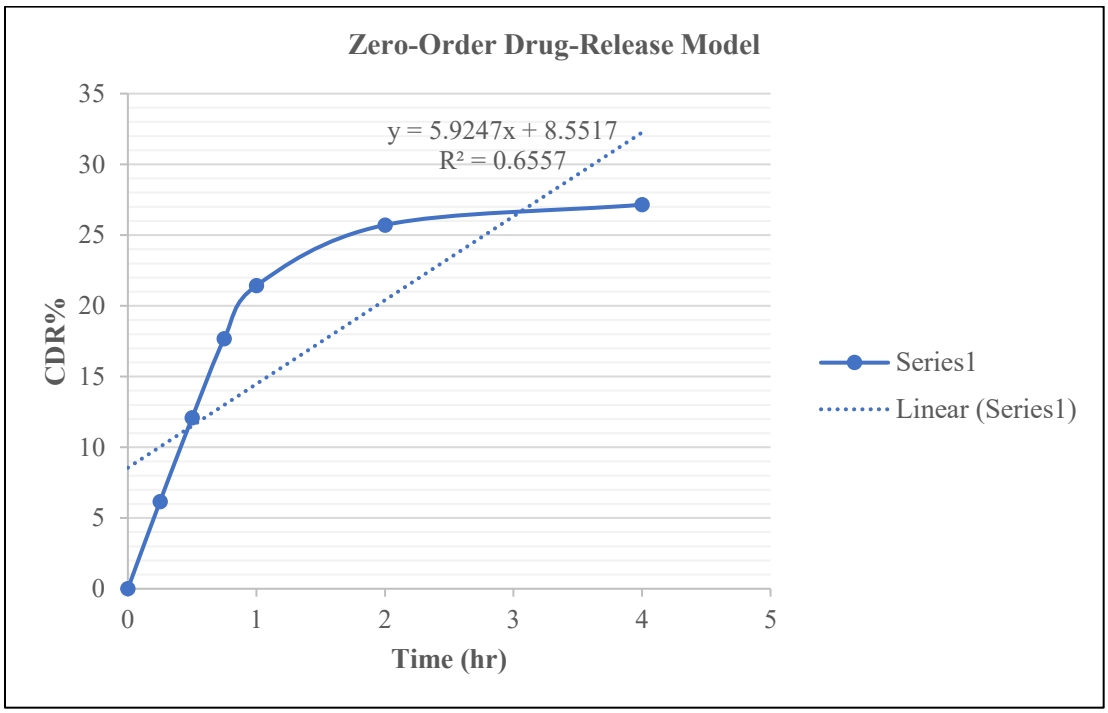

Figure A6. Release of 5-FU from chitosan hydrogels containing 24 mg/ml of magnetic nanoparticles using zero-order drug-release model.

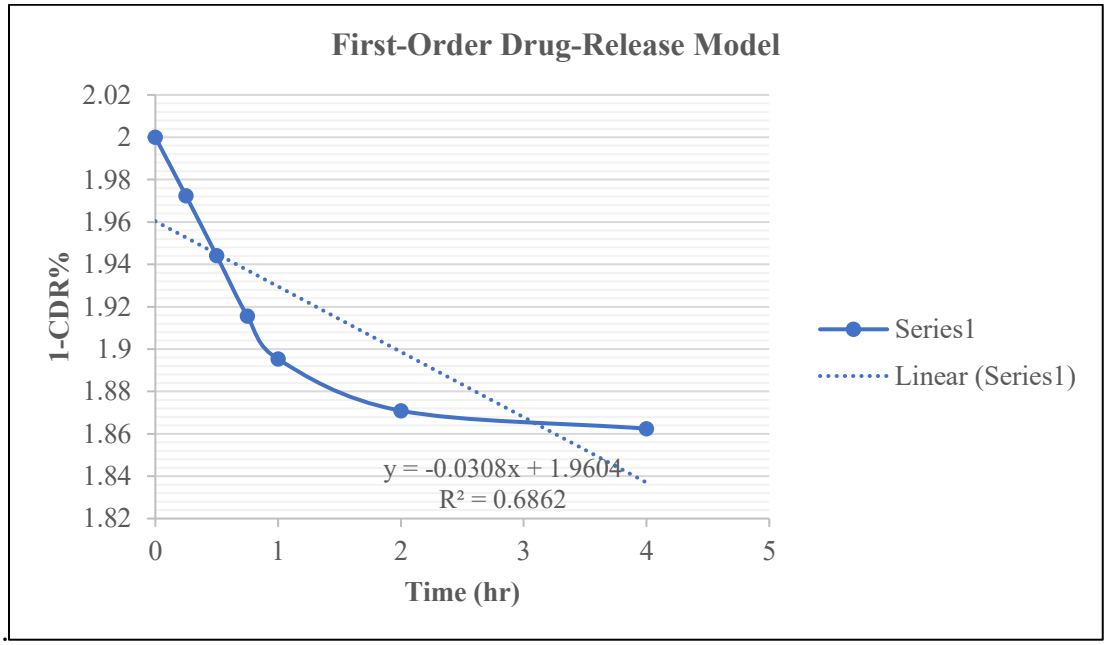

Figure A7. Release of 5-FU from chitosan hydrogels containing 24 mg/ml of magnetic nanoparticles using first-order drug-release model.

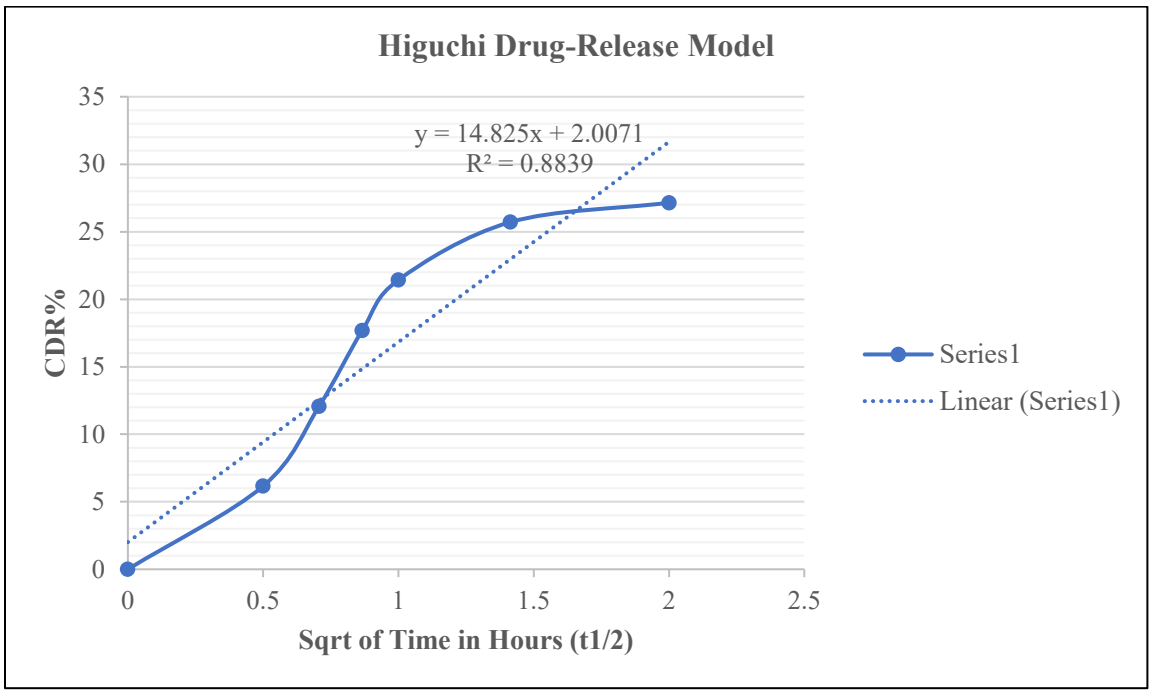

Figure A8. Release of 5-FU from chitosan hydrogels containing 24 mg/ml of magnetic nanoparticles using Higuchi drug-release model

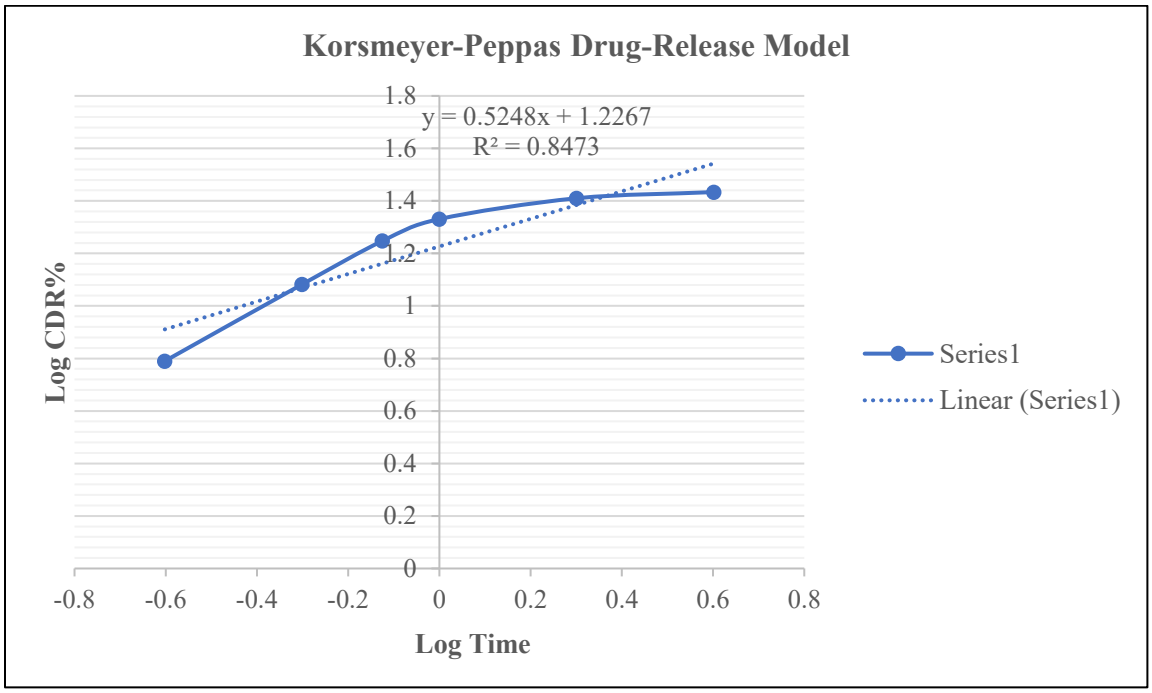

Figure A9. Release of 5-FU from chitosan hydrogels containing 24 mg/ml of magnetic nanoparticles using Korsmeyer-Peppas drug-release model.

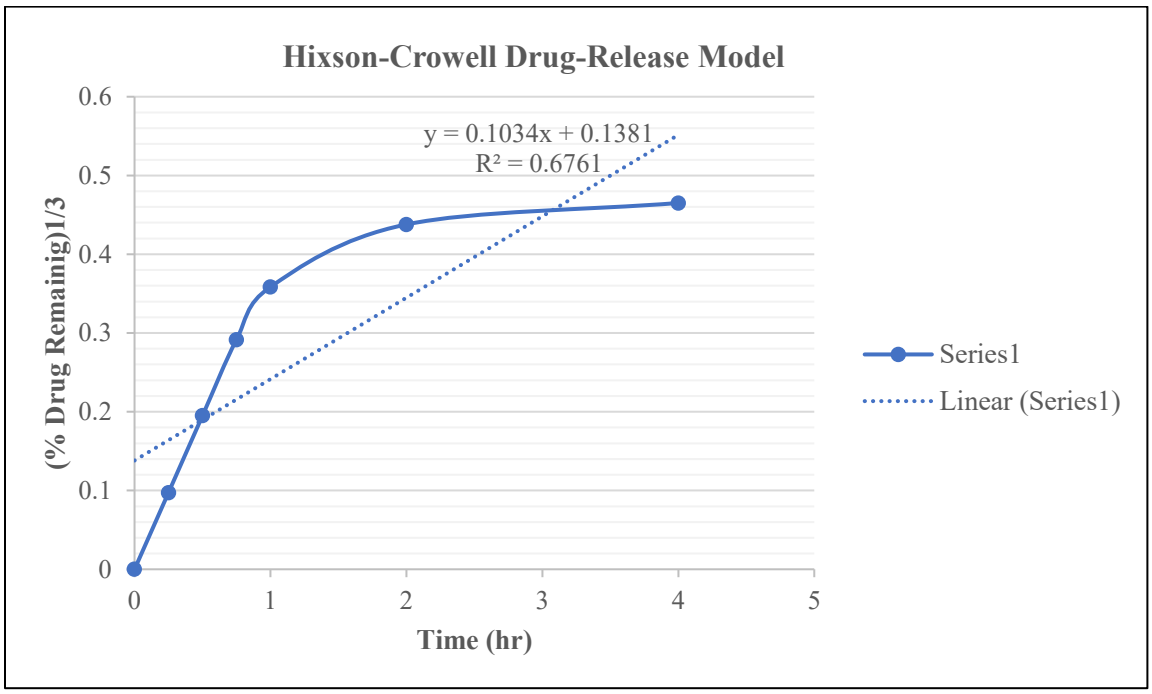

Figure A10. Release of 5-FU from chitosan hydrogels containing 24 mg/ml of magnetic nanoparticles using Hixson-Crowell drug-release model.

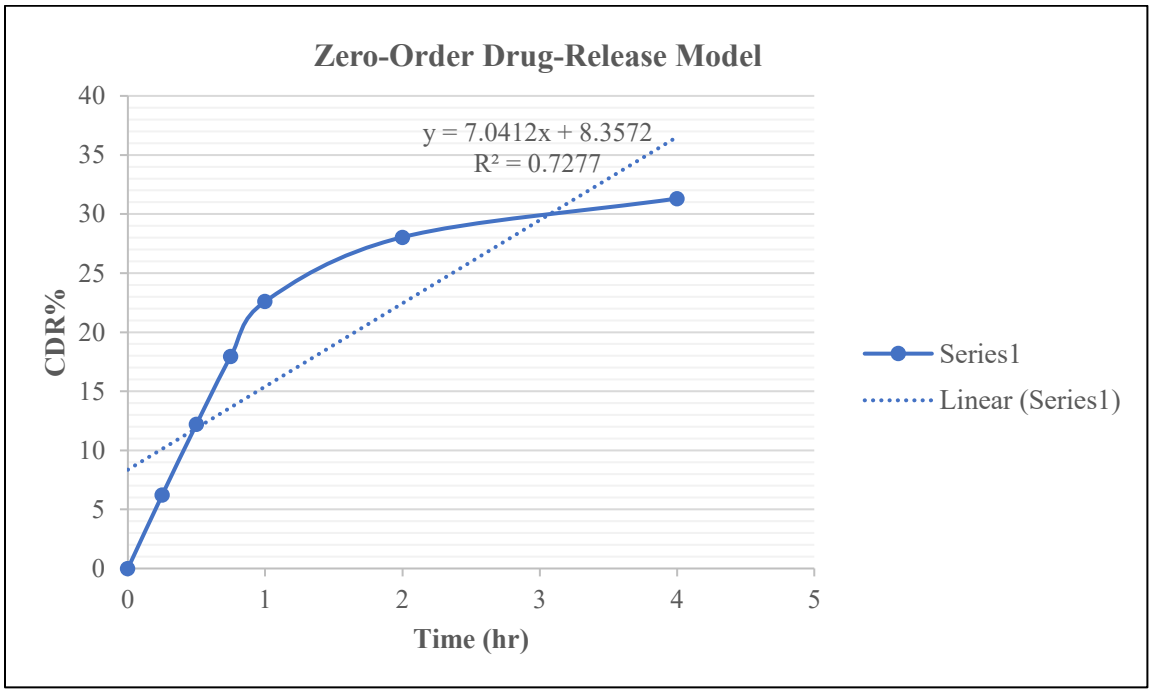

Figure A11. Release of 5-FU from plain chitosan hydrogels using zero-order drug-release model.

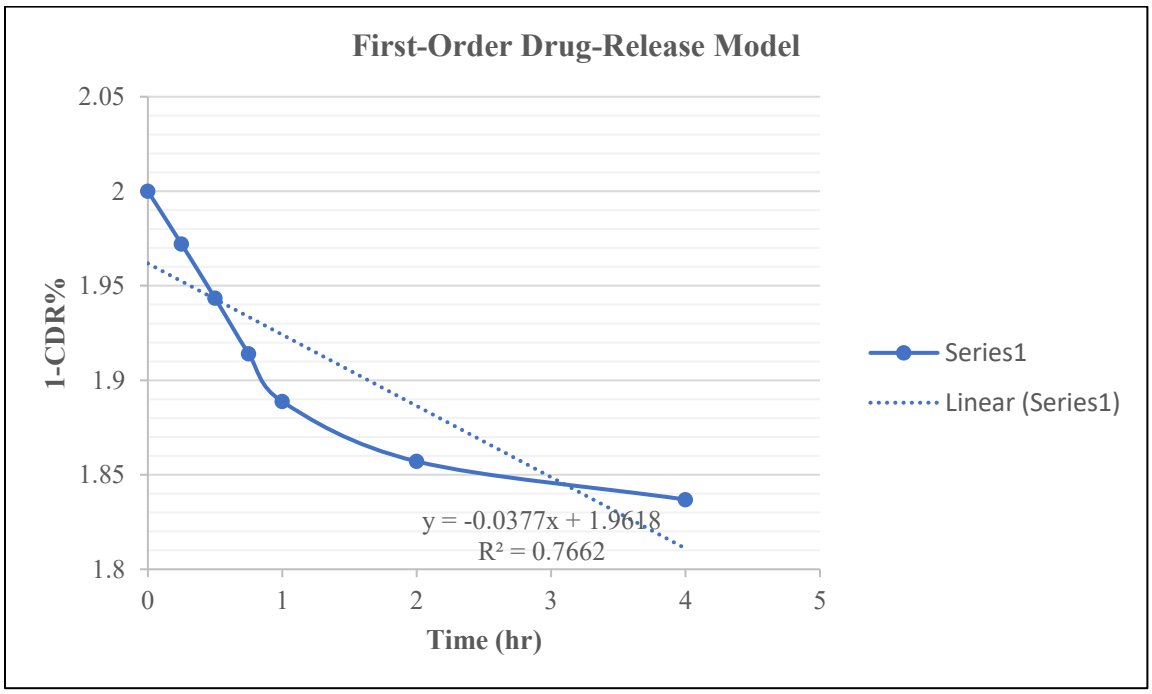

Figure A12. Release of 5-FU from plain chitosan hydrogels using first-order drug-release model.

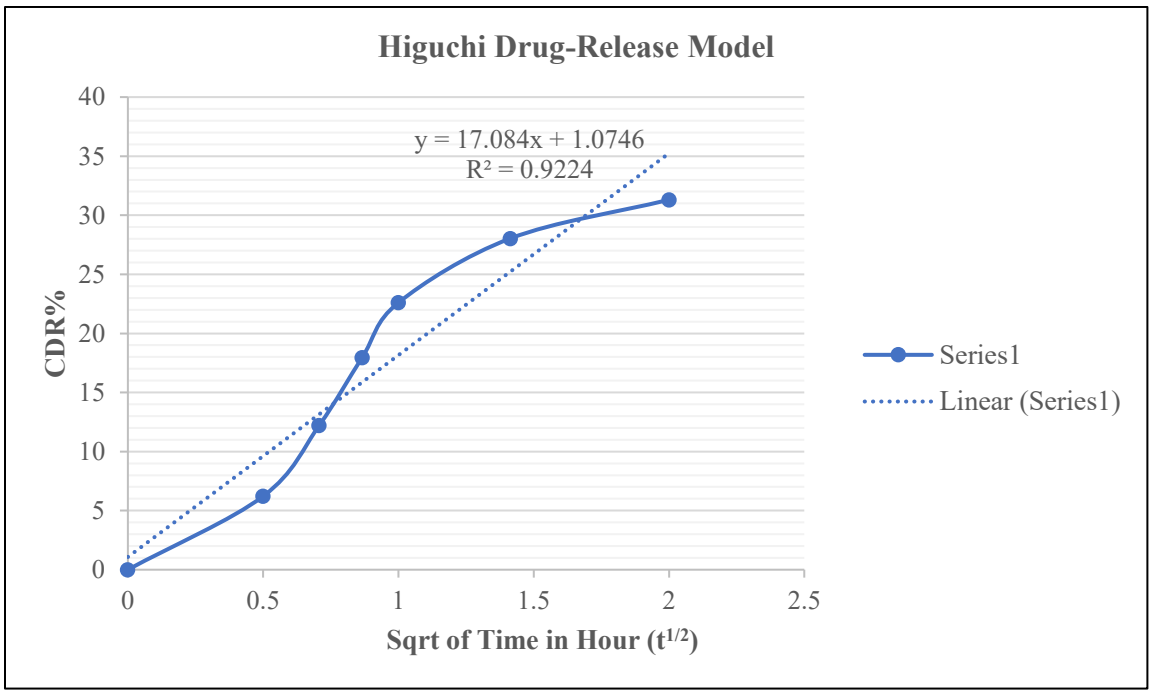

Figure A13. Release of 5-FU from plain chitosan hydrogels using Higuchi drug-release model.

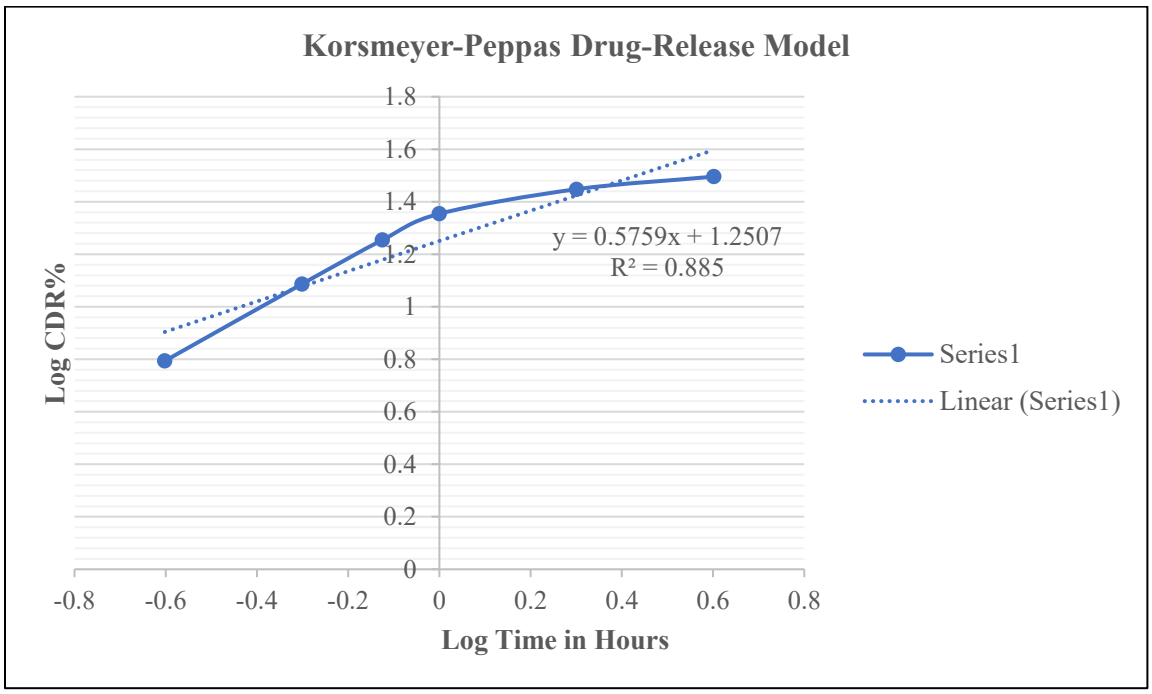

Figure A14. Release of 5-FU from plain chitosan hydrogels using Korsmeyer-Peppas drug-release model.

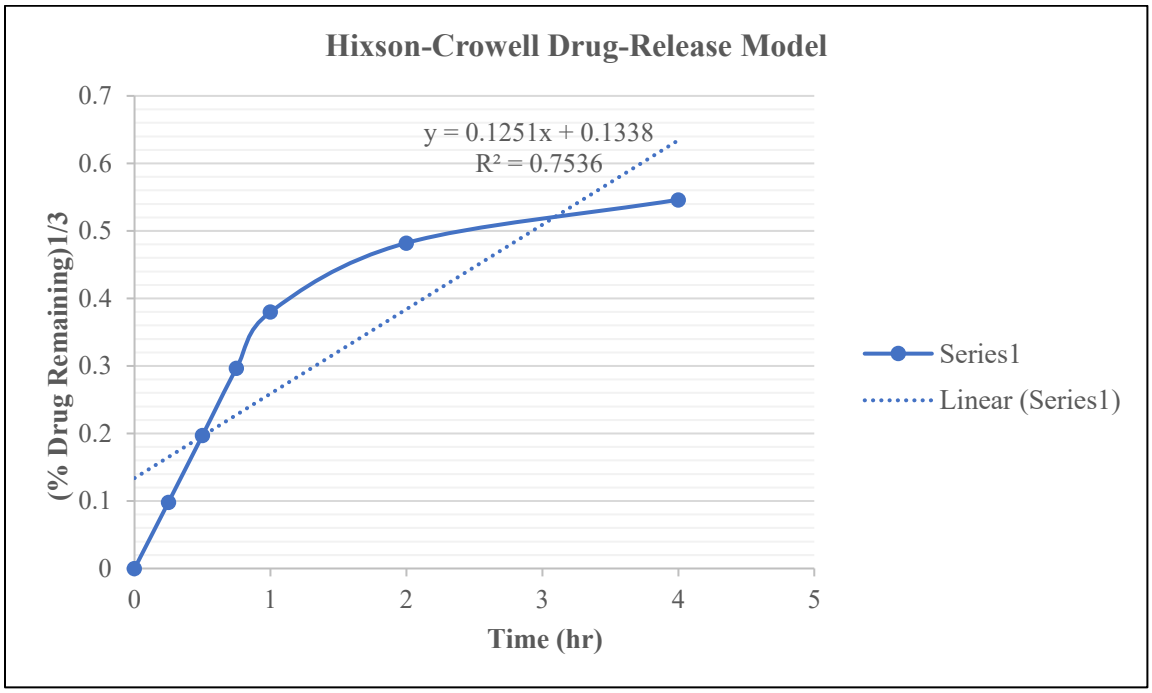

Figure A15. Release of 5-FU from plain chitosan hydrogels using Hixson-Crowell drug-release model.

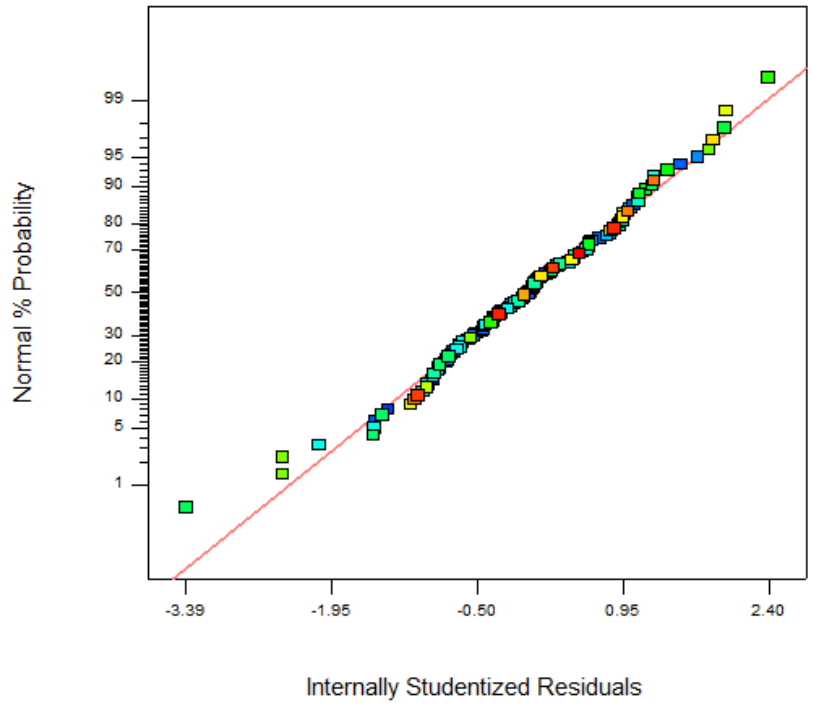

Figure A16. Normal probability plot of residuals.

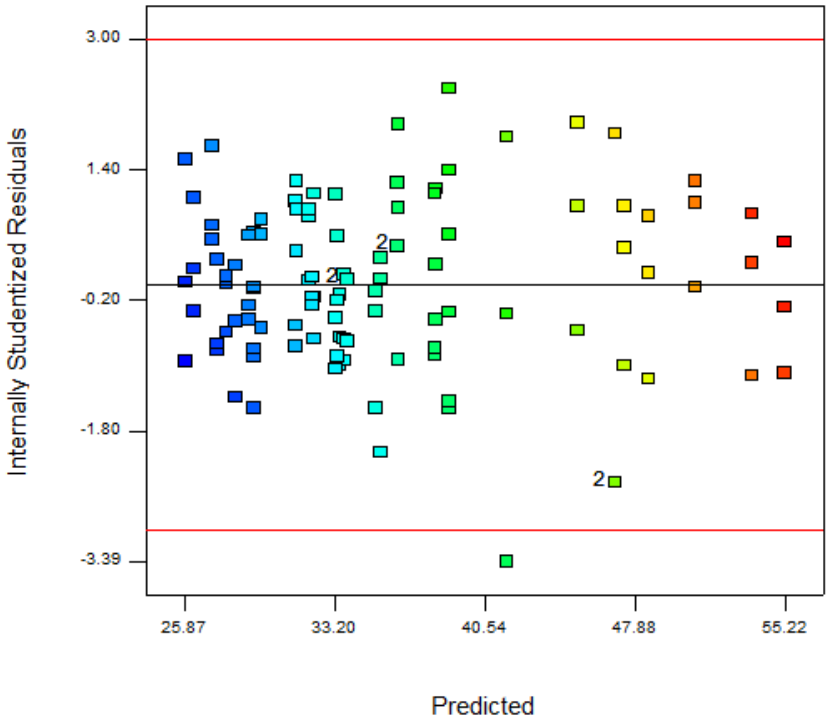

Figure A17. Plot of residuals versus predicted responses.

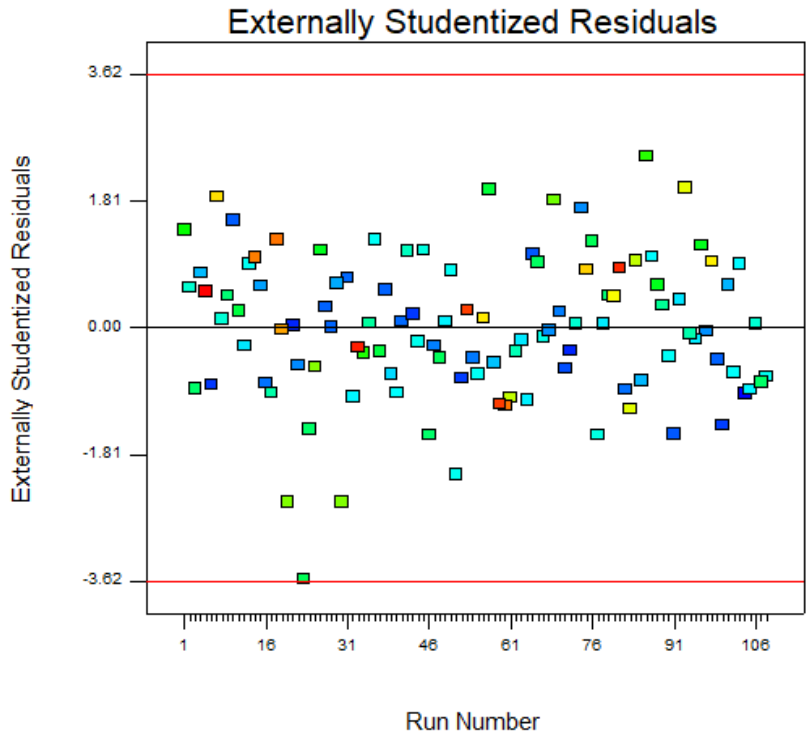

Figure A18. Plot of externally studentized residuals.

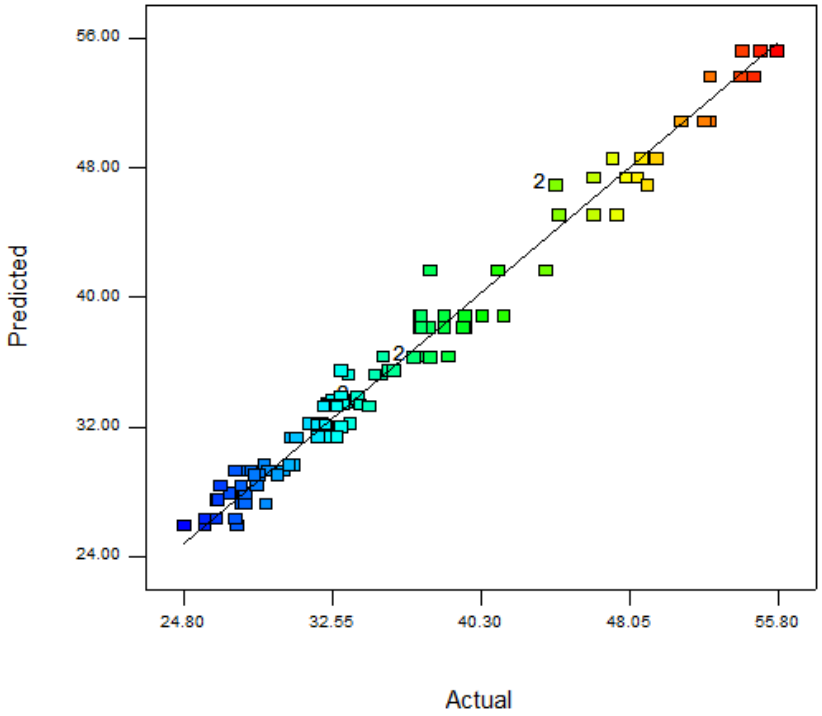

Figure A19. Plot of predicted responses versus actual responses.

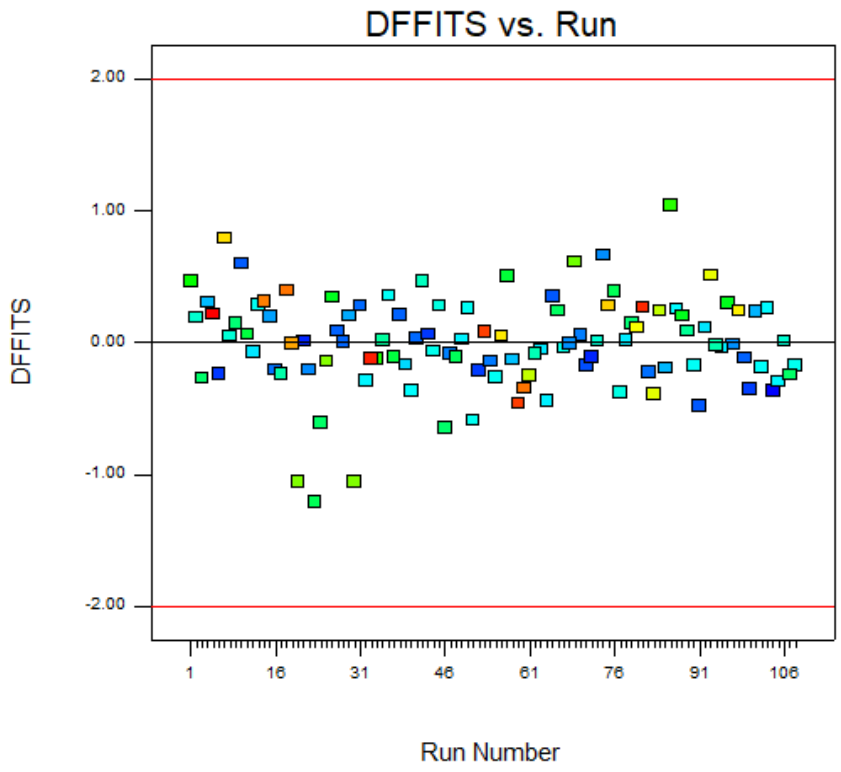

Figure A20. Plot of difference in fits versus run.